Programme: VLT

Project/WP: Science Operations

MUSE User Manual

Document Number: ESO-261650

Document Version: 12.2

Document Type: Manual (MAN)

Released On:

Document Classification: Public

Prepared by: Fuyan Bian

Validated by:

Approved by:

Name

Authors

Name	Affiliation
J.Richard and R. Bacon	Original authors from MUSE Consortia
J. Vernet, D. Wylezalek, E. Valenti	Upgrade the manual with AO information
F. Bian	Editor and maintainers DOO
F. Selman, E. Johnston	Past editors

Change Record from previous Version

Sections(s)	Date	Changes / Reason / Remarks
all	2017-01-13	All cross-references corrected and fixed (EJo)
5.1	2017-06-14	Update to include information about p2 and the unified GuideCam tool (EJo)
8.0	2017-06-29	Added information on GALACSI and GLAO observations. All sections affected.
8.1	2017-12-20	Updated information regarding AO. Fixed broken symbols. (FSE)
8.3	2018-05-24	Updated template description to be aligned with IP P102. Added numerical table with resolution vs wavelength in Sec. 3.2. (FSE)
8.5	2018-06-20	Updated range of Na notch cut off wavelengths.
8.10	2018-07-05	Changed references from P2PP to p2
8.10.x	2018-07-26	Updated to add information on the Narrow Field mode. All sections affected. (JVE, DWY)
8.12	2018-08-14	Version ready for P103 (EVA, FSE, FBI)
8.15	2018-12-19	Version for P103 Phase II. (FSE, EVA)
8.24	2018-12-23	P103: added 3 lasers performance section (FSE)
9.1	2019-03-01	For P104 Phase I. (FSE)
9.7-9.11	2019-06-15	For P104 Phase II (FSE, EVA, and FBI)
9.12-14	2019-08-22	For P105 Phase 1.
See page 9	2019-12-19	For P105 Phase 2

See page 9	2020-06-24	For P106 Phase 1 and 2
See page 9	2021-05-31	For P108 Phase 1 and 2
See page 9	2021-09-06	For P109 Phase 1.
12.1	2023-12-15	For P112 Phase 1. Correct typos and update the NFM NGS limited magnitude.
4.4	2024-01-15	For P113 Phase 2. NFM degraded 3LGS mode
4.4,5.4	2024-08-01	For P115 Phase 1. Some minor change for clarity
5.3	2025-01-21	For P116 Phase 1 Define the FWHM threshold (300mas) for unresolved and resolved objects for MUSE NFM NGS.
4.1.2	2026-07-13	Add the PSF profile difference WFM-AO between WFM-NOAO modes.
5.1	2026-09-03	no TTS for WFM-AO is necessary to provide in Phase 1

Page left intentionally almost blank

Contents

1. INTRODUCTION 7
1.1 SCOPE 7
1.2 THE MUSE FACILITY IN A NUTSHELL 7
1.3 MORE INFORMATION ON MUSE FACILITY 9
1.4 NEW IN THIS VERSION 9
1.5 LIST OF ABBREVIATIONS & ACRONYMS 10
2 TECHNICAL DESCRIPTION OF THE MUSE FACILITY 13
2.1 TECHNICAL DESCRIPTION OF MUSE 13
2.2 TECHNICAL DESCRIPTION OF GALACSI AND THE AOF 25
3 OVERALL MUSE PERFORMANCES AND CHARACTERISTICS 34
3.1 ABSOLUTE THROUGHPUT AND LIMITING MAGNITUDE 34
3.2 SPECTRAL RESOLUTION AND SAMPLING 36
3.3 EXPOSURE TIMING 37
3.4 OVERALL ILLUMINATION AND UNIFORMITY 37
3.5 DISTORTION AND ASTROMETRIC PRECISION 38
3.6 NFM ADC PERFORMANCE 39
3.7 SECOND ORDER CONTAMINATION 40
3.8 INSTRUMENT STABILITY 41
3.9 PROBLEMS TO BE AWARE OF 43
3.10 PERFORMANCE REPORTED IN THE LITERATURE 46
4 AO MODES PERFORMANCE 48
4.1 MAXIMUM AIRMASS OF OBSERVATION IN AO MODE 48
4.2 IMAGE QUALITY GAIN IN WFM AO 48
4.3 DEGRADED THREE LASERS MODE IN WFM-AO 51
4.4 DEGRADED THREE LASERS MODE IN NFM-AO 54
4.5 ADAPTIVE OPTICS PERFORMANCE IN NFM 55
4.6 CONTAMINATION CAUSED BY NA LASER DURING AO OBSERVATIONS 65
5 OBSERVING WITH MUSE 67
5.1 GENERAL INFORMATION 67
5.2 MUSE OBSERVING MODES 70
5.3 MUSE TARGET ACQUISITION 71
5.4 MUSE SCIENCE OBSERVATIONS 75
5.5 ATTACHED CALIBRATIONS 81
5.6 INSTRUMENT AND TELESCOPE OVERHEADS 82
6 TEMPLATES 85
6.1 MUSE ACQUISITION TEMPLATES 86
6.2 OBSERVATION TEMPLATES TABLES 90
6.3 CALIBRATION TEMPLATES TABLES 93
7 CALIBRATING AND REDUCING MUSE DATA 105
7.1 MUSE CALIBRATION PLAN 105
7.2 MUSE DATA REDUCTION 110
8 REFERENCE MATERIAL 113
8.1 DETECTOR COSMETICS 113
8.2 ARC LAMPS LIST 114

8.3 DESCRIPTION OF THE WFM_SMP MASK 119
8.4 LOG OF INSTRUMENT CHANGES 120
8.5 DS9 TEMPLATE 120
8.6 VERSION HISTORY 121

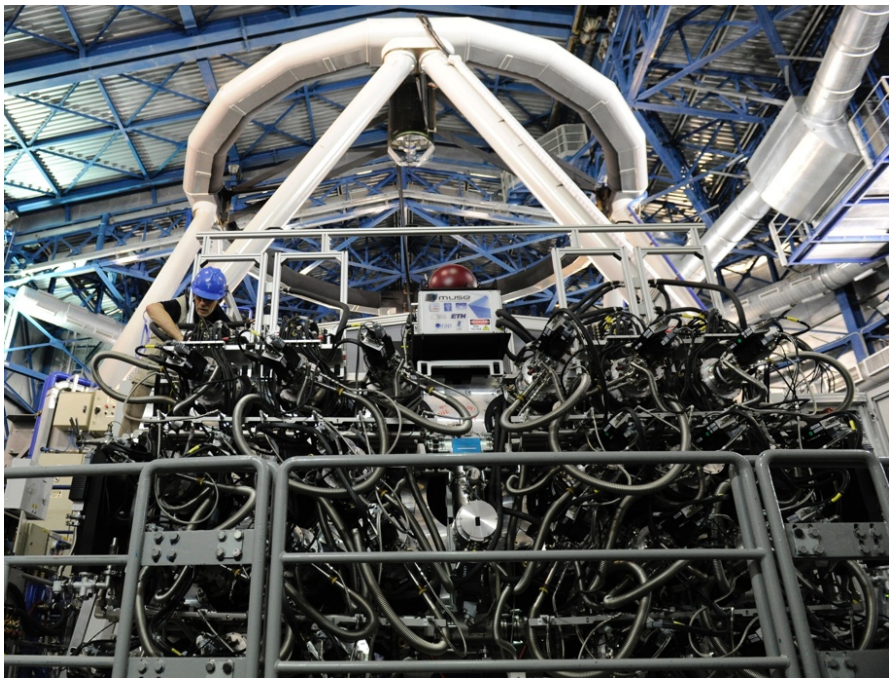


Figure 1 MUSE at the Nasmyth B focus of Yepun (UT4).

1. Introduction

1.1 Scope

The MUSE User Manual was written and provided to ESO by John Richard and Roland Bacon from the MUSE consortium. It is maintained by the ESO Paranal Instrument Scientist and the MUSE Instrument Operation Team (IOT). It provides extensive information on the technical characteristics of the instrument, its performances, observing and calibration procedures and data reduction. The goal is to provide all pieces of information and advice necessary for MUSE users to prepare their observations. It is intended for MUSE users, and as such it is written from an astronomer's perspective.

We welcome any comments and suggestions on this manual; these should be channeled through our Operations Helpdesk at https://support.eso.org/.

1.2 The MUSE Facility in a nutshell

MUSE, the **M**ulti **U**nit **S**pectroscopic **E**xplorer, is a second-generation VLT instrument located on the Nasmyth platform B of the VLT UT4. It is a large-format integral-field spectrograph, based on image-slicing technology, and has a modular structure composed of 24 identical Integral Field Unit modules that together sample a contiguous 1 arcmin^2 field of view in Wide Field Mode (WFM) sampled at 0.2 arcsec/pixel. Spectrally, the instrument samples most of the optical domain, with a mean resolution of 3000.

MUSE exploits the VLT Adaptive Optics Facility (AOF) at the VLT UT4 (Yepun) with its 4 Laser Guide Stars (4LGSF) and the Deformable Secondary Mirror (DSM) in combination

with GALACSI, the Ground Atmospheric Layer Adaptive Corrector for Spectroscopic Imaging, which provides Ground Layer Adaptive Optics (GLAO) correction for the WFM. In addition, a Narrow Field Mode (NFM) is also available and covers a ~7.5 arcsec^2 field of view sampled at 0.025”/pixel with Laser Tomography AO correction (LTAO). The combination of MUSE and GALACSI is named MUSE Facility. A view of the instrument attached to the telescope is shown in Error! Reference source not found.. The main i nstrument characteristics are summarized in Table 1.
The MUSE instrument was built by a Consortium involving institutes from France, Germany, The Netherlands, Switzerland and ESO. The GALACSI AO module was built by ESO as part of the AOF project. The names of the institutes and their respective contributions are given in Table 2.

Table 1: *MUSE in a nutshell.*

Number of modules	24
Wavelength range	480 – 930 nm (nominal) 465 – 930 nm (extended)* Wavelength range excluded for AO observations (Na Notch filter): WFM-AO-N: 582 – 597 nm (nominal) WFM-AO-E: 576 – 601 nm (extended) NFM-AO-N: 578 – 605 nm
Resolving power	1770 (480 nm) – 3590 (930 nm) (WFM) 1740 (480 nm) – 3450 (930 nm) (NFM)
Spectral sampling	0.125 nm/pixel
Detectors (per module)	4k x 4k e2V CCD
Field of view	59.9” x 60.0” (WFM) 7.42” x 7.43” (NFM)
Spatial pixel scale	0.2” / pixel (WFM) 0.025” / pixel (NFM)
Throughput (total atmosphere, telescope and instrument)	WFM: 18 % - NFM: 13% (480 nm) WFM: 33 % - NFM: 26% (750 nm) WFM: 14 % - NFM: 11% (930 nm)

(*) *only available for WFM instrument modes. Suffers from 2nd order contamination*

1.3 More information on MUSE Facility

All MUSE Manuals are available on the MUSE instrument WEB pages, together with the most updated information on the instrument:
http://www.eso.org/sci/facilities/paranal/instruments/muse/

Information and software tools for the preparation of service and visitor mode observations with MUSE are available at:
http://www.eso.org/sci/observing/phase2
http://www.eso.org/sci/observing/phase2/SMGuidelines.html

Work based on MUSE observations should cite the paper:
Bacon et al., Proc of the SPIE, Vol. 7735, 7 (2010)
Work based on observations with Adaptive Optics should also cite:
Stroebele et al., Proc. of the SPIE, Vol. 8447, 11 (2012) and
Arsenault et al., Proc of the SPIE, Vol. 7736 (2010).

Visiting astronomers will find further instructions on the Paranal Science Operations WEB page and the Paranal Observatory home page:
http://www.eso.org/sci/facilities/paranal/
http://www.eso.org/sci/facilities/paranal/sciops/

1.4 New in this version

- Version for P109 Phase 1
  - New NFM IRLOS limiting magnitudes: non-extended reference objects down to J < 18.0 any TC and (J<18.5 for TC=10% and airmass < 1.2), and extended sources down to J<17.0 are now possible.

- Version for P108 Phase 1 and 2
  - Changed band for NFM limiting magnitude specification from H to J
  - Added section giving details of NFM AO performance versus airmass and TC.
  - Added section about the MUSE NFM PSF
  - Added section for very bright star observations in NFM (Sec. 4.5.4).
  - Added WFM-AO performance figures from Hartke et al. (2020) SPIE.
  - Added section with NFM IRLOS+ commissioning info (Sec. 2.2.3).
  - Reduced NFM off-axis maximum distance for non-extended NGS from 5.90” to 5.00”.

- For other version changes see Appendix 0

- Version 1.0

  The first version of this manual has been delivered by the MUSE consortium, P.I. R. Bacon, for Phase I, P94, on 28 Feb 2014.

1.5 List of Abbreviations & Acronyms

This document employs several abbreviations and acronyms to refer concisely to an item, after it has been introduced. The following list is aimed to help the reader in recalling the extended meaning of each short expression:

4LGSF:	Four Laser Guide Stars Facility
ADC:	Atmospheric Dispersion Corrector
ADU:	Analog / Digital Unit
AO:	Adaptive Optics
AOF:	Adaptive Optics Facility
e-APD:	electron Avalanche Photo Diode
CCD:	Charged Coupled Device
CU:	Calibration Unit
DDT:	Director's Discretionary Time
DQ:	Data Quality
DRS:	Data Reduction Software
DSM:	Deformable Secondary Mirror
EE:	Ensquared Energy
ESO:	European Southern Observatory
FO:	Fore Optics
FOV:	Field Of View
FWHM	Full-Width At Half Maximum
GALACSI	Ground Atmospheric Layer Adaptive Corrector for Spectroscopic Imaging
GLAO:	Ground Layer Adaptive Optics
GLF:	Ground Layer Fraction
HST:	Hubble Space Telescope
IFU:	Integral Field Unit
IOT	Instrument Operation Team
IRLOS:	Infrared Low Order Sensor
IS	Instrument Scientist
LGS:	Laser Guiding Star
LSF:	Line Spread Function
LTAO:	Laser Tomography Adaptive Optics
MAOPPY:	Modelization of the Adaptive Optics Psf in PYthon
MUSE:	Multi-Unit Spectroscopic Explorer
MUSF	Multi-Unit Spectroscopic Explorer Adaptive Optics Facility
NFM:	Narrow Field Mode
NGC:	New Generation Controller
NGS:	Natural Guide Star
OGS:	On-axis Guide Star
p2:	Phase 2 tool (Visitor and servicemode)
P2PP:	Deprecated phase 2 tool
QE:	Quantum Efficiency
RON:	Read Out Noise
RMS:	Root Mean Square
RTD:	Real Time Display

SGS: Slow Guiding System
SH: Shack-Hartmann wavefront sensor
SNR: Signal to Noise Ratio
SPARTA: Standard Platform for Adaptive optics Real Time Applications
SRO: Splitting and Relay Optics
TBC: To Be Confirmed
TC: Turbulence Category
TSF: Template Signature File
TTS: Tip-Tilt Star
USD: User Support Department
UT: Unit Telescope
VLT: Very Large Telescope

Table 2: *collaborating institutes and their contributions.*

Collaborating institutes	**Contribution**
Leibniz-Institut für Astrophysik Potsdam	Development of the Calibration Unit, testing of the preassembled spectrograph-detector units, data reduction software
Centre de Recherche Astrophysique de Lyon	Overall management of the project, image slicer sub system, spectrograph opto-mechanical design and integration, data analysis software.
ESO	Detector systems (24 detectors and their cryogenic environment, Adaptive Optics Facility (AOF) including the GALACSI Adaptive Optics module, the Laser Guide Star Facility (4LGSF) and the Deformable Secondary Mirror (DSM)
ETH – Institute of Astronomy (Zurich)	Procurement of the 24 spectrographs
Institut für Astrophysik Göttingen	Design, analysis and procurement of the instrument mechanics, the support and handling structures as well as for the optics that apply the field splitting and the relay optics.
Institut de Recherche en Astrophysique et Planétologie (Toulouse)	Electronic and Software Control of the whole Instrument, Opto-mechanical development of the Fore-Optics module.
Leiden Observatory	Interface between the MUSE spectrograph and the adaptive optics system, definition of the top-level requirements for the adaptive optics system.

Page left intentionally almost blank

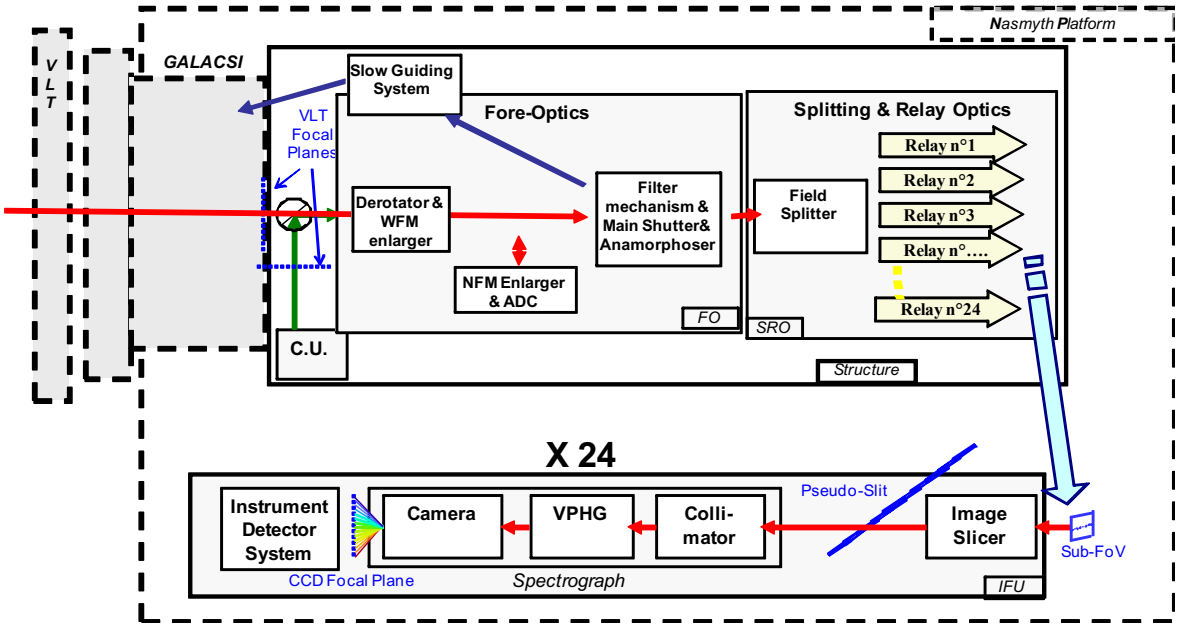


Figure 2: *Overview of MUSE subsystems*

2 Technical description of the MUSE Facility

2.1 Technical Description of MUSE

2.1.1 Overview of the opto-mechanical design

shows a schematic view of the layout of MUSE. The instrument is composed of the following sub-systems:

- The Calibration Unit (CU) provides different illumination fields to calibrate the MUSE instrument. It includes functions to switch on and off the lamps, motors to position the chosen mask and to insert a Calibration pick-up mirror in the MUSE instrument light path. These functions are controlled through calibration and maintenance templates.
- The Fore Optics (FO) reshapes the VLT focus image to adapt it to the next sub-system, which splits the image in 24 channels. It rotates the field, magnifies it, and reshapes it into a 2:1 ratio.
- The Splitting and Relay Optics (SRO) sub-system divides the Field of View (FOV) in 24 horizontal sub-fields and feeds each Integral Field Unit.
- Each of the 24 Integral Field Units (IFU) is composed of 3 sub-systems: the Image Slicer, the Spectrograph, and the Detector. Each IFU covers one of 24 sub-fields, or stripes, within the field-of-view, and each image slicer further subdivides this sub-field into 48 slices.

2.1.2 Description of the instrument sub-systems

This section describes the different sub-systems of MUSE in the order they are encountered along the optical path going from the telescope to the detectors (see , Figure 3, and Figure 4). The functionalities of the different sub-units are explained, and reference is made to their measured performance.

2.1.2.1 Calibration Unit

The calibration unit (CU) is a mechanical structure with calibration lamps, an integrating sphere, and a set of masks used to produce calibration fields for MUSE. A calibration pick-up mirror is used to direct light into the instrument from either the telescope or the CU.

The CU allows for a choice of 6 calibration lamps as input light sources:

- Two flat-field halogen lamps providing uniform continuum flux over the MUSE wavelength range
- 4 arc lamps used for wavelength calibration:
  - One Ne pencil-ray lamp
  - One Xe pencil-ray lamp
  - One HgCd pencil-ray lamp
  - One Ne High Power lamp

Two pico-ampere meters placed at the CU focal plane are used to monitor the absolute flux sent by the lamps into MUSE. Details on the line wavelengths and relative fluxes produced by each lamp are provided in Section 8.2.
The focal plane mask wheel allows for a choice of 5 masks covering the CU FOV, two of them:

- The CLEAR (no mask) position is used for flat-field and wavelength calibrations.
- The WFM_SMP is a mask containing a grid of small (50 μm diam.) pinholes covering the WFM FOV. It is used to perform the geometrical calibration (see Section 8.3).

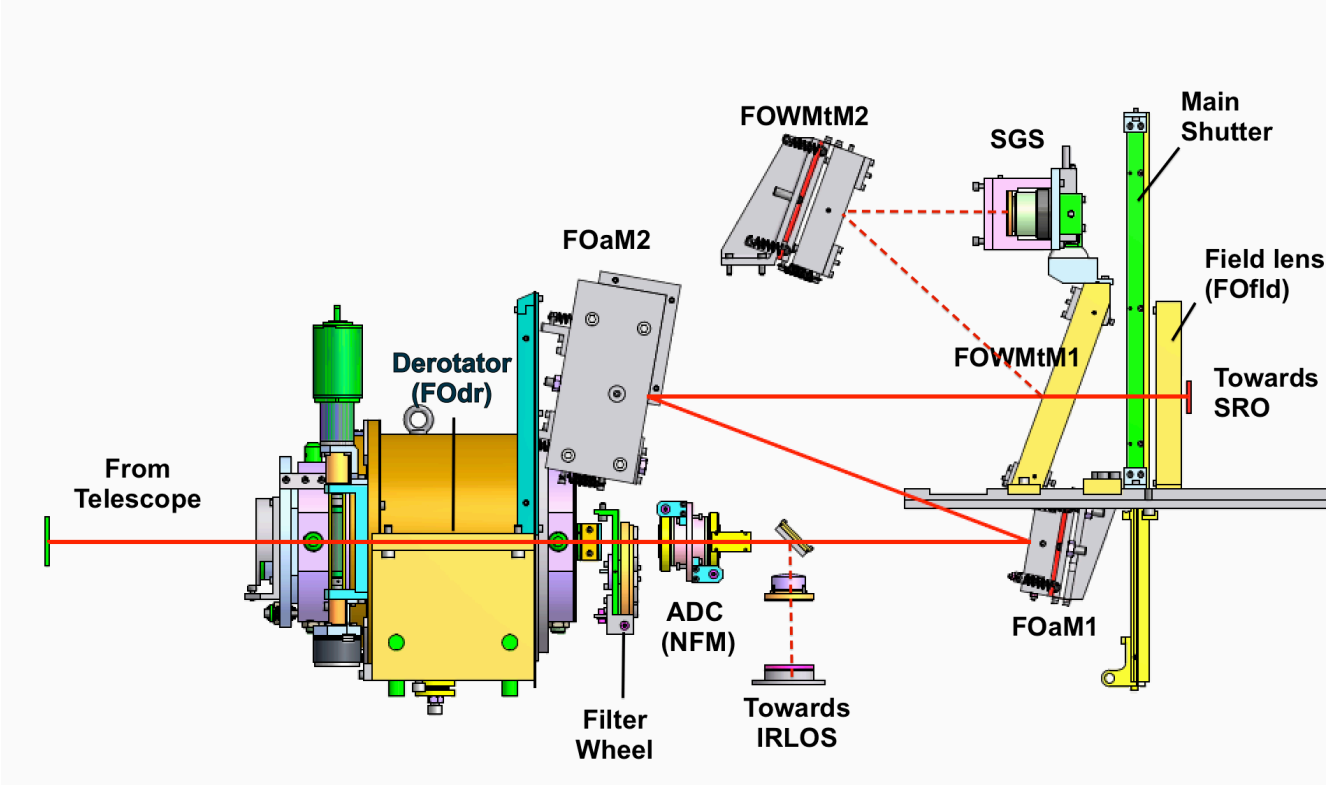


Figure 3 *MUSE fore-optics schematics in NFM configuration*

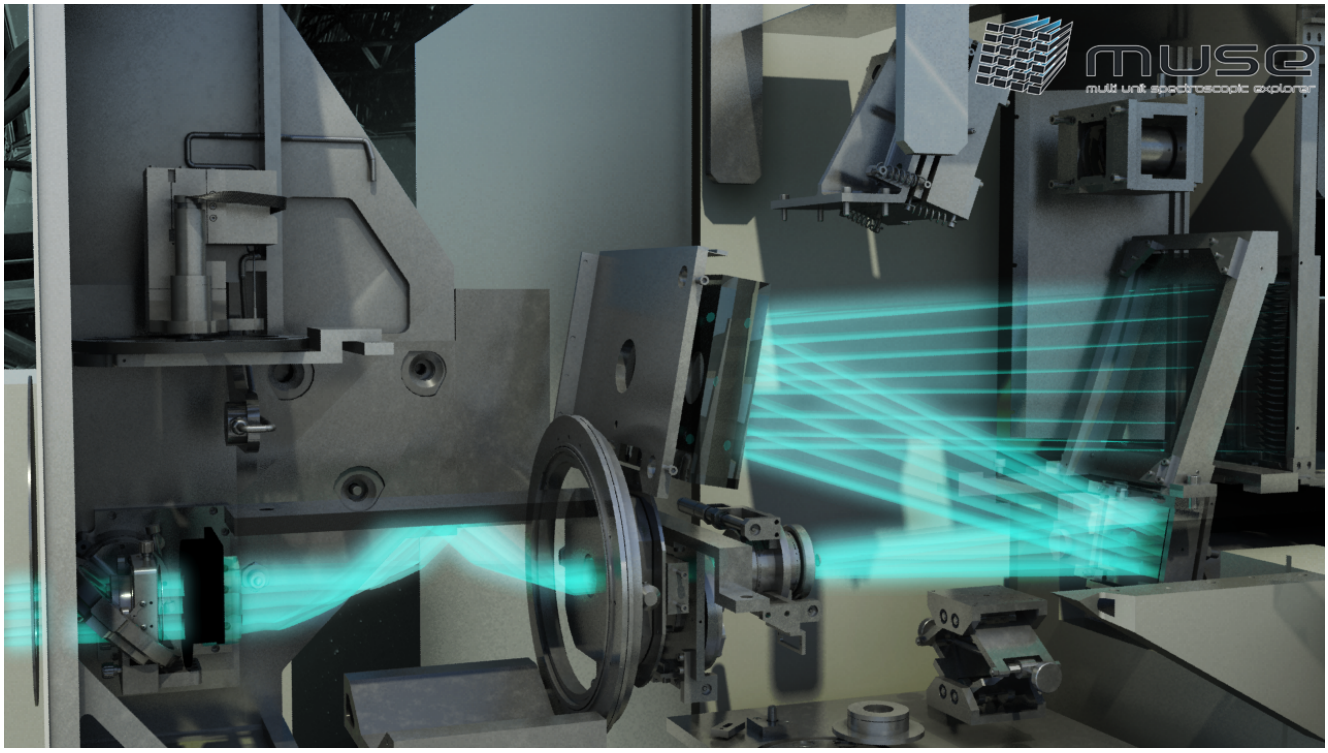


Figure 4: *Drawing of rays in the fore-optics, from the de-rotator to FOWMtM1.*

2.1.2.2 Fore Optics

The fore-optics system is shown in Figure 4. The top panel presents the optical elements (details in the text), and the bottom 3D view shows the path of light rays. It comprises the following subcomponents:

- **Derotator**

  The derotator compensates for the field rotation at the VLT Nasmyth focus. It is a classical derotator based on two prisms: when rotated by an angle θ, the image plane rotates by the angle 2θ.

- **Filter Wheel**

  A filter wheel is included in the fore-optics to adjust the spectral coverage according to the desired instrument mode:
  - The nominal wavelength range of MUSE corresponds to 480-930 nm, which allows for suppression of second-order contamination in the red. In nominal mode, the blue cut-off filter is used to cut the wavelength range in the blue and avoid ghosts in that region.
  - An "extended" wavelength range is available in WFM only, allowing observations down to 465 nm. However, strong second-order contamination appears in that case at λ>900 nm (see Section 3.7 for details).
  - In AO modes the ranges 582-597 nm (for WFM-AO-N), 576-601 nm (for WFM-AO-E), and 578 – 605 nm (for NFM) are blocked to avoid contamination by sodium light from the LGS.

In total, 5 filters are available in the wheel. The relationship between instrument mode and filter name is provided in Section 0.

- **Mode-switching and Atmospheric Dispersion Corrector (NFM only)**

  The Mode-switching unit prepares the FOV when the instrument is used in NFM. It magnifies by 8 in each direction and includes the Atmospheric Dispersion Corrector (ADC). Note that the ADC is used, in NFM only, to correct for atmospheric dispersion. It consists in two Amici prisms working in counter-rotation.

- **IRLOS (NFM only)**

  In NFM, a dichroic reflects the infrared light towards InfraRed Low Order Sensor (IRLOS), with IRLOS measuring the wave front errors invisible to the LGS-AO system. It is a Shack Hartman sensor with 2 by 2 sub apertures working in the MUSE FOV at a wavelength range of 980nm to 1800nm. The IRLOS assembly includes a filter wheel, a field selector and a plate scale changer carrying 2 optical barrels containing a pupil relay lens and the sub-aperture array. The detector is a SAPHIRA

Mark2b detector, 320x256 pix e-APD array, capable of sub-electron readout-noise[1] (RON). The pixel scales are 0.078”/pixel for point sources (SEQ.NGS.EXTENDED=F) and 0.314”/pixel for extended sources (SEQ.NGS.EXTENDED=T). IRLOS senses image drifts occurring in NFM and corrects them by means of the AO loops. Due to the reduced RON the measuring/correction frequency is now 500 Hz for point sources, and 200 Hz for extended and very faint sources.

- ### Anamorphoser

  Two cylindrical mirrors (FOaM1 and FOaM2, Figure 4) provide a magnification of 0.5 to the beam in the horizontal direction within the fore-optics to ensure sufficient sampling in the dispersion direction.

- ### Slow Guiding System (SGS)

  When in WFM mode, an elliptical pick-up mirror (FOWMtM1, Figure 3) separates the central FOV (corresponding to 1 x 1 arcmin^2 on sky) from the four metrology fields surrounding it, which are reflected towards the WFM Slow Guiding System after removing the magnification using the FOWMtM2 mirror. Incoming light is recorded by the SGS using an ESO NTCCD, 1k x 1k Technical CCD (having a 0.09” pixel scale). The system automatically detects astrophysical sources in the metrology fields of stacked exposures (Figure 5) and corrects for small motions by sending commands to the Telescope in a closed loop. These corrections are sent on average every 2 min. Therefore, in practice, the first offset sent happens after the second stacked exposure is recorded (i.e. 4 min.). The minimum and maximum brightness of stars useful for the SGS are approximately R=21.5 and R=9.5 respectively. Note that some useful parameters, such as image quality and transparency, are monitored by the SGS during an observation and saved in the FITS file of the science exposure as extension SGS_DATA (see Section 7.2).

[1] The new SAPHIRA detector was retro-fitted to IRLOS during March 2021 and started operations on April 2021. It replaces the old HAWAII 1 detector which pixel scales of 60 mas and 250mas in non-extended and extended scales, and a RON of 11 e RMS. See Finger et al., Proc. SPIE **2019**, 11180, 111806L

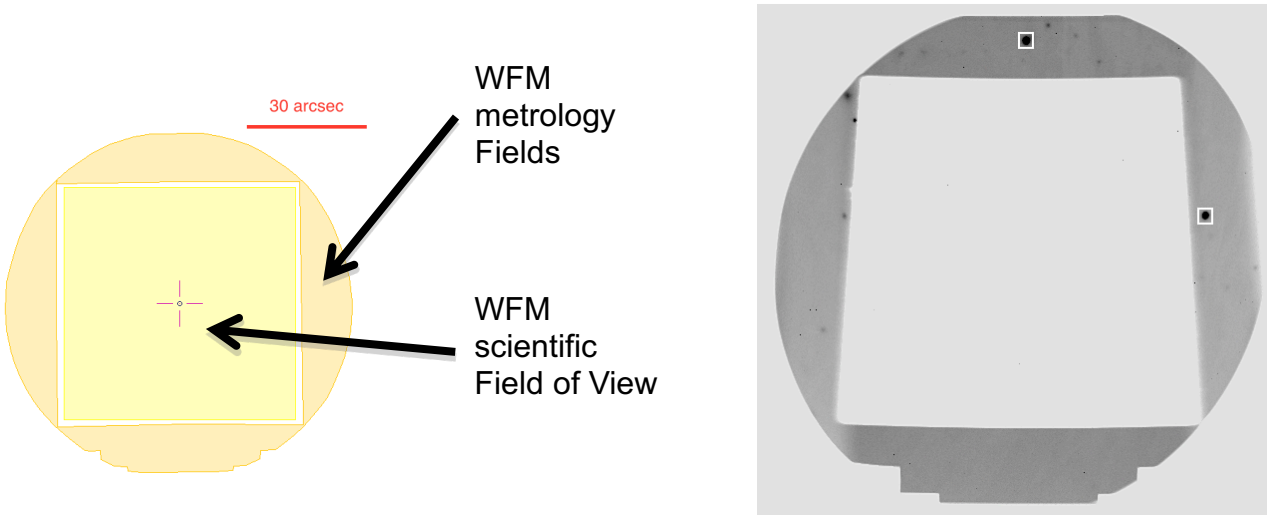


Figure 5: *left, shows the location of the metrology field used by the SGS, as seen on the detector[1]. On the right there is an example of SGS image showing the detected stars used to monitor small motions (white squares). Note that the SGS image is flipped vertically when oriented on sky.*

- Exposure shutter

  This shutter is located between the SGS pick-up mirror (FOWMtM1, Figure 3) and the exit beam. It is a Bonn shutter with a rectangular aperture moving along the vertical direction. Shutter delay has been measured at 7.0-7.5 ms.

2.1.2.3 Splitting and Relay Optics (SRO) system

The SRO system splits the MUSE FOV into 24 channels and redirects the light of each channel towards the entrance of an IFU. It is composed of a field-splitter and a field separator, which separate the field into 24 horizontal beams (Figure 6).

These sub-fields feed 24 relay optics, which correct for the variations in optical path from one channel to another (Figure 7).

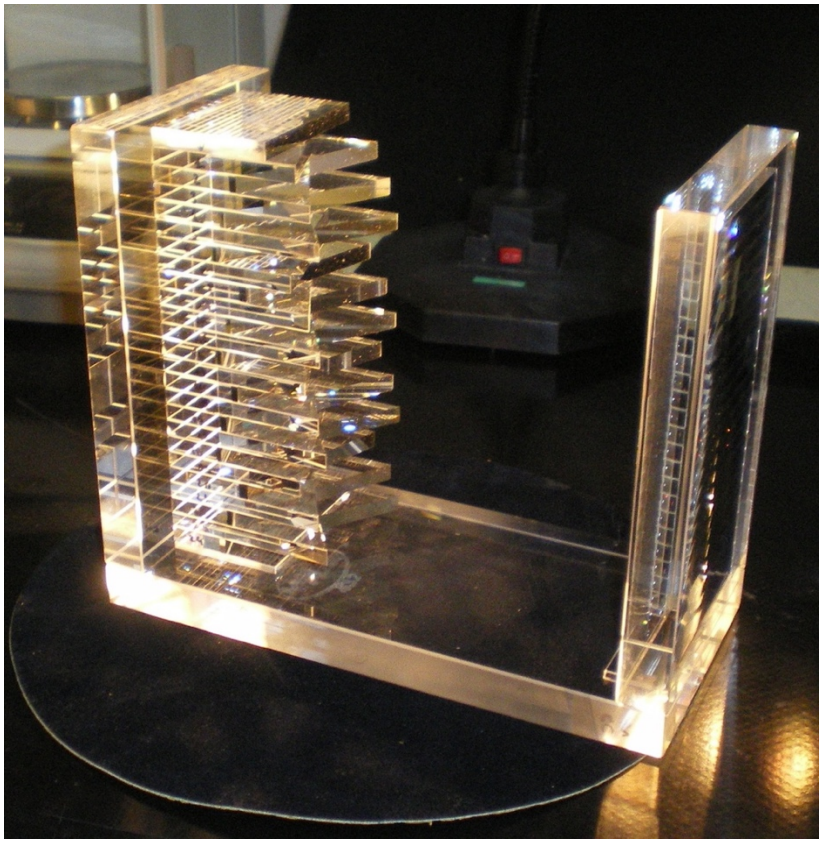
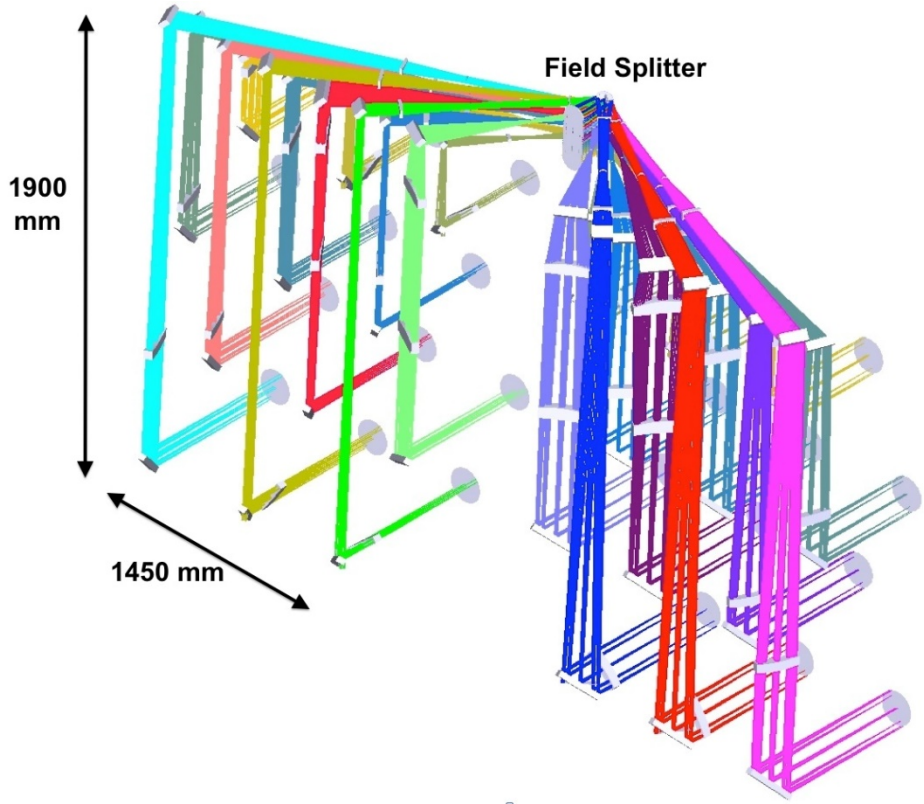


Figure 6*: MUSE Field splitter and field separator optics. The 24 mirrors positioned at varying angles split the MUSE field-of-view in 24 horizontal bands.*



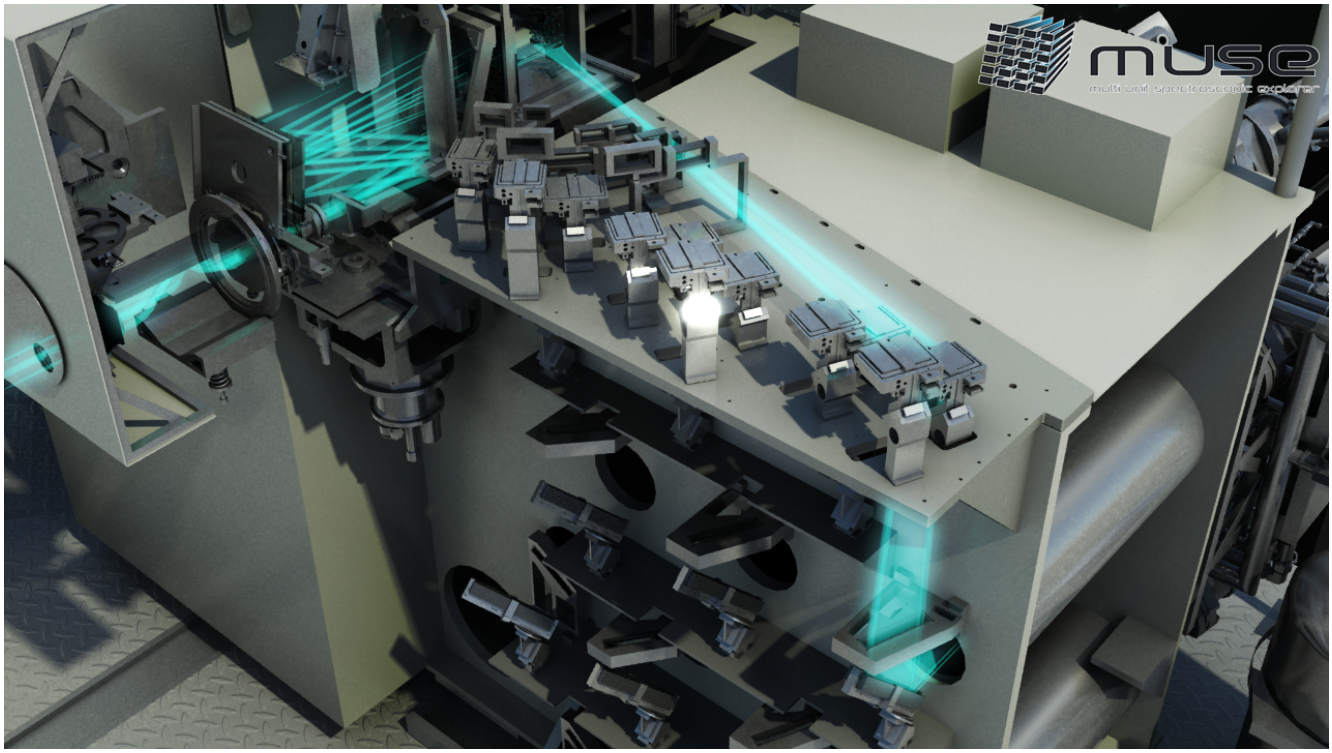


Figure 7: *3D view of optical paths for all channels due to the relay optics splitting of the field-of-view into 24 channels. The bottom figure shows the path of light rays for one of the channels, as seen from the Fore-Optics.*

2.1.2.4 Integral Field Unit

Each of the 24 Integral Field Units (each assigned to a given channel) is formed by the combination of an image slicer, a spectrograph, and a detector, which we describe below. The optical layout of one of the IFUs is presented in Figure 8.

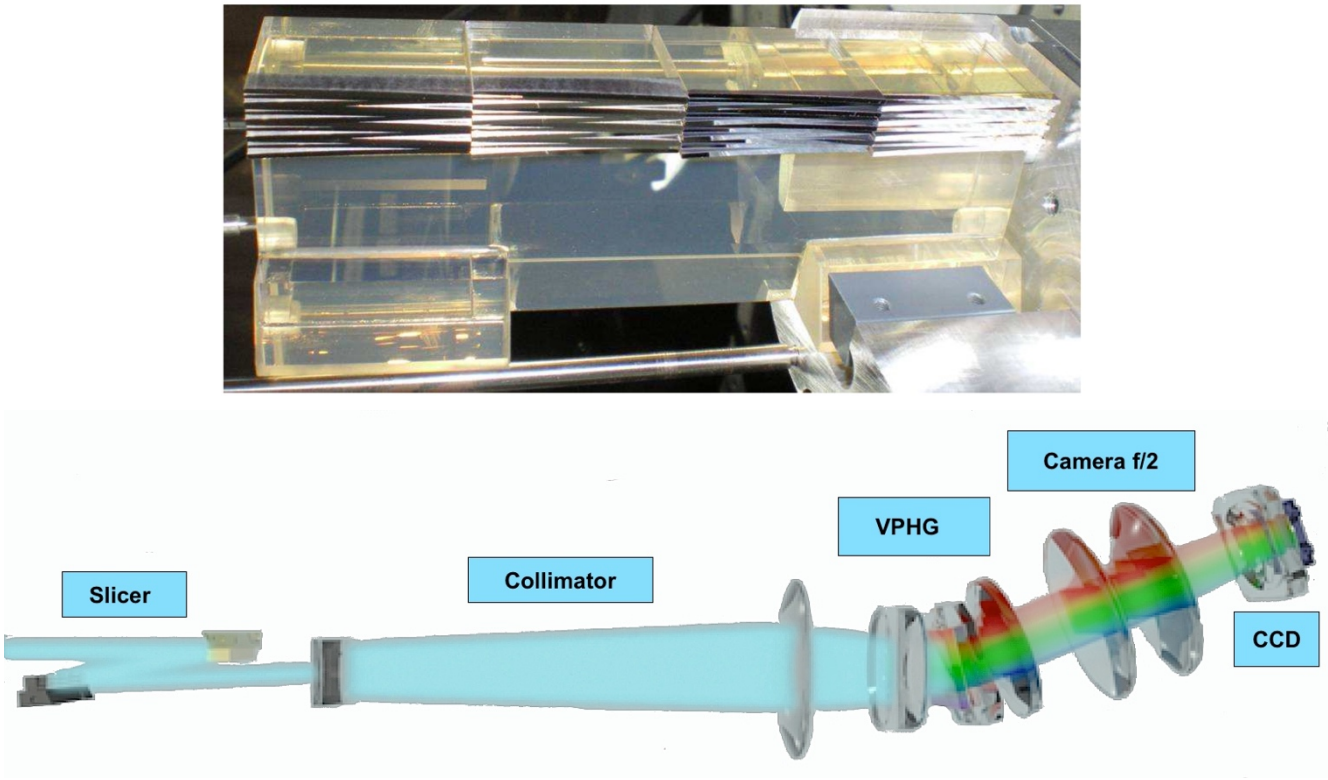


Figure 8*: Overview of the optical layout for one of the IFUs. The top panel shows one of the slicers, which cuts the FOV of each channel into 4 stacks of 12 slices. The bottom panel shows the optical elements in the IFU and the path of light to the CCD.*

2.1.2.4.1 Slicer

The slicer cuts and rearranges the 2D sub FOV in a 1D pseudo slit of 0.2" width. The main function of the image slicer is to slice the fraction of the FOV coming from the SRO into 48 slits that are rearranged in a long slit at the entrance of the spectrograph. The slicer is composed of:

- an image dissector array separating the beam in 48 slices (as represented on top of Figure 8)
- a focusing mirror array, which rearranges and aligns the slices
- a pupils/slits mask reducing scatter light and ghost images before entering the spectrograph.

2.1.2.4.2 Spectrograph

The main function of the spectrograph is to produce the spectra of the mini slits and image them onto a detector. It is composed of a collimator, a Volume Phase Holographic Grating and a camera. The grating disperses the mini slits in the perpendicular direction and achieves a spectral resolution of 1609 at 465nm to 3506 at 930nm (Figure 18). There is no moving part in the spectrographs and all 24 spectrographs are identical.

2.1.2.4.3 Detector

The light exiting each of the 24 spectrographs is sent onto a 4k x 4k, 15 μm pixel CCD, operating at 163 K. The nominal characteristics of these detectors are given in Table 3.

Parameter	Value
CCD Type	E2V Deep depletion, AR graded coated
Active pixel format	4096*4112 pixels (X*Y)
Pixel size	15*15 μm^2
Pre-scan pixels in X direction	32
Overscan pixels	32
Detector gain	~1.1 ADU / e-
Saturation	65000 e-
Linearity	<0.5% non-linear residuals
Binning factor	1x1 only
Readout noise	2.6 e-
Number of readout ports	4
Readout speed	100k pix/s
Readout time to RTD	40 sec
Dark current at 160K	3 e-/pix/hr

Ta**ble 3:** *Properties of the MUSE detectors.*

The twenty-four scientific detectors of MUSE are controlled using four New Generation Controllers (NGC). The readout is always used without binning during observation.

The detector imaging area consists of four individually read quadrants of 2048 x 2056 pixels (X , Y) each, separated by pre-scan and over-scan regions. In the normal (science) readout mode, both pre-scan and over-scan regions have 32 pixels in size (Figure 9). Each quadrant is characterized by its own RON, gain, and bias level.

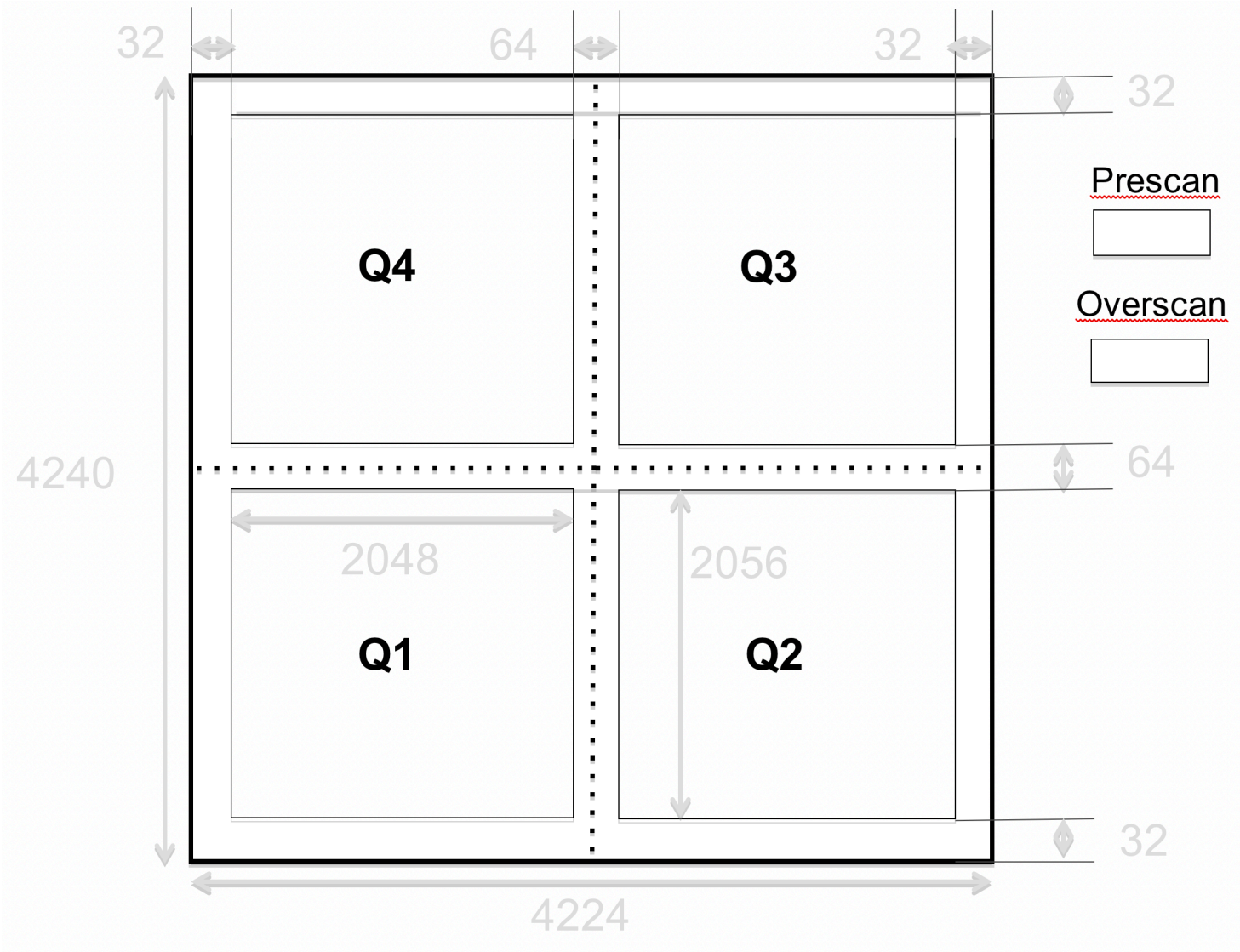


Figure 9: *Overview of the pixel map of one of the detectors, showing the 4 quadrants and the pre-scan / over-scan regions. All scales are given in pixels.*

2.1.2.5 Spectral format

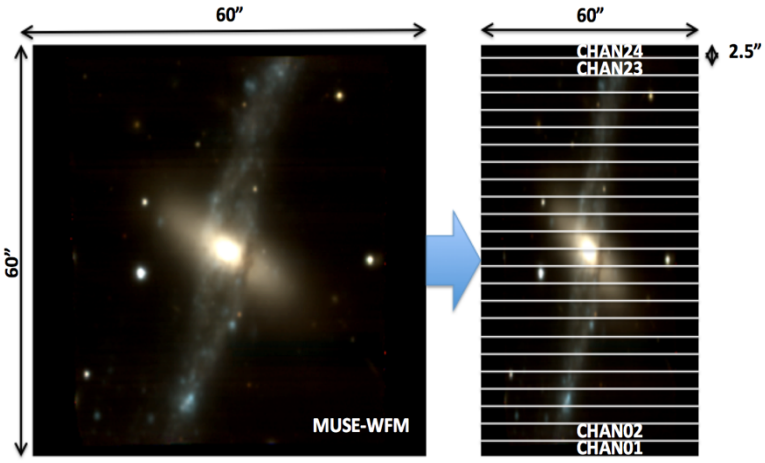
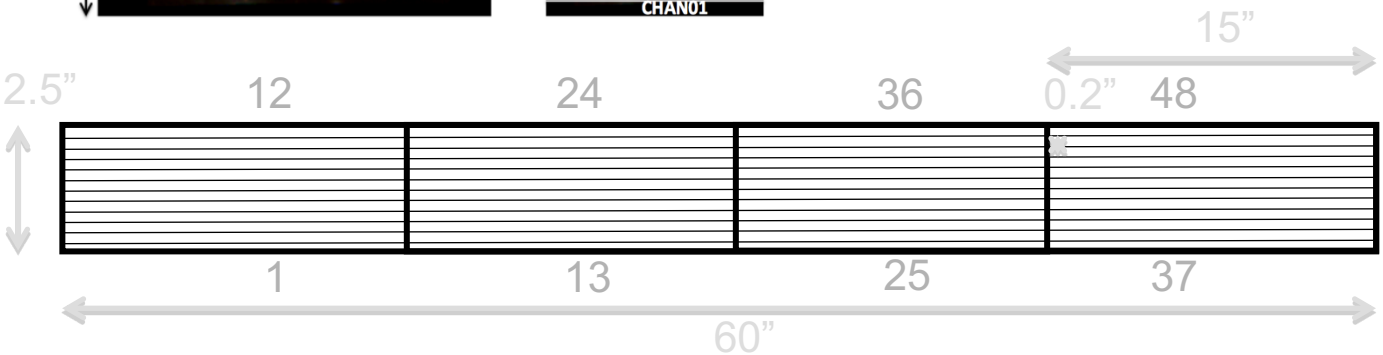


Figure 10: *Overview of the splitting of the field-of-view from the fore-optics to one of the MUSE detectors. Left: splitting of the MUSE FOV into 24 sub-fields entering each channel. Center: shape of the entrance slicer on sky, with 4 stacks of 12 slices (numbered in grey from 1 to 48) covering a 2.5” x 60” field. Bottom: location of each slice on the detector, with the corresponding wavelength range.*



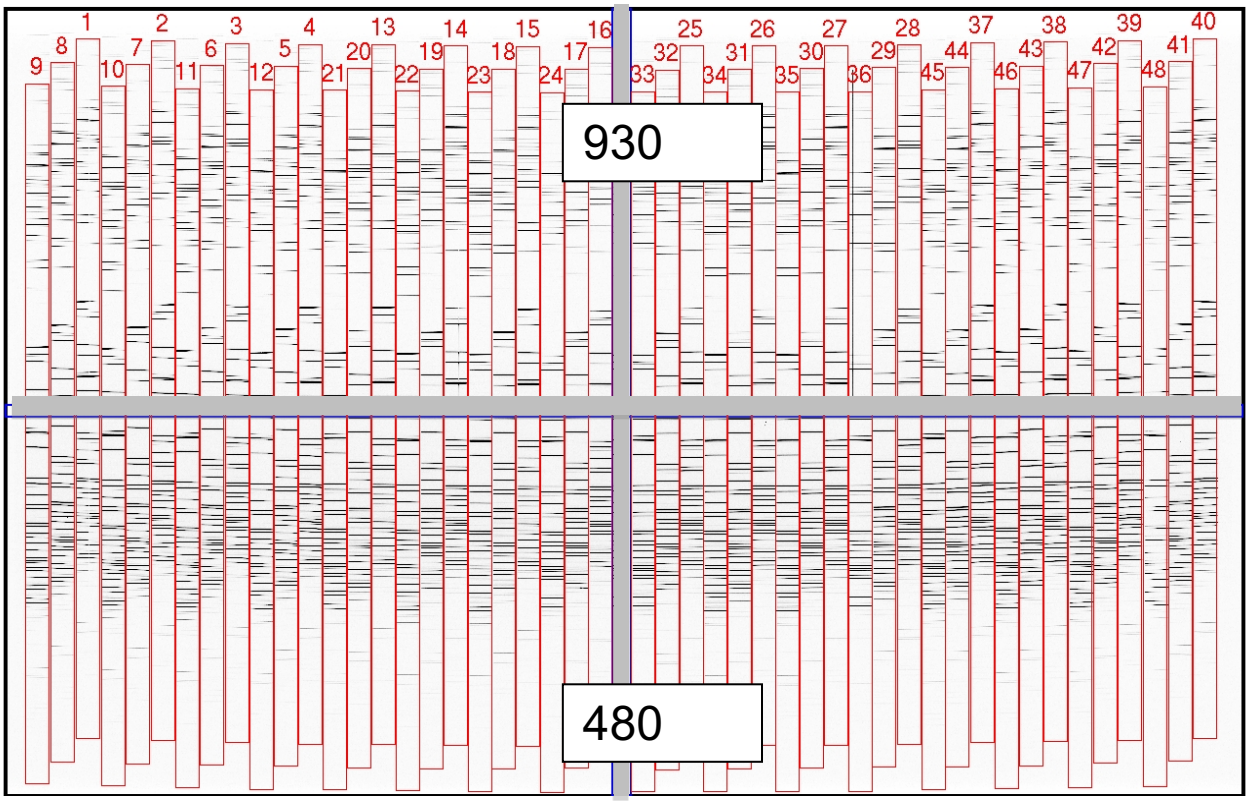


Figure 10 gives an overview of the spectral format as seen on one of the detectors, and the relationship with the splitting and slicing of the field of view in the sky frame, when used in WFM. The spectral format is identical in NFM, except that the field-of-view is 7.5” x 7.5”. After splitting the magnified FOV into 24 sub-fields entering each of the 24 IFUs (top-left panel), the image slicer separates a sub-field into 48 slices (middle panel) and aligns them along the horizontal axis of the detector (bottom panel). The numbers 1-48 show the relationship between the image slicer mapping and the CCD mapping. Each slice is ~ 75 pixels wide and dispersed in the spectrograph along the vertical axis of the CCD, with the bluest wavelengths located at the bottom of the detector and the reddest wavelength at the top. The 48 slices are offset vertically from one another by ~ 125 pixels, following a repeating pattern of 3 slices.

2.2 Technical Description of GALACSI and the AOF

2.2.1 Overview of the Adaptive Optics Facility (AOF)

The ESO Adaptive Optics Facility consists in an evolution of the ESO VLT UT4 (Yepun) to a laser driven adaptive telescope with a Deformable Secondary Mirror (DSM) and four Laser Guide Stars (4LGSF). In addition, two Adaptive Optics wavefront sensing modules have been developed: GALACSI for MUSE described in this manual and GRAAL for HAWK-I.

2.2.1.1 The Deformable Secondary Mirror (DSM)

The DSM is the heart of the new facility. The design and manufacturing were done by Microgate and ADS (Italy). It implements all the VLT required functionalities plus the needed adaptive optics functions. 1170 force actuators are used to modify the shape of a 1.95 mm thick Zerodur thin shell (see Figure 12). Voice coils are attached to a cold plate that serves two functions: mechanical holding systems for the actuators and heat evacuation. The cold plate is also supporting the reference body: this piece of optics, made of Zerodur, is used as an optical reference and is facing the thin shell rear surface with a gap of almost 100 microns in between. Magnets are glued onto the thin shell applying the deformation when the voice coils produce a magnetic field. Metallic coatings deposited on the reference body and collocated on the thin shell form 1170 capacitive sensors that are used in an internal control loop to maintain the mirror at the proper shape. A picture of the full DSM assembly is shown in Figure 11.

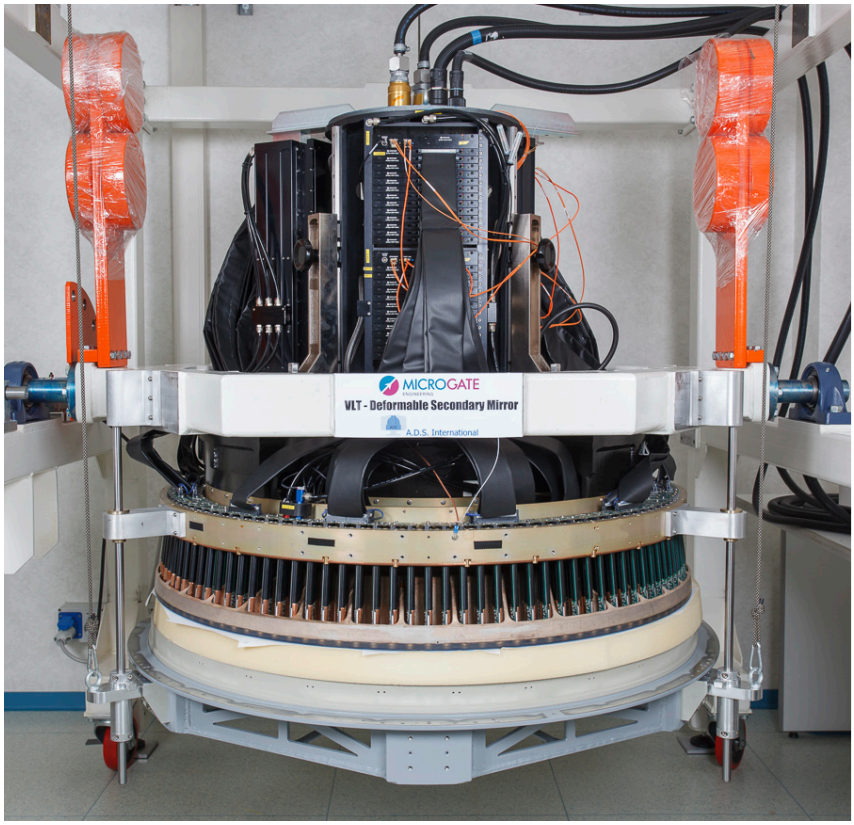


Figure 11: *The Deformable Secondary Mirror on its test stand before shipping to Paranal.*

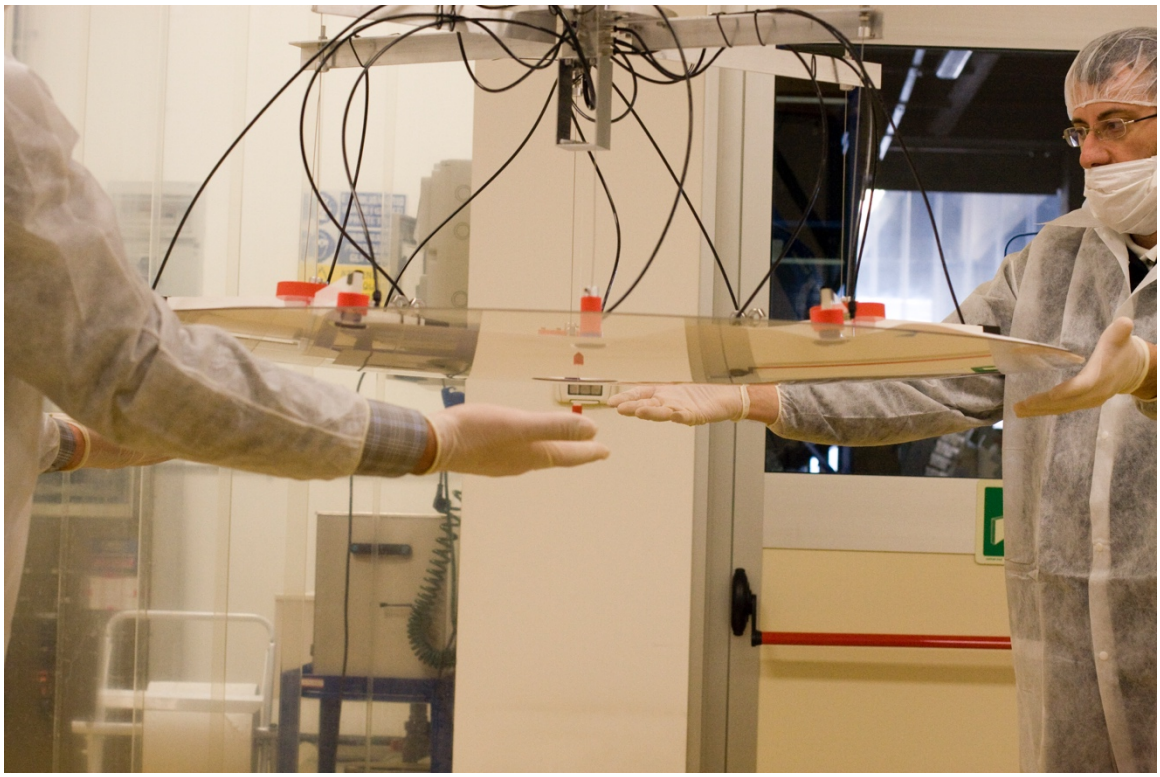


Figure 12: *careful handling of the DSM 1.95mm thin shell during manufacturing.*

2.2.1.2 The Four Laser Guide Star Facility (4LGSF)

Attached to the main structure of the telescope itself, the Four Laser Guide Star Facility (4LGSF, see Figure 13) provides all required hardware and software to launch the laser beams in the atmosphere. Each of the four laser units provides a 20 W beam launched through a 40 cm telescope. The laser design is based on a Raman Fiber Amplifier (RFA) technology first developed at ESO and subsequent frequency doubling realized by a Second Harmonic Generation resonant cavity. The laser also generates the Na D_{2a} and D_{2b} lines to promote back-pumping of the Na atoms and thus maintaining an efficient return flux for the wavefront sensors. Systems are compact and the lasers, plus beam diagnostic and launch telescopes are mounted directly on the telescope Center-Piece. The launch telescopes are x20 athermal beam expanders including only 2 single lenses with, in between, a 45deg steering mirror that can be tilted to point the beam at the appropriate location in a ±6 arcmin field-of-view. At the entrance of each launch telescope, a fast tip-tilt mirror controlled at 1 kHz is used to correct for laser jitter. The 4LGSF also includes an aircraft avoidance system and interlocks to ensure a safe operation of the system.

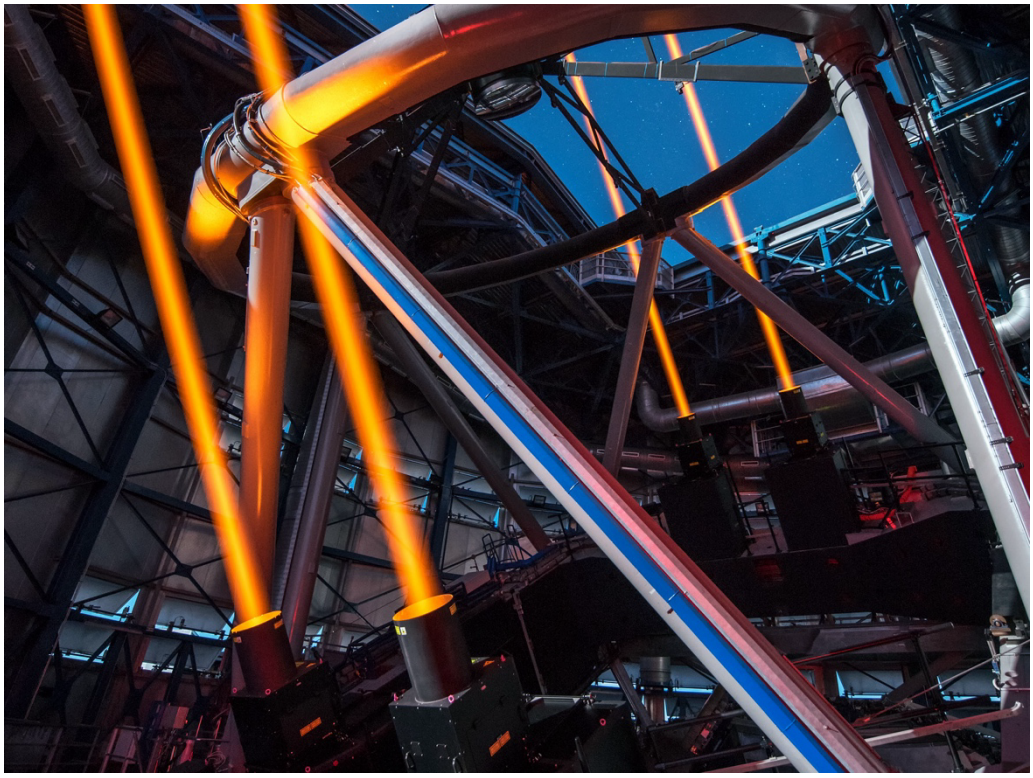


Figure 13: *the 4LGSF in action*

2.2.2 Overview of GALACSI's Wide Field Mode

The aim of the GLAO correction in WFM is to increase the ensquared energy (EE) within MUSE spatial pixels homogenously over the whole MUSE WFM field-of-view. In this mode, the four LGS are located at 64" off-axis i.e. outside the scientific field of MUSE. The visible Tip-Tilt natural guide Star (TTS) is located within a 3.5' technical field-of-view but outside the 1' field-of-view of MUSE. The scientific beam path is not affected by any of the optical components within GALACSI (i.e. scientific beam simply goes through GALACSI).

The separation of the technical light path from the scientific beam path is done with an annular mirror located near the Nasmyth focal plane. It lets the central 1.4 arcmin of the field pass through towards MUSE and reflects the technical light towards a Sodium (Na) Dichroic which reflects the laser light and transmits the Tip-Tilt star patrol field.

The tip-tilt patrol field is then collimated by a three-element lens. A field selector located on the pupil image given by this lens group, can pick up a star on a 3.5 arc min field of view and sends it towards the guiding detector through an objective.

The reflected LGS light is sent to the focus compensator, and a telecentricity lens. A reflecting pyramid sends then the four LGS beams towards their respective wavefront sensor paths. Each of them consists of a pupil re-imaging lens, a jitter actuator, and an additional pupil relay to create the pupil on the wavefront sensor lenslet array.

The LGS wavefront sensors measure the turbulence in each of the four directions. The beam overlap depends on the turbulence layer height and is largest for the Ground Layer. The reconstructor estimates the deformable mirror commands for each wavefront sensor and averages them before being applied to the ground conjugated DSM. The averaging of the DSM commands from each wavefront sensor implies that only the correlated part of the wavefront error is corrected, corresponding to the Ground Layer turbulence.
A sketch of the optical layout in WFM is presented in Figure 14.

Note that it is possible to observe in WFM-AO mode without a tip-tilt star. To do this just set the Boolean parameter SEQ.AO.TTS to F. Although the mode is not well characterized it has been seen to provide some improvement (see Fig. 12 of Hartke et al. (2020) SPIE).

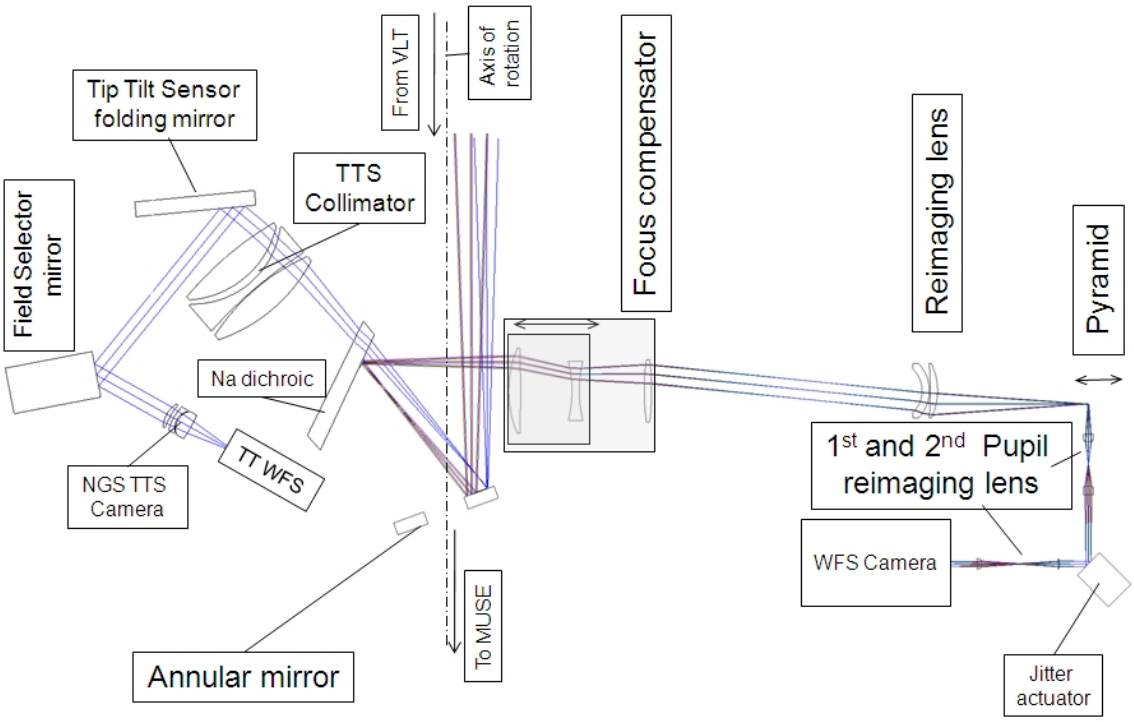


Figure 14: *GALACSI WFM layout of the optical paths to the tip-tilt sensor and to one of the LGS wavefront sensor. The MUSE science beam runs unaffected along the axis of rotation.*

2.2.3 Overview of GALACSI's Narrow Field Mode

The aim of the LTAO correction in NFM is to provide near diffraction limited images over the 7.5"x7.5" MUSE NFM field-of-view. In this mode, the four LGS are launched at 10" off-axis and the laser beams overlap with the scientific field of MUSE. The separation of the laser light from the scientific beam path is done with a dichroic located inside GALACSI near the Nasmyth focal plane.

In NFM, the reference TTS star is sometimes referred to as On-axis Guide Star, OGS. It serves more than just tip-tilt sensing and also is used to correct for defocusing. To distinguish it from the WFM TTS which is done off-axis, we will call it Natural Guide Star, or NGS. NGS sensing is done in the near-IR by the IRLOS (described in 2.1.2.2) on a source located within a 3.35" radius from the MUSE NFM field centre when using an extended source (SEQ.NGS.EXTENDED=T) as IRLOS NGS star, and 5.00" when using a point source (SEQ.NGS.EXTENDED=F) as IRLOS NGS. The separation between the science light and the NGS is done with a dichroic mirror in the MUSE fore-optics (see section 2.1.2.2 and Figure 3).

The LGS wavefront sensors measure the turbulence in each of the four directions. The reconstructor optimizes the correction on axis by estimating the turbulence in a volume via a tomographic process, then projecting the turbulence profile onto a single deformable

mirror in the pupil close to the ground, the DSM (for details on the tomographic reconstruction, see Oberti et al. 2016, SPIE Vol. 9909, p 20).

2.2.3.1 The upgraded Infrared-Low-Order wavefront sensor

During March 2021, IRLOS was retrofitted with a new SAPHIRA Mark2b detector, 320x256 pix e-APD array, capable of sub-electron readout-noise (RON). This new detector can be readout with a frequency of 500 Hz making it able to correct faster turbulence. The pixel scales are 0.078”/pixel for point sources (SEQ.NGS.EXTENDED=F) and 0.314”/pixel for extended sources (SEQ.NGS.EXTENDED=T). Although the user only needs to specify the J-band magnitude of the IRLOS reference star, or NGS star, we provide below some details of the modes used by IRLOS. Prior to the upgrade the NGS needed to be brighter than magnitude H=15. After the upgrade a first commissioning was carried out and the system was able to go 2 magnitudes fainter down to J=17 starting April 1st 2021.

Although the IRLOS bandpass is similar to a J+H band, the upgraded IRLOS requires the J-band magnitude (2MASS) of the NGS star to be specified (previously the system required the H magnitude). The predicted performance for stars with spectral types between A0V and M5V was estimated to be less dependent on the colour of the star if J magnitudes were used. Simulations showed that for a magnitude J=15 A0V star the system, when readout at 500 Hz, and assuming a wave-front error of 120 nm rms HO loop, would detect around 173 photoelectrons/readout within the FWHM of the PSF core, which would result on 43.25 photoelectrons/readout per sub-aperture (of the 2x2 SH). Therefore, at J=17 the system is working with approx. 6.8 photoelectrons/readout per sub-aperture.

A second commissioning of the new IRLOS system was carried out during July 12- 18, 2021. After this commissioning a new faint mode of operation, which increases the detector gain and decreases the readout frequency from 500 Hz down to 200 Hz, was introduced that permits the use of stars as faint as J=19 with some of the best conditions (10% turbulence category) for a short period of time. The system can close the loop with approximately 2.7 photoelectrons/readout per sub-aperture. In the recent science operation and technical activities, we did find that the near-IR color and object type (star vs quasar) can affect the IRLOS ability to close the loop at the limiting magnitude J-19. Starting with Phase 1 for P112 reference objects with J < 18.0 are accepted for turbulence categories <= 50%; for turbulence category of 10% and airmasses below 1.2 this can be increased up to J<18.5.

It should be noted that with the pre-upgrade IRLOS the 2MASS catalogue was perfectly adequate for searching for feasible NGS stars as this catalogue had completeness limits of J=15.8, H=15.1. The situation is more complex now that the system can operate down to fainter magnitudes. During commissioning we used the VIKING catalogue[2], but not being an all-sky catalogue, it cannot be used for general feasibility assessment of candidate NGS stars. The following relation between J magnitude and the Gaia magnitudes using the VIKING and Gaia catalogues

[2] https://www.eso.org/qi/

$$J = G + 0.019 - 2.221 \times (G-G_RP) - 0.108 \times (G-G_RP)^2$$

This relation has been implemented to the ObsPrep in P2. Please use the predicted J magnitude with caution, if the NGS is a non-stellar object, such as a quasar.

Work was also done to improve functionality at the bright end with an automatic and transparent process. A waiver is still required for stars brighter than J=7, but as can be seen in Table 4, the bright end has been expanded considerably (but the full range not offered yet). *Caveat emptor*: bright star observations do suffer from several issues not completely characterized: AO performance penalty due to wider laser constellation results in one half the Strehl obtained under similar conditions with the nominal laser constellation; the overheads are large because at these magnitudes MUSE integration times must be kept short; internal reflections and other features such as the *Ferris Wheel* patterns are guaranteed to be present (then offset and rotated observations are recommended to be able to identify and mitigate them), see Sec. 3.9.1, Figure 22. Therefore, observations will be carried out in shared risk mode requiring a waiver.

After the IRLOS upgrade there was a small decentering of the optics and the field selector ranges in different directions are not the same, forcing a reduction of the maximum NGS off-axis distance from 5.90" to 5.00".

Table 4 IRLOS modes as of 19 July, 2021. Note that the 4LGSF column indicates the laser asterism: wide or normal. For P109 all orange and green modes can be requested, orange mode with waiver.

J-band	Name AOS MAIN MODES IRLOS	4LGSF	gain	Freq.	Filter
Small scale: pix: 78 mas, FoV 20 pix x 20 pix – 1.56" x 1.56"					
0.5..3.5	20x20_SmallScale_500Hz_LowGain	W	1	496	1600BW20nm
3.5..5.5	20x20_SmallScale_500Hz_LowGain	W	1	496	1600BW190nm
5.5..7.0	20x20_SmallScale_500Hz_LowGain	W	1	496	CLEAR
7.0..10.5	20x20_SmallScale_500Hz_LowGain	N	1	496	CLEAR
10.5..16.0	20x20_SmallScale_500Hz_HighGain	N	68	496	CLEAR
16.0..18.5	20x20_SmallScale_200Hz_HighGain	N	100	200	CLEAR_8as or CLEAR[1]
Large scale: pix: 314 mas, FoV 20 pix x 20 pix -- 6.28" x 6.28"					
7..10.5	20x20_LargeScale_200Hz_LowGain	N	1	200	CLEAR
10.5..17	20x20_LargeScale_200Hz_HighGain	N	68	200	CLEAR

[1] For these fainter modes a field stop with 8" diameter is inserted to reduce background contamination. If the OB performs offsets that brings the field selector beyond a radius of 4", then this field-stop must be removed. This should be clearly indicated in the README file.

The performance of the fainter mode, 16..18.5, has not been extensively characterized yet. The preliminary estimates from commissioning show AO performance to be quite flat down to the faintest magnitudes and then rapidly degrading. Furthermore, the operational robustness has not been tested under a wide variety of turbulence

conditions. Users should stay tuned for news in the MUSE web pages for updates on performance and the exact modes offered.

Page left intentionally almost blank

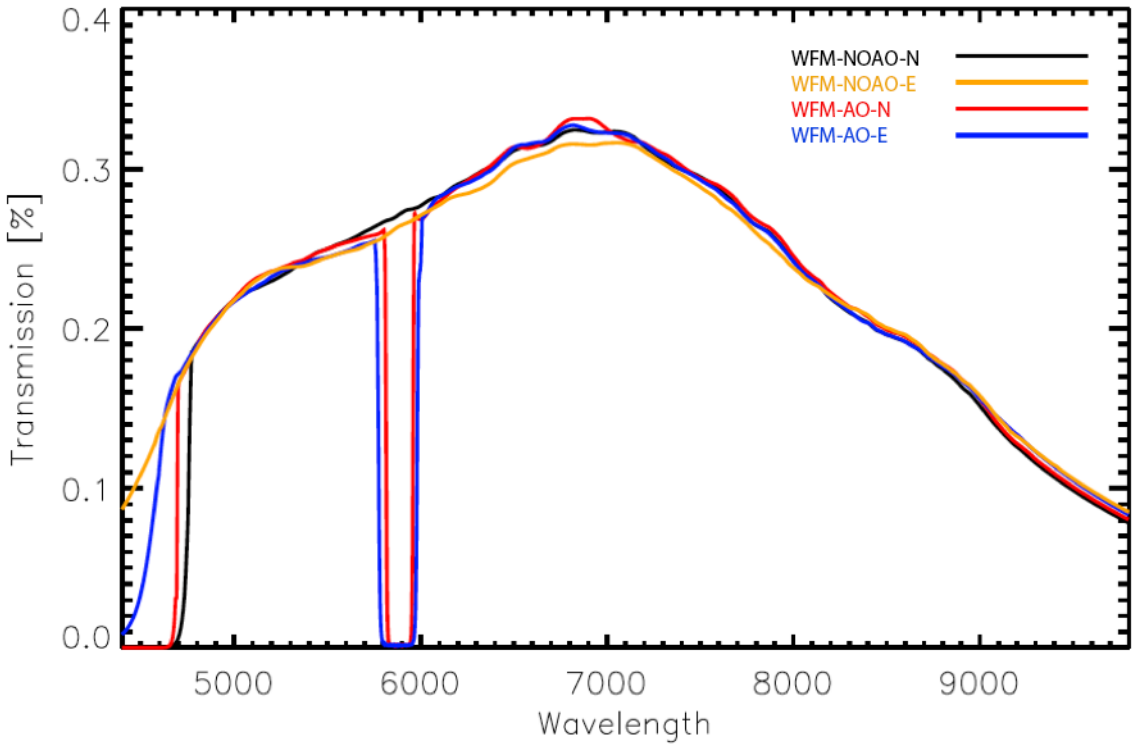


Figure 15 End-to-end MUSE+VLT/UT4 throughput in WFM, as derived from spectroscopic standard star observations. The blue cutoffs of the extended modes in this graph are affected by smoothing and extrapolation effects and should not be relied upon.

3 Overall MUSE performances and characteristics

3.1 Absolute throughput and limiting magnitude

The absolute throughput of the overall system (MUSE+UT4) has been measured by observing spectrophotometric standard stars during commissioning. The throughput in both WFM-NOAO and WFM-AO modes peaks at a high value >30% around 700 nm and is overall > 15% (Figure 15 and Figure 16). At shorter wavelengths, the throughput in the nominal mode (WFM-NOAO-N and WFM-AO-N) drops around 480 nm, while the extended mode gives a high throughput down to 465 nm. Due to the additional optics required for the NFM, the throughput in this mode is ~80% that of the WFM (see Figure 16). Note that in the AO modes, the wavelength around the NaD lines is blocked to avoid contamination and saturation of the detector by the strong laser light.

We have used this measured efficiency curve to predict the performances of the instrument in spectral continuum observations. We are assuming a 1 hour observation of a

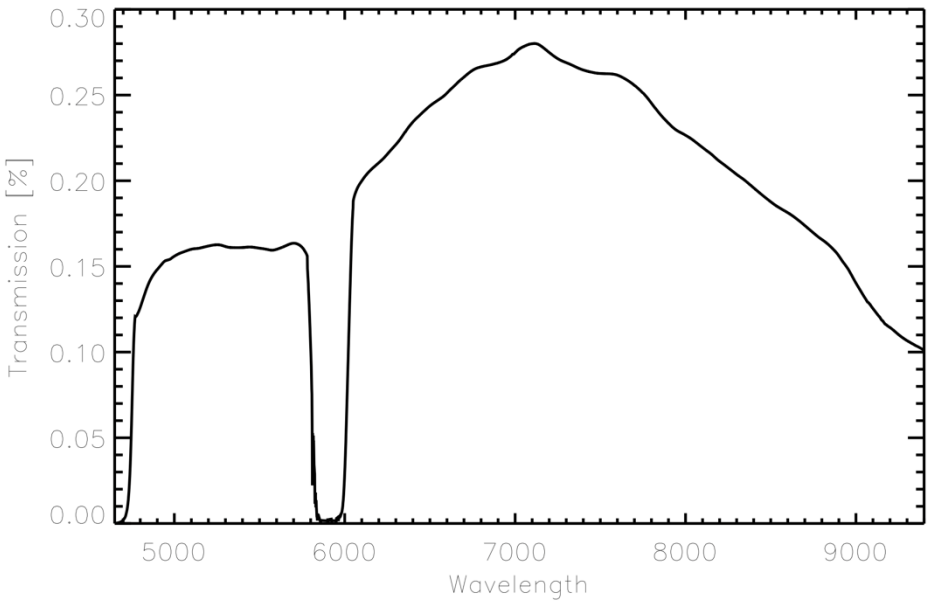


Figure 16: *End-to-end MUSE+VLT/UT4 throughput in NFM, as derived from spectroscopic standard observations.*

point source at airmass = 1.0 and a seeing of 0.8" in V-band. The limiting magnitude at S/N=10 per spectral resolution element, in regions free of sky lines, is reached for the following AB magnitudes (Table 5).

Filter	Wavelength	AB mag (S/N=10)
V band	550 nm	22.64
R band	640 nm	22.70
I band	784.9 nm	22.28

Table 5: Limiting magnitudes of MUSE WFM per spectral resolution element.

Similar results for different sources/conditions, as well as more detailed performances, can be obtained using the dedicated Exposure Time Calculator available on the ESO website: http://www.eso.org/observing/etc/bin/gen/form?INS.MODE=swspectr+INS.NAME=MUSE

If the spectral region of interest is the very blue part of the extended mode users should be careful with the throughput curves in Figure 15 or the throughput curves in the ETC as the smoothing applied can affect the edges of the spectral range. To help users with a decision we have determined the relative throughput, using the same standard star, and extracting the spectrum from the slitlet that reaches most to the blue in both WFM-NOAO-E and WFM-AO-E. The result is presented in Figure 17.

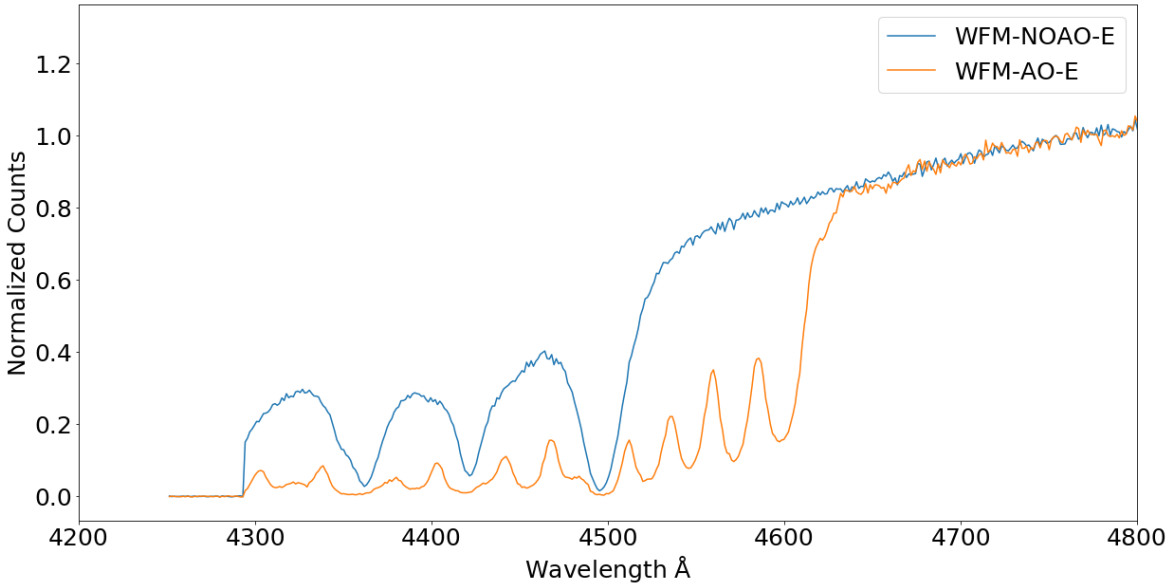
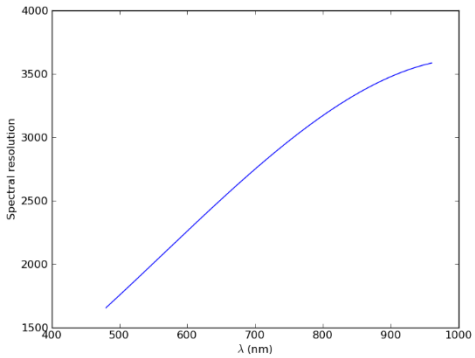


Figure 17 Relative throughput of the extended modes measured placing the standard star in a slitlet that reaches most to the blue.

3.2 Spectral resolution and sampling

In all instrument modes, the spectral resolution increases from 1609 at the bluest wavelengths (465 nm) to 3506 at the reddest wavelengths (935 nm). This was measured on wavelength calibration data (Figure 18). Each resolution element is sampled by 2.5 pixels along the spectral direction. Note that in contrast to a slit spectrograph the spectral resolution of MUSE does not depend on seeing.



λ	R	Range[1]
4650.0	1609 ± 6	
5000.0	1750 ± 4	1680 -> 1813
5500.0	1978 ± 6	
6000.0	2227 ± 6	2132 -> 2330
6500.0	2484 ± 5	
7000.0	2737 ± 4	2658 -> 2824
7500.0	2975 ± 4	
8000.0	3183 ± 4	3126 -> 3284
8500.0	3350 ± 4	
9000.0	3465 ± 5	3211 -> 3589
9350.0	3506 ± 10	

Figure 18: *Spectral resolution, R = λ/Δλ, as a function of wavelength, as measured in the lab using calibration lamps. [1]Range over channels. From Technical Note ESO-318117.*

3.3 Exposure timing

The performances of the Bonn[3] shutter have been estimated to provide an error < 300 μs on the total exposure time. In addition, and due to the shutter mechanisms, variations in the exposure time across the FOV are possible but have been estimated to be < 1ms over the entire FOV. Recent measurements estimate the shutter delay at approximately 7.0 – 7.5 ms, that is, to every exposure you should add 7ms to the value in EXPTIME header keyword to get the actual exposure time.

3.4 Overall illumination and uniformity

There are several factors that are decreasing the MUSE throughput in some specific locations within the FOV. The first factor is the Field Splitter: the gap between the Field Splitter lenses causes a small light loss that affects the 4 slices at the bottom and the 4 slices at the top for each channel. The gap is smaller than 50μm for a spaxel size of 580μm, so the light loss is lower than 8.3% for these channels. The effect is visible as horizontal regions of lower illumination in a continuum flat-field image (Figure 19).
The second factor is the gap between the 4 stacks of 12 slices in each channel that is 20μm for spaxel size of 465μm in this direction. The 4.3% of light loss affects only the spaxels at the edges of the slices and is visible as vertical regions of lower illumination in the continuum flat-field image (Figure 19).
Finally, there is the geometrical shadowing of some slices by the neighbouring slices at the slicer level. In the worst case, there is 7% of light loss. But integrated over the entire slicer stacks, the light loss is only 0.4% per channel.
Very high SNR flat-field exposures obtained in the laboratory have been used to characterize the global illumination as a function of position (Figure 19). The median flux value is used as a reference to measure the flat-field variations. The main characteristics are the following:

- The small vertical distortion is visible as the global trapezoidal shape of the FOV: slices from the top channel have a larger horizontal extent than the bottom channel.
- In general, the flat-field is quite uniform, with variations of ±2% within a given channel / stack.
- At the top/bottom edges of each channel, a horizontal drop of ~ 10% in illumination due to the field splitter vignetting.
- In between the 4 stacks in each channel, there is a vertical drop of ~ 30% in illumination due to the inter-stack vignetting
- A small flux variation (~2-3%) is visible between the central 2 stacks and the leftmost and rightmost stacks. This is predicted by design.

[3] Bonn shutters are travelling slit type shutters characterized by high exposure uniformity across the aperture. For more info see http://www.bonn-shutter.de

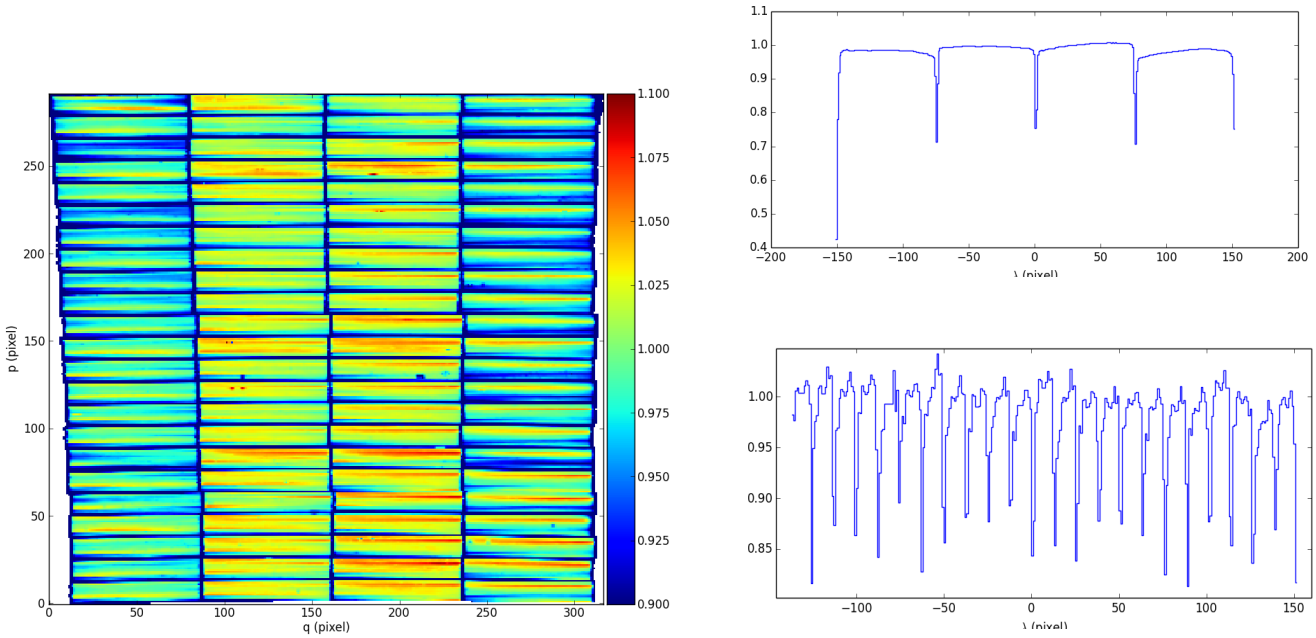


Figure 19: *(left) normalized reconstructed image of the continuum flat-field in WFM. (right) horizontal (top) and vertical (bottom) cuts through the normalized image showing the horizontal and vertical variations in illumination.*

3.5 Distortion and astrometric precision

The instrument distortion is calibrated by using a regular multi-pinhole mask as part of the overall calibration plan (see Table 17). The overall FOV of the instrument shows a trapezoidal shape (Figure 19), with channel 01 having a 3.5” smaller angular view in the horizontal direction. The MUSE astrometric precision is calibrated/monitored on a regular basis by observing stellar cluster fields that have HST data of high astrometric quality. The astrometric solution has been obtained during commissioning on these fields with an overall rms precision of 0.04” in each direction in WFM.

3.6 NFM ADC performance

In NFM there is an ADC in the path of light, common to the MUSE science field and IRLOS, which has been specified to give a maximum residual of 10 pix (i.e., 250 mas) over the whole MUSE wavelength range. During commissioning we have measured 2 pixels (i.e., 50 mas) residual dispersion between 480 – 930 nm. Most of the residual dispersion becomes noticeable bluer than 500 nm. In an observation taken on 2019-12-04 (MUSE.2019-12-04T01:33:06.866.fits) at airmass 1.71 we get a total shift of 3.6 pixels from 930 nm to 480 nm with a wavelength dependence as follow: from 900 nm to 600 nm the centroid shift is +0.3 pix; from 600 nm to 500 nm the centroid shift is -2.2 pix; and from 500 nm to 480 nm the centroid shift is -1.1 pix (signs to be consistent with Figure 20).

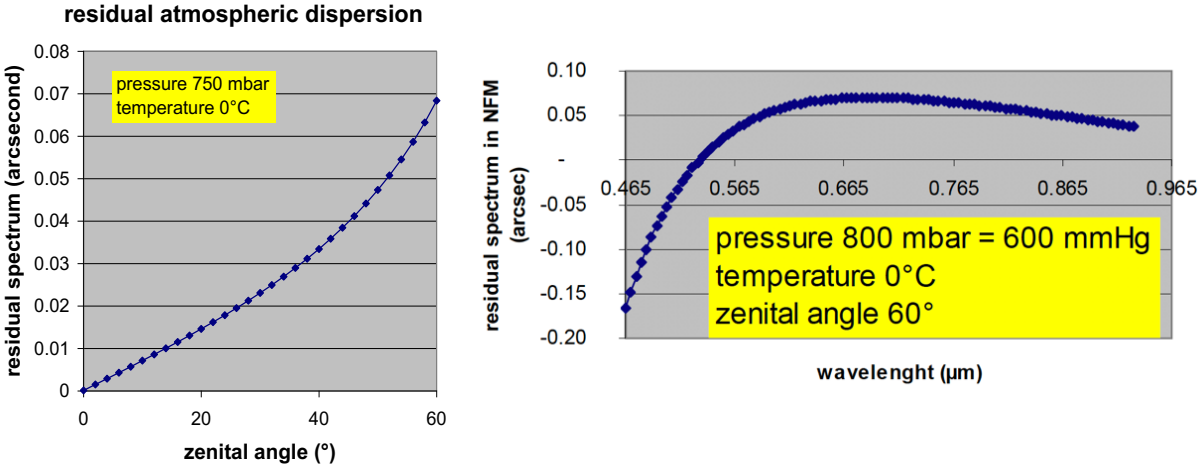


Figure 20: Expected ADC performance

3.7 Second order contamination

In the nominal wavelength range (i.e. using the cut-off blue filter at 480 nm), the second orders appear, as expected, above the 930 nm wavelength limits (as shown as the red boxes in Figure 21). One can nevertheless see a faint contamination in the 920-930 nm region. In addition, the second orders are defocused and therefore extend beyond the slice. Because of their 3 steps pattern, the slices extending higher on the detector are impacted by the adjacent second orders. The impact is nevertheless very limited.

In the extended mode (i.e. without any blocking filter), the impact of second orders is significant and starts already at 790 nm. The contamination reaches levels of ~12% at wavelengths redder than 850 nm.

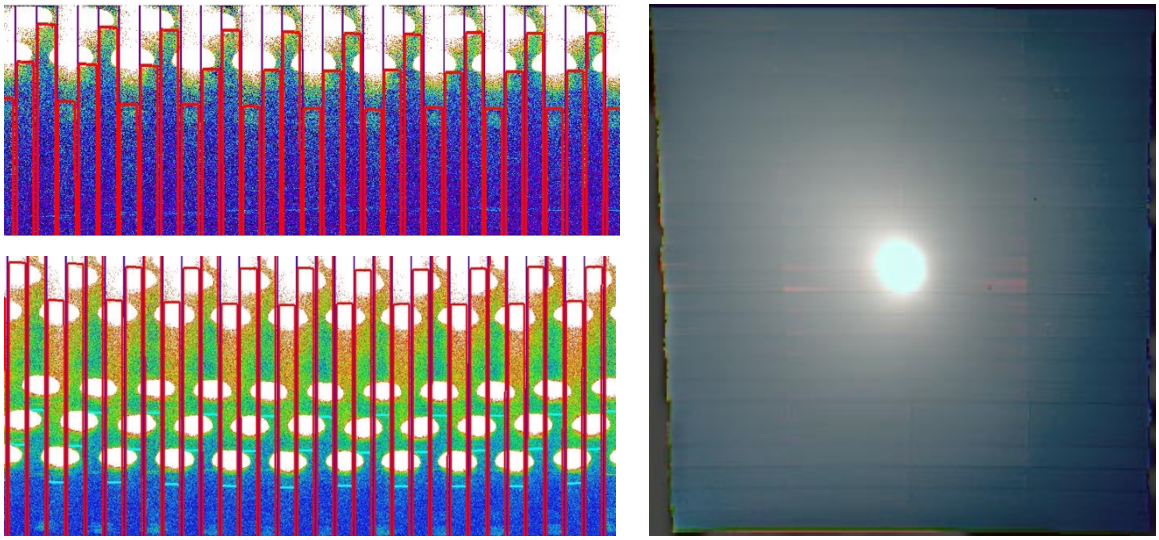


Figure 21: *Left, second order effect in nominal (top panel) and extended (bottom panel) modes, shown here for a bright exposure with arc lines. The red boxes mark the slice limits up to 930 nm. The impact of second order is visible as the white ellipses illuminating the top of the detector. The nominal instrument mode is not much affected by contamination, but it is more significant in the extended instrument mode. Right, second order contamination as it appears in the reconstructed image of a comet: the RGB image has been created using the red end, the center, and the blue end for the RGB channels. The second order contamination is visible as the non-uniform redder slices where the out of focus bright comet light in the blue contaminates the red end of the spectrum.*

3.8 Instrument stability

Two kinds of instabilities have been observed. The first one affects the detector system in the form of varying bias structure, difficult to subtract. The second one is a temperature dependent flat-field effect. The former instability has been very much reduced by improving the detector hardware and the introduction of a new continuous clocking scheme introduced after 19 July 2015. The latter has been addressed by the use of illumination frames taken several times during the night.
The long-term stability of the instrument is still being monitored, and the details in this section will be updated continuously with new findings.

Wobble:

The MUSE derotator produces a residual mechanical wobble, which produces a repeatable pattern as a function of the derotator position. When the instrument is used in WFM, the effect of this wobble will be compensated by the SGS.
When the SGS is not available (e.g., no suitable stars in the metrology fields), the impact of this wobble was estimated for the worst case of a 1 hour observation of a target close to the zenith (4 deg. Zenithal distance). We can reach a total displacement of 0.28”, which has an impact of 10% on image quality in good observing conditions (0.6” seeing). In most cases, the impact will be much smaller.

Thermal stability:

MUSE has been submitted to thermal tests in the lab to assess its stability with regards to the ambient temperature. The resulting displacements in the spatial and spectral directions are provided in the Tables below. To predict the effect of temperature changes on observations we have used the Paranal statistics that give the median and peak temperature variation (ΔT) for various periods (1 hour, 1 night, 1 season, see left columns in Table 6 and Table 7).
The stronger impact appears in the wavelength direction. During a one-hour exposure, the inferred motion is still small (<0.05 resolution element) and the impact on the LSF is negligible: e.g. assuming a Gaussian shape its FWHM will increase by a maximum of $(1+0.03^2)^{1/2}$ = 1.0004, i.e. 0.04%. Across one night, the offset is larger and can reach 0.4 Å. However, it is always possible to use bright sky emission lines to correct for this offset. This is currently implemented in the sky subtraction pipeline recipe

Table 6: *Thermal stability in the spatial direction.*

Conditions	Maximum offset in spaxel
1 hour median ΔT (0.5 °C)	0.01
1 hour peak ΔT (1.5 °C)	0.03

Table 7: *Thermal stability in the spectral direction.*

Conditions	Maximum offset in Å	Maximum offset in resolution element
1 hour median ΔT (0.5 °C)	0.06	0.03
1 hour peak ΔT (1.5 °C)	0.19	0.08
1 night median ΔT (3.2 °C)	0.42	0.17
1 night peak ΔT (6.0 °C)	0.78	0.31
Seasonal median ΔT (7.0 °C)	0.91	0.36
Seasonal peak ΔT (20.0 °C)	2.60	1.04

3.9 Problems to be aware of

3.9.1 Ghosts, straylight, spikes and Ferris wheels

Ghosts: a ghost analysis has been performed on the detectors when illuminating the slices with bright saturated emission lines. The only detected ghosts have been observed at a very low level (<0.001%).

Straylight: similarly, contaminating straylight appears at a very low level (< 10^{-5}) when illuminating a channel with a very bright light source. This effect is seen at the level of the detector, with a background affecting the neighbouring slices.

Ferris Wheels: Observing close to bright sources with MUSE leads to the presence of strong artefacts within the datacube in the form of concentric rings and fainter spokes, similar to a Ferris Wheel. Typically, these effects become obvious when observing within a few arcminutes of a bright source, e.g. V < 6. Figure 22 shows one of these artifacts near the star Sirius. It has been observed that sometimes changing telescope guide star or observing at a different hour angle can eliminate the effect.
Analysis of all these issues is still preliminary at this stage and will be updated after a full analysis has been completed and the origin and solutions have been determined.

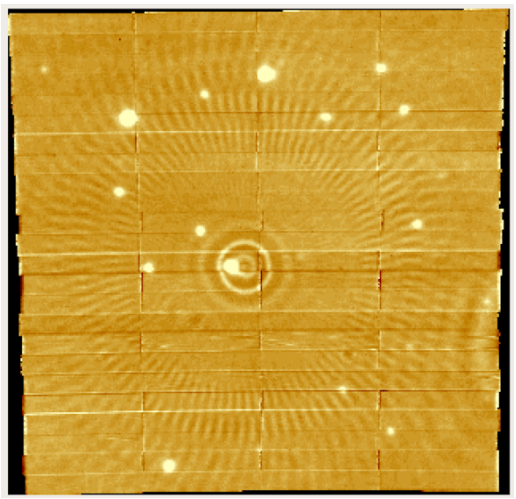


Figure 22: *Ferris Wheel on a field of stars near Sirius.*

3.9.2 Remanence

The remanence of the detectors has been measured by performing long dark exposures shortly after a saturated exposure. Remanence measured in these dark exposures is very low (0.04 ± 0.23 e-) and its effect can be ignored.

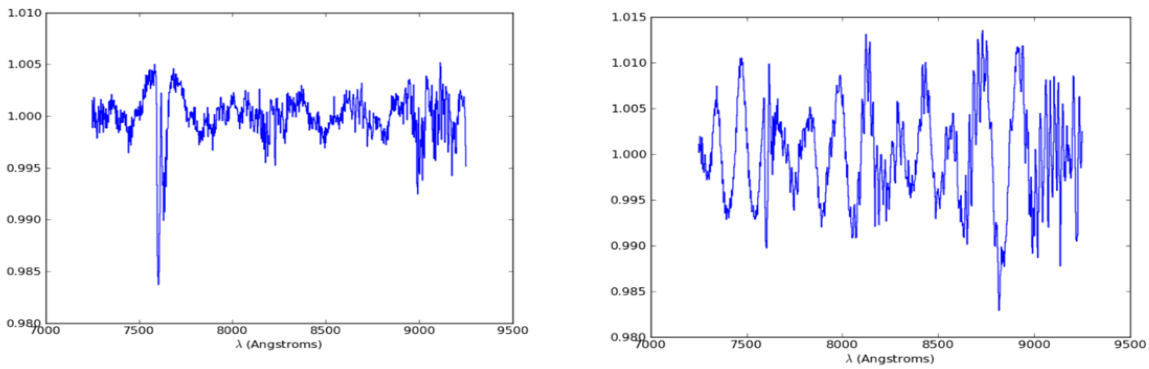


Figure 23: *Fringing in the red on normalised flat-fields. (left) WFM, (right) NFM.*

3.9.3 Detector defects

Fringing: The choice of detectors for MUSE keeps the effect of fringing to a very low level. Fringing is apparent on very high signal-to-noise flat-field exposures in the 750-870 nm wavelength range and is measured at a peak-to-peak level of 0.3% in WFM and 0.6% in NFM (Figure 23).

3.9.4 Bad columns/pixels

The MUSE detectors are generally of high quality, with only very limited regions of bad pixels. 17 out of the 24 detectors do not show any strong defect automatically flagged by the pipeline as a data quality (DQ) issue, and the remaining 7 detectors show between 1 and 3 bad columns. The full details of bad pixels flagged are given as reference for each detector in Table 19 in Section 8.1.

3.9.5 Regions of reduced sensitivity on flat fields

MUSE flat field images for all channels show regions of lower transmission of varying strengths, which is believed to be due to dust on the field splitter. These regions stretch the full length of the spectrum, and appear as small spots on the reconstructed flat fields, as shown in Figure 24



Figure 24: Dark features in the MUSE flat fields due to dust in the field splitter. Top: the regions of low transmission extend the full length of the spectrum. On the left is an N-mode flat and on the right is an E-mode flat. Bottom: the 'spots' of low transmission in a reconstructed datacube.

3.9.6 Faint sky lines in NFM

Calibrating science data using exclusively the arc frames taken during the morning calibrations results in a wavelength calibration accuracy no better than 0.4 Å in all MUSE modes. The wavelength calibration accuracy can be improved during pipeline processing measuring sky lines in the science frames if not too crowded, or in SKY frames if not too shallow. The wavelength shift that is determined from sky lines needs for its determination SKY frames with integration time above 150s, allowing wavelength calibration errors below 0.4 Å. The final accuracy that can be obtained depends in many other factors, but values around 0.1 Å or better have been reported.

3.9.7 Failure of the Atmospheric Dispersion Correctors in NFM

The atmospheric dispersion correctors, ADC, are used during NFM observations so that the centroid of objects does not change with wavelength. The ADC is vital for proper TTS handling because IRLOS uses a wide bandpass similar to a J+H-band. We have found out that in some occasions the ADCs can fail without raising an error condition, leading to exposures that can complete but which are affected by atmospheric dispersion. The telltale sign is that on reconstructed intermediate to wide pass-band images stars are elongated along the parallactic angle, as shown in Figure 25.

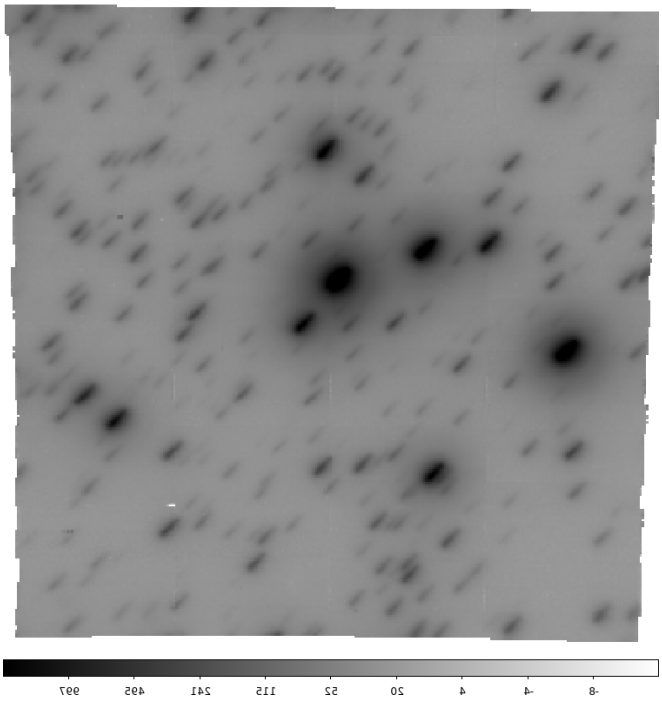


Figure 25: *Reconstructed Cousins I band image from a NFM cube obtained after the ADC failed.*

3.10 Performance reported in the literature

In this section a small survey of some performance reported in the literature is presented. It should be a quick guide to assess the potentialities of MUSE for different types of projects.

3.10.1 General data fidelity

The work by Weilbacher et al. 2015, A&A, 582, A114 is particularly valuable. They investigate the central region of the Orion nebula and report comparisons with previous literature values of different variables: coordinate system determination accuracy, spectro-photometric calibration, magnitudes and colours synthesized from the extracted flux calibrated spectra, derived velocities, absolute line fluxes and line ratios. The actual understanding of all effects affecting the data is quite complex and the readers are invited to study that source. We summarize below some of their findings:

- WCS: matching sources with the HST ACS catalogue of the Orion nebula (Robberto et al. 2013, ApJS, 207, 10) they find a mean and std. deviation of 0.163” ± 0.078”.
- Spectro-photometry: Comparison of reference spectrum with spectrum extracted from calibrated cube show deviation typically below 5%. This work is based on WFM-NOAO-E data so they dealt with 2nd order contamination extracting the spectrum with circular apertures for wavelength planes bluer than 8334 Å and a Moffat fit for redder planes.
- Synthetic photometry on the extracted spectra: Comparison of Johnson V band magnitudes of selected stars with previous photometry show a deviation of only 2%. The photometric comparison of the synthesized magnitudes in Cousins R and I filter show deviations of up to 0.18%. Another work, Castro et al. 2018, A&A, 614, A147, performs synthetic photometry on the extracted spectra in cubes of 30 Doradus and finds zero point offsets of 0.60 magnitudes in V. These deviations are currently under investigation.
- Velocities of emission lines: Figure 4 of Castro et al. (2018) provides a line by line comparison of determined velocities with prior published work. They produce two cubes, one with wavelength sampled at the standard 1.25 Å, and another at 0.85 Å sampling. They find for $\lambda < 5250$ Å an issue with the wavelength calibration of up to 0.1 Å. For $\lambda > 5250$ Å they report no systematic deviations larger than 3 km/s. To study the spatial characteristics of the velocity field traced by emission lines they strongly recommend the 0.85 Å sampling.
- Absolute fluxes of emission lines: Although Castro et al. (2018) find a few large deviations in the measured fluxes compared to the literature of up to 28%, more typical values range from 2 – 7%. They convincingly explain that most of the differences come from errors in the reported positions of the slits in the comparison work.

- Line ratios of emission lines: Using [O III]/Hβ, Hα/ Hβ, [S II]/ Hβ, and He I/Hβ Castro et al. (2018) find typical deviations of line ratios below 5%, with maximum deviations of up to 6.5%.

3.10.2 Stellar velocity determination from spectrum correlations

The determination of accurate velocities from stellar spectra has been reported by several investigator since MUSE started operations. We report here the work by Husser et al. A&A 588, A149 (2016) and Valenti et al. A&A 616, A83 (2018). Figure 26 shows measured and simulated errors for radial velocity determination from spectral fits to stellar absorption spectrum. The data of Husser at al. 2016 is inserted in the Valenti et al. 2018 plots. It appears that there is a limit around 2 km/s for very high signal to noise data.

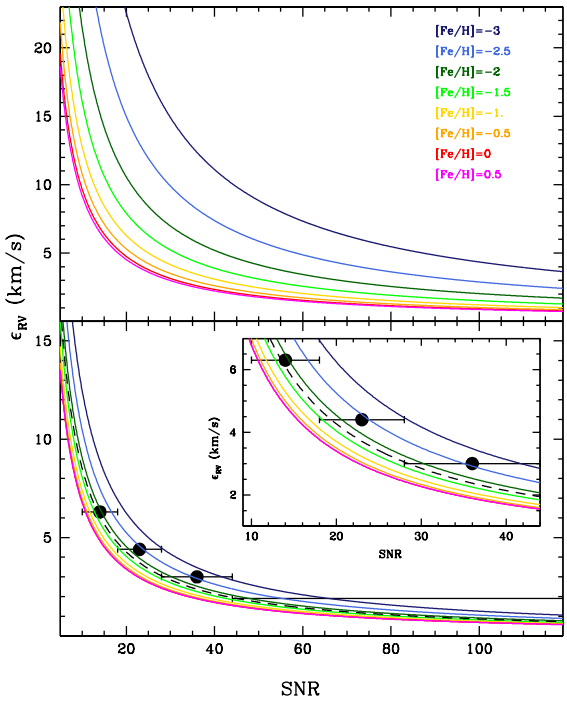


Figure 26. *Error in radial velocity determination versus S/N of the stellar spectrum, for dwarfs, upper plot, and giants, lower plot. The black dots represent the NGC6397 data of Husser et al. 2016, and the dashed black line corresponds to the Valenti et al. 2018 simulations for [Fe/H] = -1.75.*

3.10.3 How deep can MUSE go?

The reference observations to answer this question are the Hubble deep field observations by Bacon et al. 2017, A&A, 607, A. The state-of-the-art observation strategy and data reduction procedures described in that work permits to reach a 1σ emission line limit of 2.8×10^{-20} erg s^{-1} cm^{-2} $Å^{-1}$ $arcsec^{-2}$ for an aperture of 1"x1" in the 7000-8500 Å range after 31h on-source time. To achieve this, they use a self-calibration method described by Piqueras et al. to be published in proceedings ADASS XXVI, 2017 (arXiv:1710.03554), and the enhanced sky-subtraction software ZAP developed by Soto et al. 2016, MNRAS, 458, 3210.

4 AO modes performance

4.1 Maximum airmass of observation in AO mode

Due to the operational range of the deformable secondary mirror, the maximum allowed airmass for AO observations is 1.9. Optimal AO performance for NFM is obtained for low airmass values (<1.2), and redder wavelengths.

4.2 Image Quality Gain in WFM AO

Ground layer adaptive optics correction essentially acts like a seeing enhancer allowing for good to excellent image quality a larger fraction of the time. Note that this Ground Layer correction is by no means aimed at providing close to diffraction-limited images. By essence, the magnitude of the correction and the ability for the system to increase the energy in a spaxel highly depends on the turbulence profile of the atmosphere. The more the turbulence arises from layers close to the ground, the better the correction is. The target performance of GALACSI is to increase the energy ensquared in a 0.2”x0.2” spaxel of MUSE by a factor of two compared to natural seeing limited images when more than half of the turbulence is concentrated in the first 900m above the telescope.

The fraction of the time with a dominant ground layer turbulence is still poorly known, therefore we cannot yet provide image quality improvement statistics. Analysis of data from P101 and P102, shown in Figure 27, gives an idea of what can be achieved. A gain of 2 indicates that the FWHM measured in the reduced cube is half what we would expect from scaling the seeing to the airmass of the observation and the wavelength range indicated in the plot.

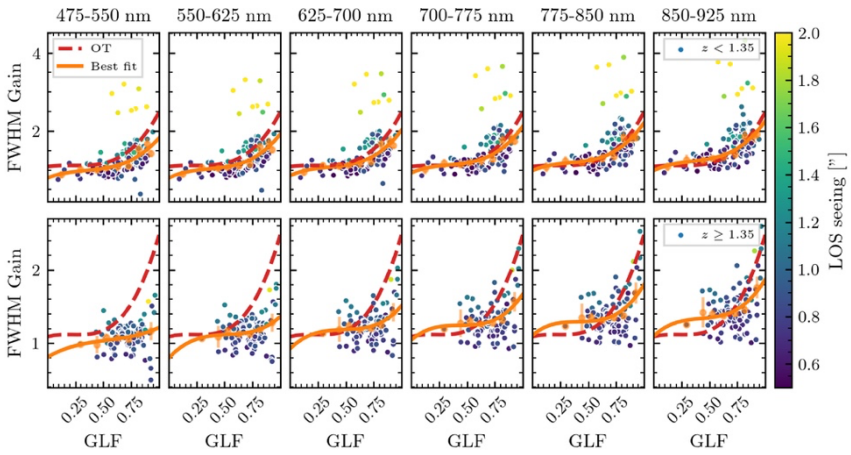


Figure 27 *WFM-AO FWHM Gain (with respect of what is expected from DIMM seeing during the time of the observation) vs GLF for different wavelength ranges. Upper set of plots for airmasses z<1.35, lower set for z>1.35. The dashed red curve is what is implemented at the observatory when deciding whether to observe a given OB. See Hartke et al. Proc. Of SPIE 11448E, id. 114480V (2020).*

4.2.1 Should I request a WFM-AO mode? Pros and Cons

MUSE WFM-AO mode is more efficient than WFM-NOAO and suitable for most science cases.

- Without AO or with AO the intrinsic optical characteristic of MUSE limits the best practical obtainable image quality in WFM to 0.55” at the blue extreme and 0.45” at the red, matching the pixel sampling. AO permits the achievement of better IQ for a larger fraction of external conditions.
- AO almost always delivers better image quality than non-AO, therefore when using the WFM-AO mode the probability of observation of a given OB is generally higher (i.e. a given requested image quality has a probability of realization larger if the AO is used).
- This improved image quality always results in improved S/N at the peak of point sources.
- For point sources, the increased overhead for WFM-AO are overcome by the improvement in S/N due to IQ gain, making WFM-AO the better choice.
- Beyond approximately 2” - 4” the wings of the PSF are the same as those without AO: all the energy redistribution occurs interior to 2” - 4”.
- The option of using the TTS-free AO mode provides 100% sky coverage. The performance gain in this mode has not been fully characterized.
- Because of the notch filter, users should refrain from selecting WFM-AO if interested in spectral features in the wavelength range between 582 nm and 597 nm, for the nominal filter, or between 576 nm and 601 nm, for the extended filter.
- The spectrum obtained in AO mode is contaminated by Raman lines. Users are strongly encouraged to consult Table 9 and Figure 44 of this User Manual, to check the wavelength and intensity of the Raman lines.
- Service Mode OBs have lower priority over Visitor Mode observations when laser collisions occur Therefore, if your target is located in highly requested RA bins (i. e. COSMOS, UDFS) then you should consider that the use of WFM-AO might not be always an advantage because of possible laser collision with other telescopes.
- For the same image quality (FWHM), the shapes of the PSF in the WFM-AO and WFM-NO-AO mode are different. The average Moffat beta parameters of WFM-AO and WFM-NOAO are 2.2 and 2.6, respectively.

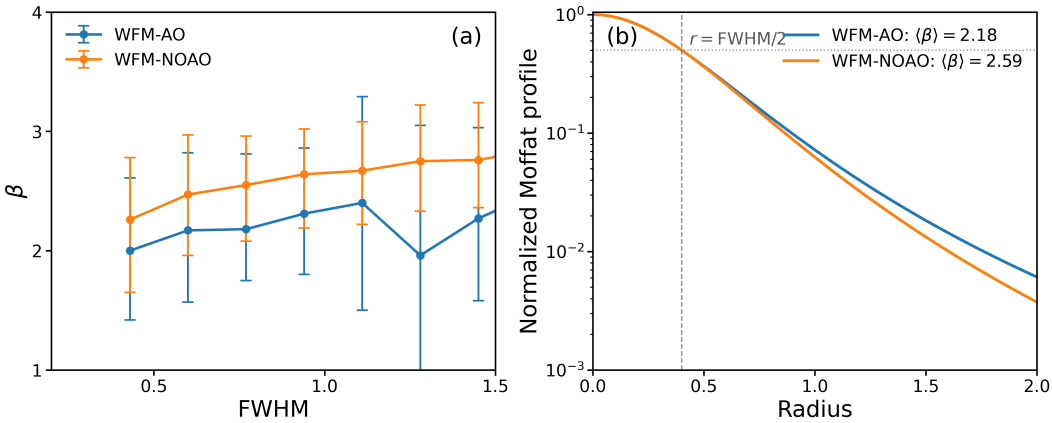


Figure 28 a) Moffat beta β parameter as a function of FWHM for WFM-AO and WFM-NOAO. (b) Normalized Moffat profiles with fixed FWHM = 0.8 using the mean beta values, <β> = 2.2 for WFM-AO and <β> = 2.6 for WFM-NOAO.

4.2.2 PSF reconstruction for WFM-AO observations

The paper by Fusco et al. 2020 A&A, 635, 208F, "Reconstruction of the ground-layer adaptive-optics point spread function for MUSE Wide Field Mode observations" describes an algorithm to reconstruct the PSF of WFM-AO data based solely on data present in the SPARTA extension of the raw frames. When there are no stellar sources in the FoV and the user needs to know the PSF this work offers a possible solution.

4.3 Degraded three lasers mode in WFM-AO

The system considers the possibility of failure of one laser in WFM-AO. We have evaluated the performance in those circumstances and reached the following conclusions (see Figure 31):

- Performance gains measured with four lasers vs three were detected but marginal, typically EE with 4 lasers is 2-3% better than with 3. No change in the spatial uniformity of the correction was measurable.
- The 3 lasers performance of FWHM versus wavelength shows the same behaviour as with 4 lasers, namely: a clear trend of lower FWHM toward longer wavelength.
- The 3 lasers performance of FWHM versus wavelength for all extracted stars also shows the same behaviour as with 4 lasers, namely: the individual profiles are much closer to the mean than without AO correction.
- The same trends can be seen with the Moffat's beta parameter.

Therefore, in case of failure of one of the laser units users could receive WFM-AO data obtained with three instead of four lasers. The status of all lasers can be found in the header keywords. The following HIERARCH ESO keywords are present with typical values as given. SWSIM stands for software simulation. In the example LGS4 is out of service. We are implementing the HIERARCH ESO keywords AOS.LGS.LIST giving the list of active lasers, and AOS.WFS.LIST giving the list of active wavefront sensors.

```
LGS4.LASR4.POWER = 22.000,
LGS4.LASR4.SWSIM = T,
AOS. LGS4.DET.GAIN = 1,
LGS4.SHUT2.ST = F
while for LGS1/2/3 :
LGS3.LASR4.POWER = 22.943,
LGS3.LASR4.SWSIM = F,
AOS.LGS3.DET.GAIN = 100,
LGS3.SHUT2.ST = T.
```

Hartke et al. Proc. Of SPIE 11448E, id. 114480V (2020) reports the performance in this degraded mode, performance which is summarized in Figure 29 and Figure 30 below.

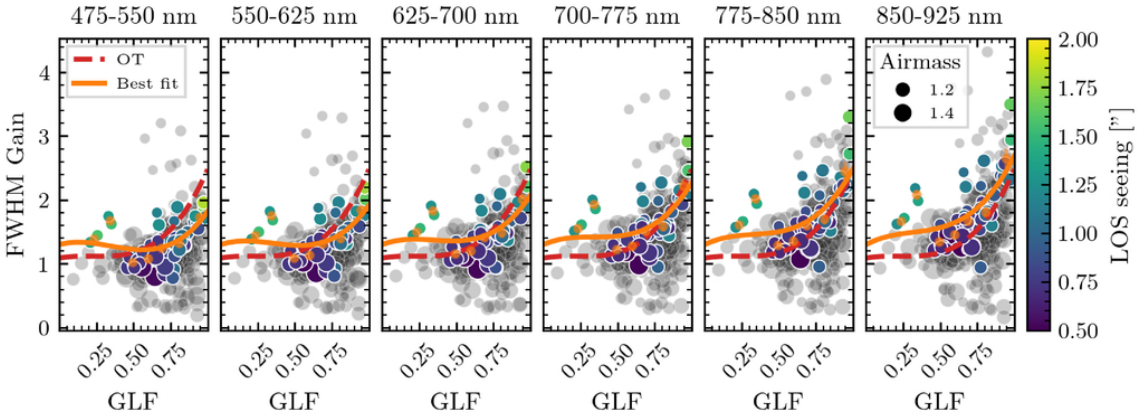


Figure 29 (top) Gain in image quality as function of GLF in six wavelength bins for observations in degraded mode (opaque points). For reference, operations in standard mode are shown with grey points, including poor data outliers (From Hartke et al. 2020).

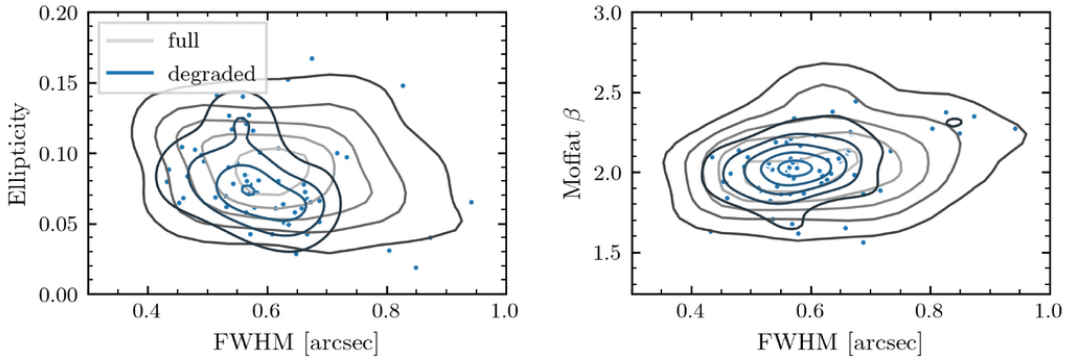


Figure 30 (bottom) Distribution of the PSF parameters ellipticity (left) and Moffat β (right) versus the PSF FWHM for observations in 3-lasers degraded mode (blue contours) and standard mode (gray contours).

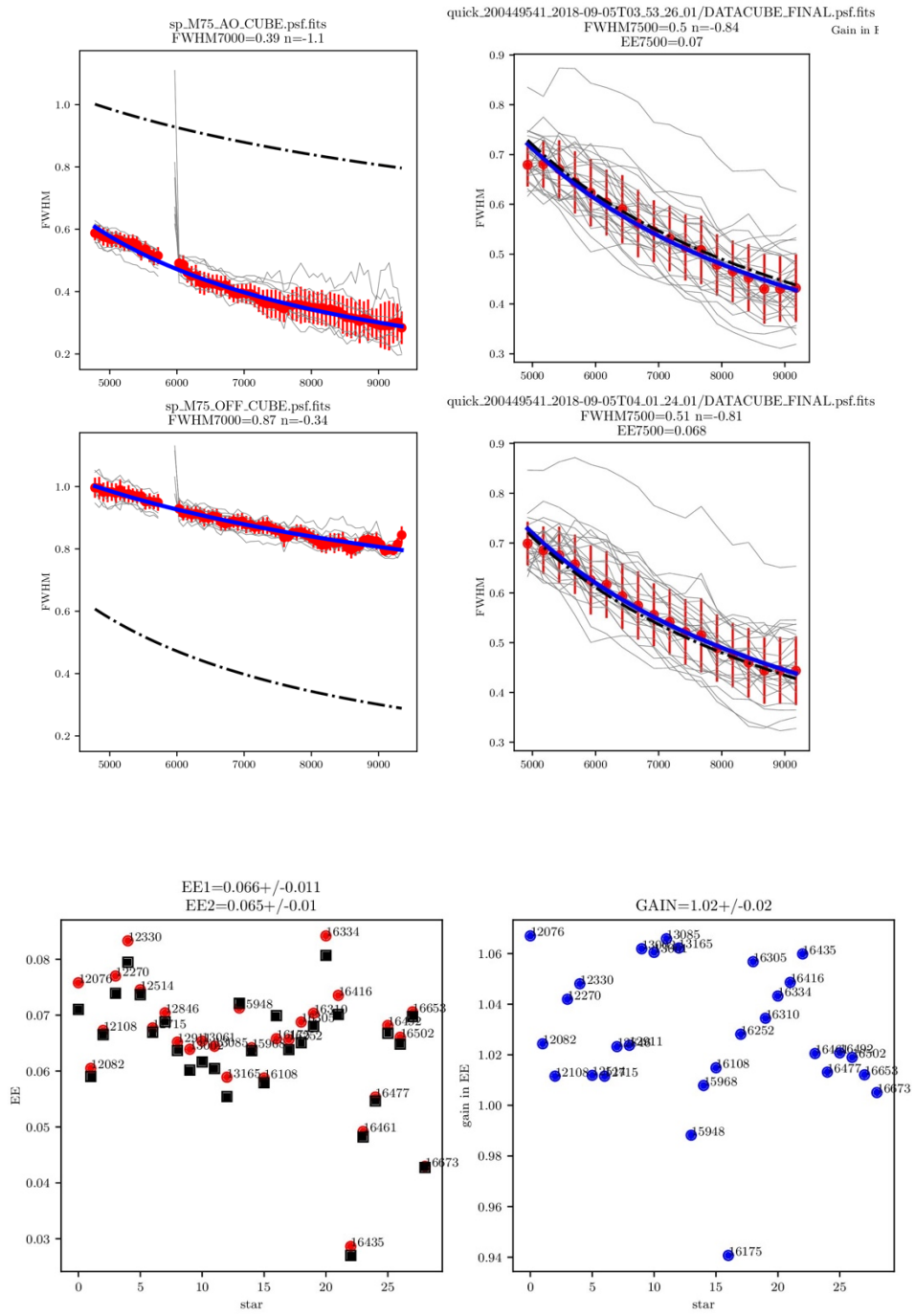


Figure 31: *Performance of 3 lasers vs 4 lasers. (a, top) FWHM versus wavelength for all stars in one of the astrometric fields. The two left panels plots the data for 4 lasers with AO ON (top) and OFF (bottom); the two right panels show the performance with 4 (top) and 3 (bottom) lasers. (b, bottom) EE for 4 lasers (red circles) and 3 laser (black squares) and gain in EE for 4 vs 3 lasers. It should be noted that conditions were very stable during the observations that led to these figures. Even so, sometimes 3 lasers were ahead. External seeing conditions at the time ~ 0.90"@550 nm.*

4.4 Degraded three lasers mode in NFM-AO

The system considers the possibility of failure of one laser in NFM-AO. We have evaluated the performance in those circumstances and summarized the results in the following plots:

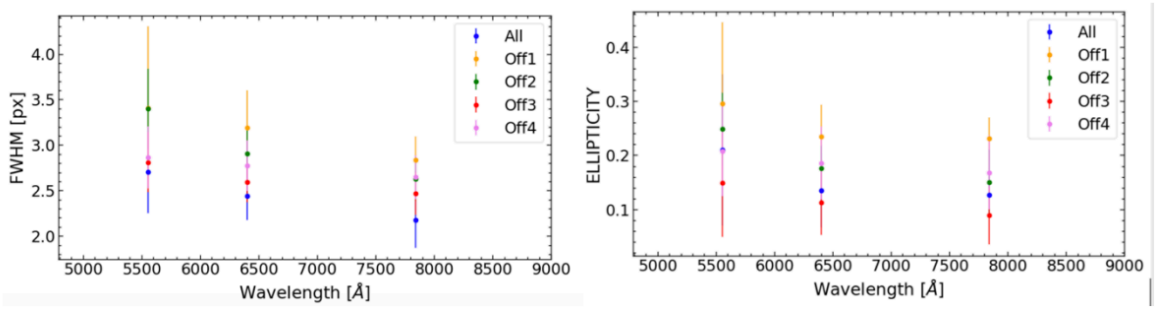


Figure 32: *Distribution of the average of FWHM and ellipticity (1-B/A) (right) as measured using the stars selected in the V ,R and I MUSE field of view images. On the X-axis we adopted the nominal peak of the throughput of the filters. A and B are the lengths of the semi-major and semi-minor axes, respectively. The FWHM is measured in pixels. The label 'All' represents all four lasers are working, and label 'Off#' represents one of the lasers is turned off.*

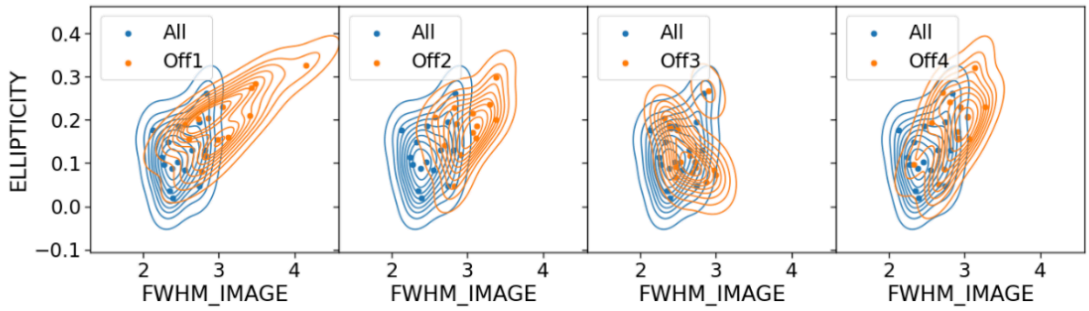


Figure 33: *Comparison of the distribution of ellipticity vs FWHM (pix) of the stars in the 4 White images taken with the support of 3 lasers (orange) on top of the image taken with the 4 lasers (blue). The labels Off1 to 4 indicate which laser was effectively not used in performing the observations (from laser number 1 to 4, respectively). The data are taken in excellent conditions (TC < 20% and airmass = 1.05)*

The FWHM and ellipticity in NFM downgraded mode are worse than those in the full 4LGS mode but can still deliver FWHM < 0.1" (4 spaxals) in excellent conditions (20% TC and airmass < 1.2), and the ellipticity is smaller than 0.2.

For slightly worse conditions (TC<20% and airmass =1.5), the differences in FWHM and ellipticity between NFM downgraded 3LGS mode and full 4LGS mode are not as significant as it is in excellent conditions (Figure 34).

In phase 2, the MUSE checklist includes a question about whether the program can be executed in NFM-3LGS mode. Enabling NFM-3LGS mode will improve the program's chances of execution, especially if one of the LGSs is unavailable for an extended period. For instance, LGS unit #3 was out of service from January 31 to March 22, 2024.

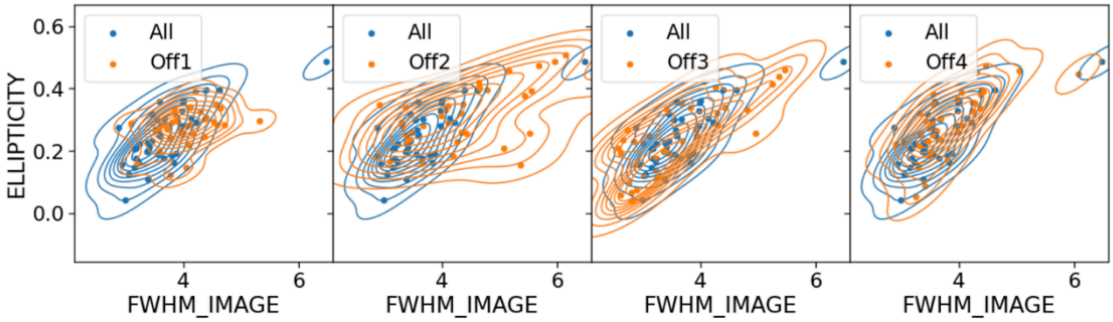


Figure 34: *Comparison of the distribution of ellipticity vs FWHM (pix) of the stars in the 4 White images taken with the support of 3 lasers (orange) on top of the image taken with the 4 lasers (blue). The labels Off1 to 4 indicate which laser was effectively not used in performing the observations (from laser number 1 to 4, respectively). The data are taken in slightly worse conditions by increasing the airmass (TC < 20% and airmass = 1.5)*

4.5 Adaptive optics performance in NFM

In NFM, the AO performance strongly depends on wavelength, on the atmospheric turbulence profile, on the airmass of observation, and on the J-band magnitude of the tip-tilt star. The observed PSF is best reproduced by using a combination of 2 Moffat PSFs as global fitting function: for PSF core and wings. Figure 35 shows the range of PSF core FWHM as a function of wavelength and Figure 36 the Ensquared Energy (EE) in a 25 mas box (i.e., 1 spaxel) as a function of wavelength. Close to the zenith and in the very best conditions, i.e. line of sight seeing (LOS) at 500nm better than 0.5”, the FWHM of the PSF core recorded on MUSE images is close to the sampling limit of ~2 pixels at 50—55 mas over the full wavelength range and the EE reaches up to 10% at 900nm. In more common conditions (LOS seeing between 0.5” and 1”) the median performance observed during the commissioning runs allows to consistently reach ~50 mas FWHM at 900nm degrading to ~80 mas at the blue edge of the wavelength range. The large variations observed are predominantly due to the details of the atmospheric turbulence profile. Note that the performance estimates shown here are still very preliminary and are continuously in progress and will be updated as the number of collected NFM frames increases.

Three important points are worth highlighting:

- Obtaining good NFM-AO performance, especially at bluer wavelengths, is very challenging and it is only possible in the very best seeing conditions, close to zenith (airmass lower than ~1.2).

- While the GALACSI system allows to reach a diffraction limited PSF core down to ~600nm (as verified on the commissioning camera), it is important to realize that with a 25 mas x 25 mas spaxel size, the diffraction limit of the VLT in the optical is heavily under-sampled by MUSE.
- As of P105: a new way to specify the constraints via an atmospheric turbulence category, TC, has been introduced (equivalent to previous Phase 1 seeing constraint). For NFM-AO mode these categories are based upon percentiles of seeing, and coherence times as described in Table 12.

It should be noted that even for the case of observations of stellar fields, the performance via the Strehl ratio cannot be reliably estimated on the final frames with MUSE due to the under-sampling. The FWHM of the PSF core of the stellar sources gives only part of the story; the fraction of the energy in the core is needed for a full assessment.

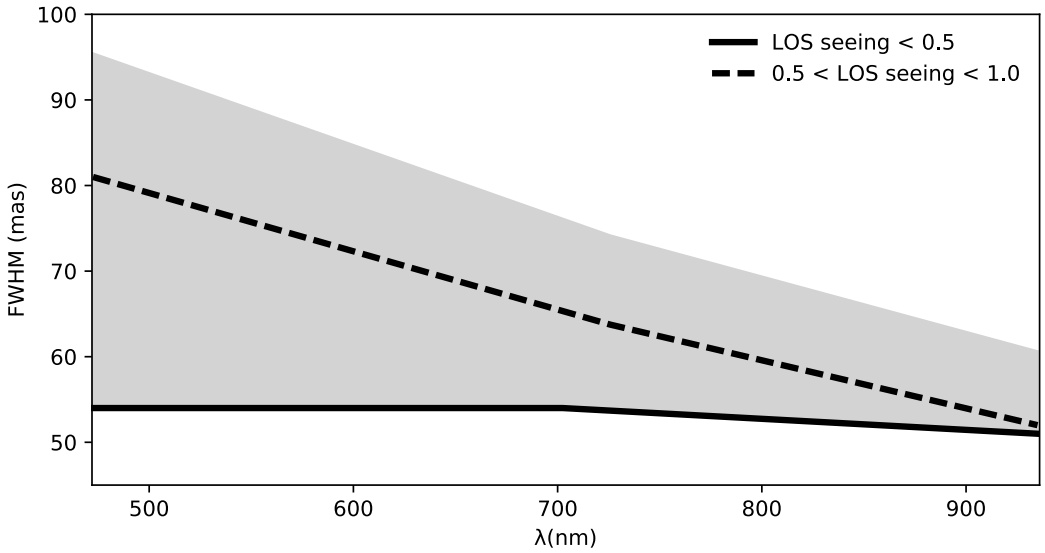


Figure 35: *FWHM of the MUSE NFM PSF core as a function of wavelength. The solid line represents the very best performance in the best seeing conditions, with a LOS seeing@500 nm<0.5". The dashed line shows the median performance for LOS seeing between 0.5" and 1.0". The grey area shows the observed variation of the PSF core FWHM recorded during the commissioning runs, depending on details of the atmospheric turbulence profile.*

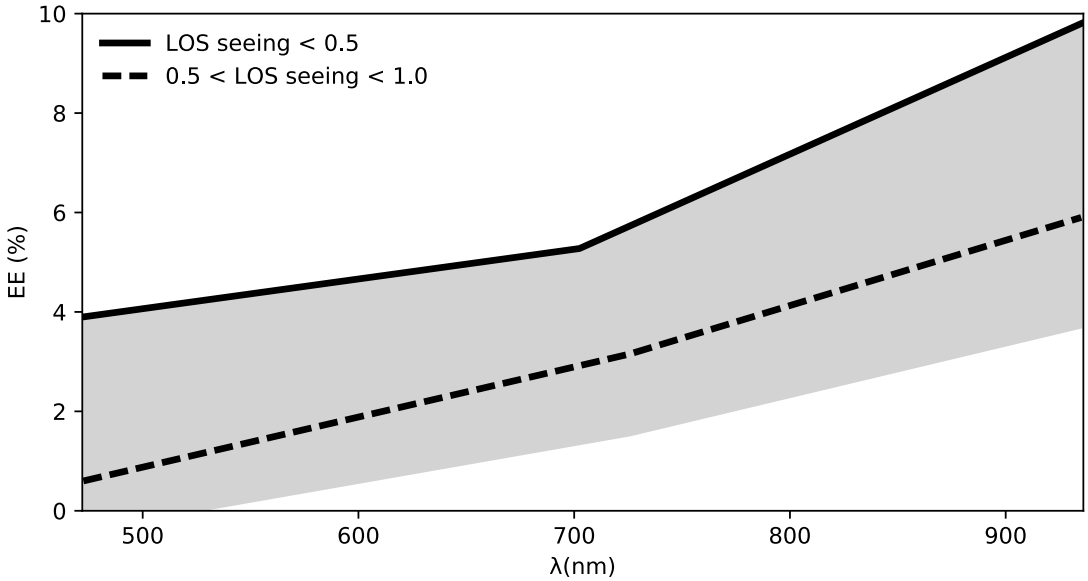


Figure 36: *Ensquared Energy (EE) in a 25mas (one spaxel) box as a function of wavelength. As in Figure 35, the continuous line shows the best performance for a LOS seeing <0.5". The dashed line shows the median performance and the grey area indicates the range observed during the commissioning runs for a LOS seeing between 0.5 and 1 arcsec.*

4.5.1 NFM performance milestones

Since the start of operation of MUSE NFM LTAO four periods should be recognized: the first one goes from start of normal operations in Oct 2018 up to Oct 2019 when a laser tomography optimization campaign was carried out during six non-consecutive half nights between 4–14 October after which our monitoring has revealed a clear improvement in AO performance as shown in in Figure 37. The second period starts after 14 Oct 2019 with the new control matrices determined during the optimization campaign and extends until the first commissioning of IRLOS+ which was carried out between 16 – 23 March 2021. The third period starts with P107, April 1st 2021, with the newly commissioned IRLOS+ with a small-scale mode using a correction frequency for its TT loop of 500Hz instead of 200Hz, and, due to the very low readout noise of its SAPHIRA detector, with the capacity of using tip-tilt stars down to J=17. A fourth period starts after July 18th when during the second IRLOS+ commissioning a faint mode was introduced permitting the use of reference object with J< 19.0. It is expected that good performance will be achieved for smaller turbulence coherence time and fainter tip-tilt stars but quantitative performance figures will need to wait a longer monitoring time.

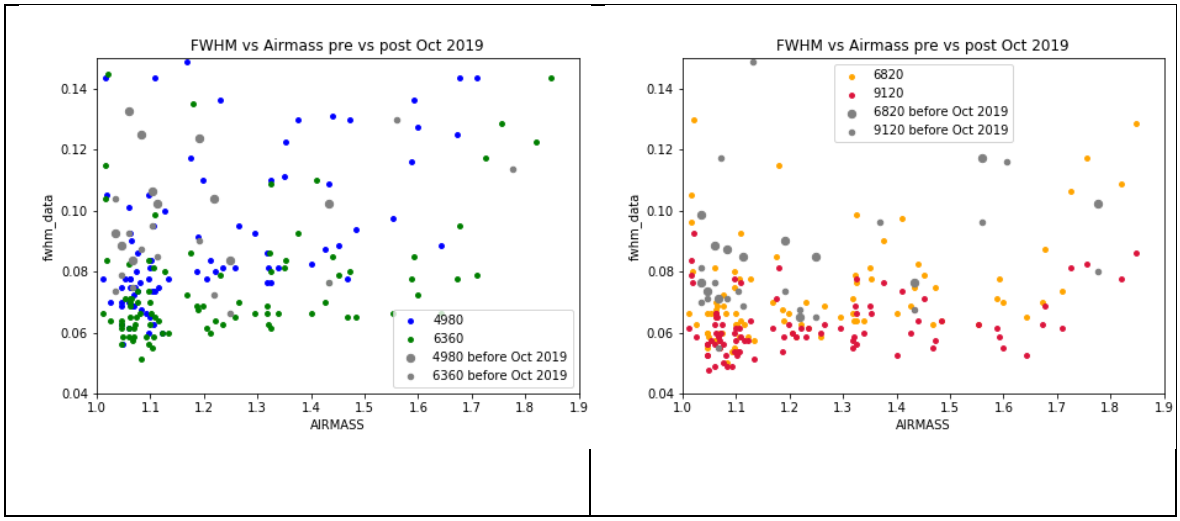


Figure 37 FWHM of the core of the NFM PSF for different airmasses before the 2019 campaign, grey, and after the campaign, in color, for selected wavelengths as indicated in the legends.

4.5.2 NFM AO performance versus airmass

A preliminary analysis of data from the first year of NFM observations, that is the first period described in the previous section, is summarized in Figure 38 below, constructed based on data from science observations of stellar sources, including stars in globular clusters. The vertical dotted lines show the coherence time values that define the turbulence categories for NFM that are defined in Table 12.

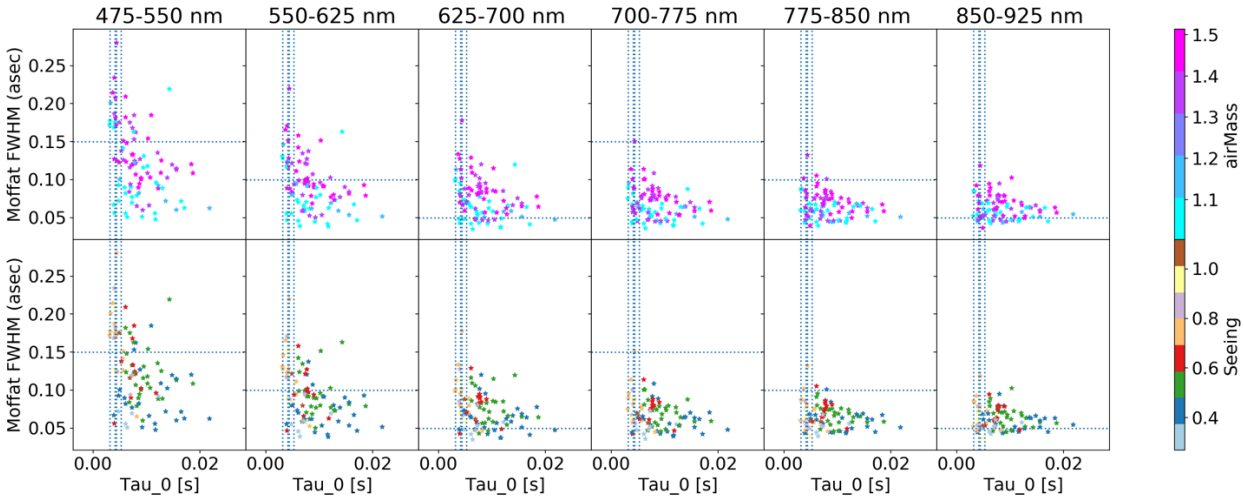


Figure 38 *NFM FWHM in milli-arcsec [mas] from Moffat fits to the core of the PSF versus coherence time for six wavelength ranges. Data points are colour-coded according to the observed airmass (upper panels) and ambient seeing (lower panels). Note the strong airmass effect, especially for the bluer wavelengths. The horizontal lines are drawn at 150 mas, 100 mas, and 50 mas.*

Table 8 and Figure 38 illustrate the strong effect that airmass has on AO performance. For airmasses above ~1.5 the SPARTA (the real time computer) reported performance is down by a factor of 10 compared to observations done near zenith. The degradation in performance comes, at least in part, due to the 3/5 power dependence of seeing on airmass and the -3/5 power dependence of the coherence time of the turbulence. This implies that an observation taken at airmass of 1.5 when seeing and coherence time at zenith are 0.6" and 5.2 ms, for a turbulence category (TC) of 10%, are equivalent to observations at zenith with TC of 30%. Note that the wavelength dependence of the turbulence parameters makes matter much worse for the blue wavelengths.

Figure 40 shows FWHM of the core of the NFM PSF as a function of airmass for several wavelength ranges and turbulence categories. All the data in the figure comes from after the Oct 2019 control matrices update; the large points are from the few observations taken after the first commissioning in March 2021 of the IRLOS detector when the tip-tilt was measured and corrected at 500 Hz (instead of the previous 200 Hz). The number of dimensions of parameter space results in very few data points per condition so a final analysis is not yet possible, but it was considered important to present these figures based on preliminary data for users to have an idea of the expected performance degradation for observations taken at large airmasses and different turbulence categories. Particular note should be taken for the strong airmass dependence for the bluer wavelength.

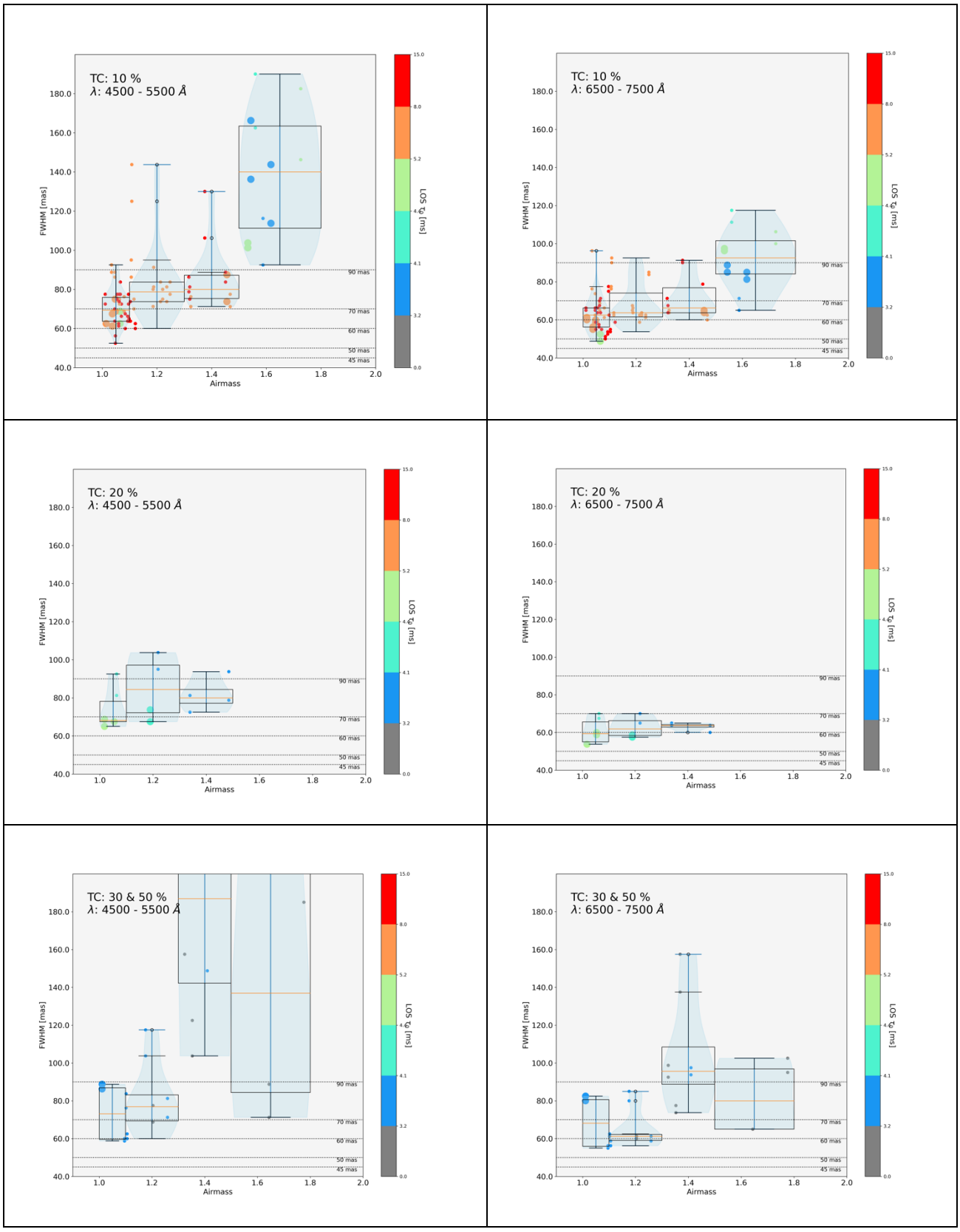


Figure 39 FWHM vs airmass for several TC and wavelength ranges. The colour bar gives the coherence time corrected to the airmass of observation.

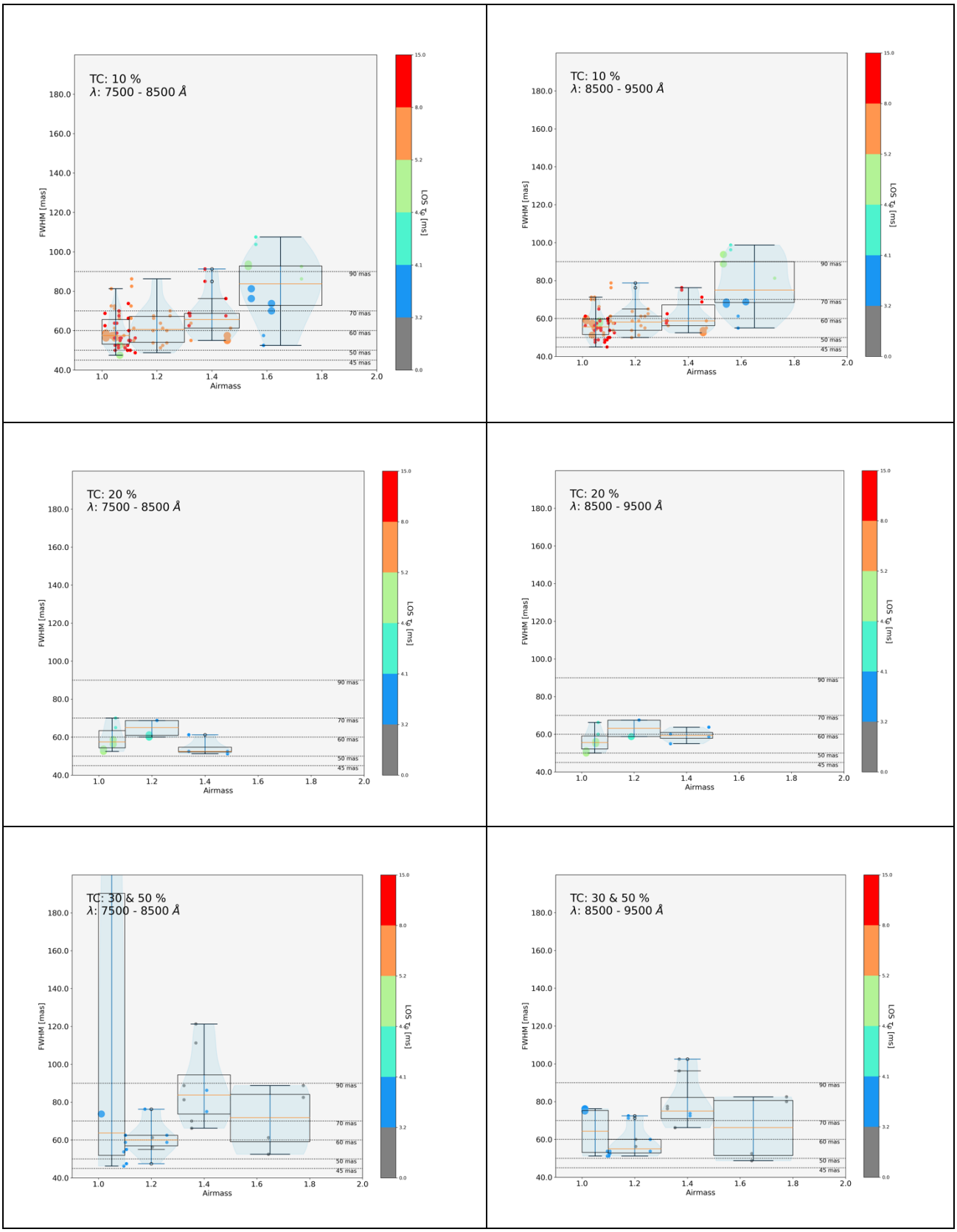


Figure 40 *(cont)* FWHM vs airmass for several TC and wavelength ranges. The colour bar gives the coherence time corrected to the airmass of observation.

The airmass AO correction degradation effect is illustrated with actual science data of a star cluster shown in
Figure **41**.

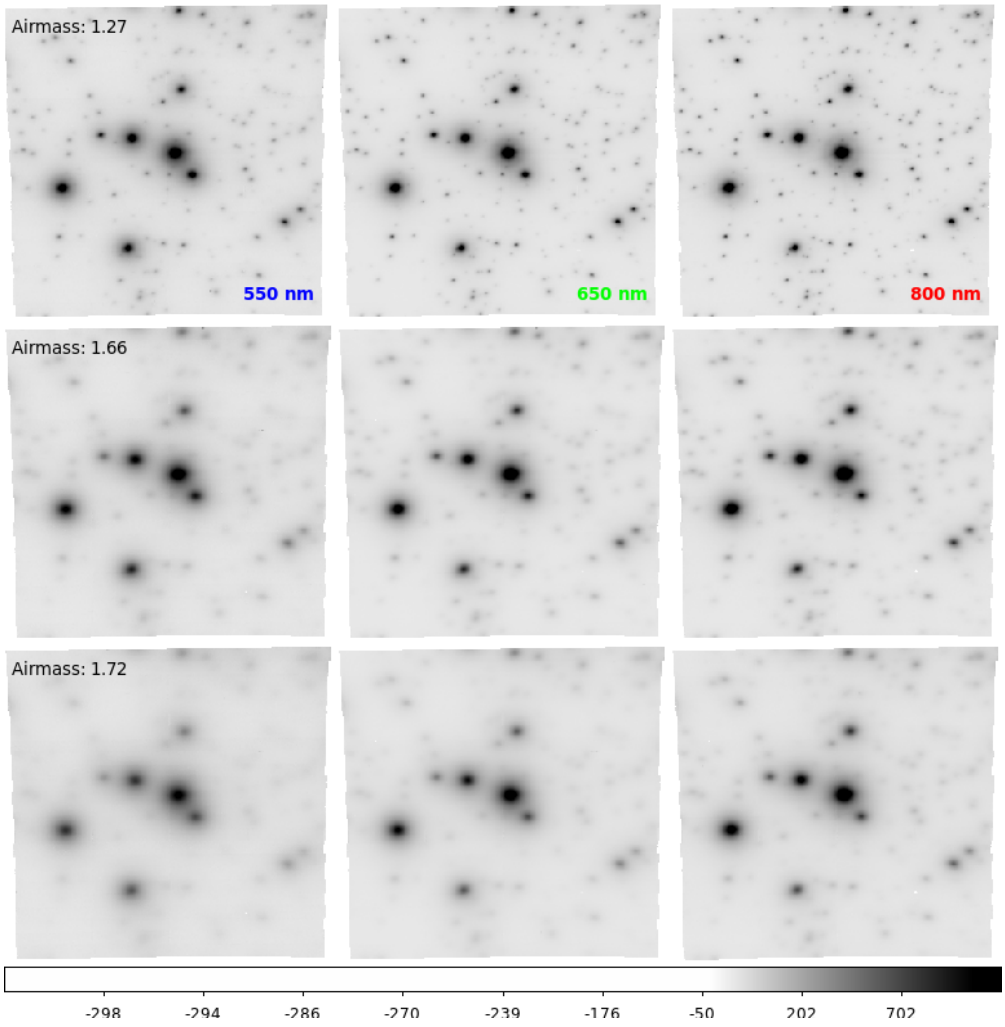


Figure 41: *Rows correspond to cubes at different airmasses, as labelled. Columns show images extracted at the given wavelength from the same cube. Data for NGC7099 obtained during the night of 4 December 2019 is publicly available.*

Table 8 *Log of NFM observations illustrating the effect of airmass*

Airmass	Seeing "	τ_0 [ms]	SPARTA Perf [%]	Gaussian FWHM of core 500 nm [mas]	700 nm [mas]	900 nm [mas]
1.27	0.77	5.4	5	124	74	57
1.66	0.62	8.7	<1	247	187	151
1.72	0.59	8.7	<1	312	227	188

4.5.3 PSF reconstruction for NFM-AO observation

Although there is no tool to reconstruct the NFM PSF from SPARTA data similar to the one for WFM-AO observations, there are some advances toward this. The user can consult the work of Fétick et al. A&A 628, A99 (2019) "Physics-based model of the adaptive-optics corrected point-spread-function." In that work the authors represent the MUSE NFM PSF as a (possibly) elongated Moffat core plus a constant out to a correction radius, r_c, and a Kolmogorov spectrum round PSF outside the correction radius, convolved with the optical transfer function of the instrument. The correction radius is defined by the minimum spacing between actuators of the deformable mirror, as ripples in the wavefront sensor cannot be corrected if they have a spatial wavelength smaller than twice this spacing. This results in a natural seeing PSF beyond r_c. In Figure 42 below the mean wavelength is 912 nm which corresponds to a r_c=0.432", marked with a loosely dashed red circle, for an inter-actuator spacing of 25 cm. The AO system redistributes the energy within r_c towards the core of the PSF.

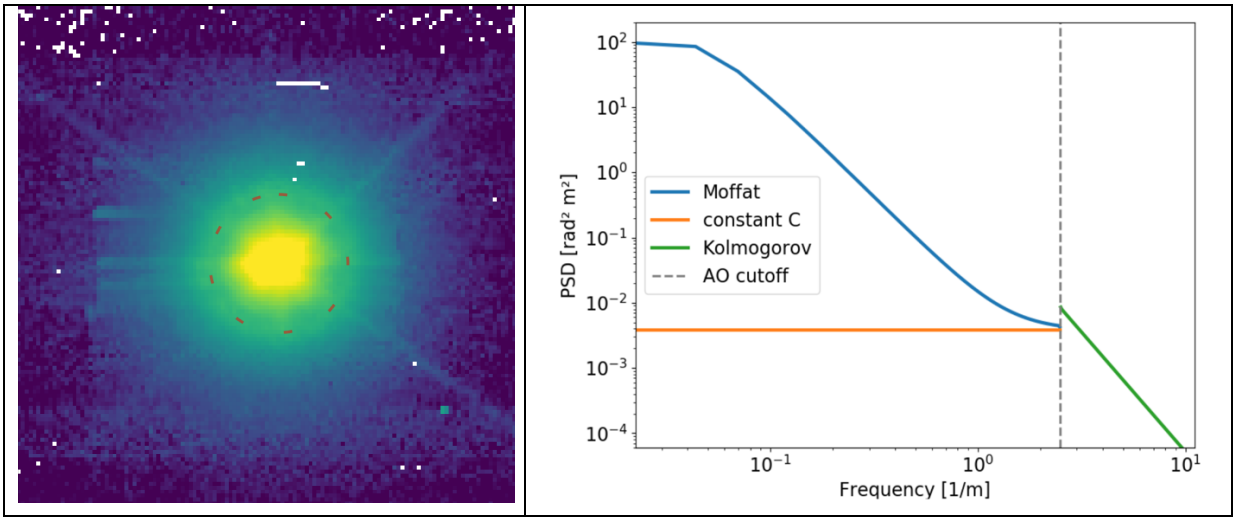


Figure 42 *(left) MUSE NFM PSF for an image extracted between 889 - 935 nm. Red circle shows the AO cutoff of 0.432". Right, Fig 2 from Fétick et al. (2019) showing the maoppy PSF described in that paper.*

4.5.4 Very bright NGSs observations in NFM

Very bright NGSs with V-band magnitudes brighter than 7.0 contaminates the FoV of the 4LGSF SH wavefront sensors focused at ~90 km. This happens because the cross-section of the telescope beams pointing to the artificial stars intersect the center of MUSE FoV at infinity, therefore a sufficiently bright star will still be visible, defocused, despite the attenuation provided by the sodium notch-filter.

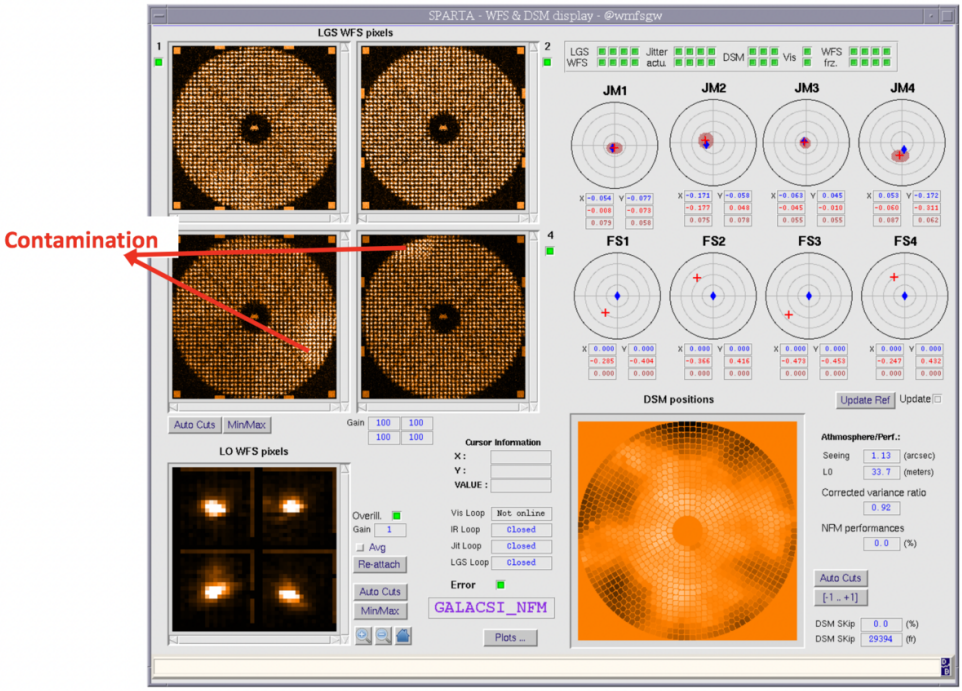


Figure 43 4LSF FoV contamination by bright star as seen in the SPARTA GUI.

Despite the above, the observations can still be carried out with a special procedure that widens the laser constellation to avoid contamination of the laser wavefront sensing, and if necessary, adds a neutral density filter in IRLOS to avoid saturation that would degrade de sensing. This requires a submission of a waiver which should be mentioned during Phase 1 and requested at Phase 2. Note that the Strehl ratio is expected to decrease by approximately a factor of two, so this procedure should be reserved for targets observable with airmasses lower than ~1.2. The observatory would follow the procedure on a best-effort basis. Users are cautioned that for bright stars artifacts from internal reflections and flat-fielding errors are hard to deal with. We are studying the feasibility and usefulness of a pupil-tracking mode which would be useful for very bright stars, but such observing mode is not yet offered.

4.6 Contamination caused by Na laser during AO observations

During the first commissioning run of MUSE+GALACSI the team discovered that the upstream beam of photons induced Raman scattering with the air molecules leading to the presence of additional lines shifted to the red of the main Na line. The spectrum seen by MUSE is contaminated by these lines to the extent shown in Table 9, and Figure 44 below. It is to be noted that the strength of the two brightest lines, those of N_2 and O_2, are comparable with a bright skyline. The MUSE commissioning team define strategies to subtract them in the data reduction pipeline and it is recommended that MUSE pipeline version equal or later than 2.8.3 is used. For details see Vogt et al., 2017, Phys. Rev. X 7, 021044.

Table 9 *Raman Lines visible with MUSE with laser on.*

Raman Line	λ_{4LGSF}	CO_2	CO_2	O_2 ($\nu_{1\leftarrow0}$)	N_2 ($\nu_{1\leftarrow0}$)	CH_4	O_2 ($\nu_{2\leftarrow0}$)	H_2O	N_2 ($\nu_{2\leftarrow0}$)
Raman shift (cm_{-1})	…	1285.8	1388.1	1556.4	2330.7	2914.2	3089.2	3651.7	4631.2
λ_{obs} (Å)	5889.959	6372.57	6414.39	6484.39	6827.17	7110.43	7200.02	7503.93	8099.23
Flux	1.9×10^{7}	11.3	18.9	**6.8×10^{3}**	**2.0×10^{4}**	≲1.1	3.2	2.7	16.1

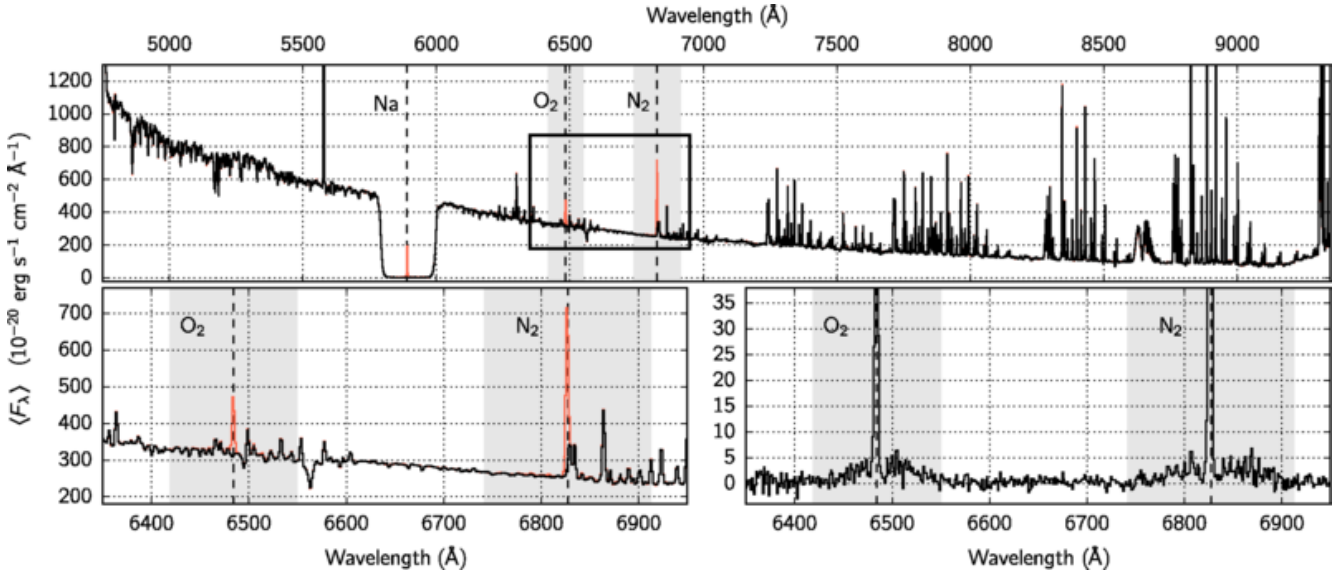


Figure 44: *Sky spectrum seen by MUSE with 4LGSF on.*

5 Observing with MUSE

5.1 General information

There are two phases in the application for time with Paranal instruments. Phase 1 starts with the Call for Proposals issued by ESO. Every User must create the proposal with p1, the web-based Phase 1 tool found at www.eso.org/p1. Using this tool, the User creates a proposal providing the scientific rational and technical information about the proposed observations. In the proposal, the User is requested to create one or more observing runs for any requested instrument and instrument modes. In addition, for each defined run, observing constraints and proposed targets must be defined. With the help of the MUSE Exposure Time Calculator (ETC) and the table of overheads (see section 5.6 or the p2demo) the User decides on the total amount of time to be requested for each run.

Important note: since P105 the previous Phase 1 seeing constraint has been replaced by a Turbulence Category. For MUSE WFM modes they are defined using the percentiles of the seeing distribution following Table 10 for WFM-NOAO modes and Table 11 for WFM-AO modes.

Table 10 *Turbulence categories for MUSE WFM-NOAO mode.*

Turbulence Category	10%	20%	30%	50%	70%	85%	100%
Seeing threshold	0.50”	0.60”	0.70”	0.80”	1.0”	1.30”	all

Table 11: *Turbulence categories for MUSE WFM-AO mode.*

Turbulence Category	10%	20%	30%	50%	70%	85%	100%
GLAO-corrected Seeing threshold	0.45”	0.50”	0.55”	0.70”	0.85”	1.10”	all

For NFM the Turbulence Categories are defined in terms of chosen points in the bivariate distribution of Seeing and Coherence time are defined in Table 12.

Table 12 *Turbulence categories for MUSE NFM.*[4] *For a plot of actual achieved performance data versus the coherence time defining the TC see Figure 38 and Figure 39.*

Turbulence category	Maximum seeing	Minimum Coherence Time	Comment
10%	0.6”	5.2 ms	replaces previous NFM:excellent
20%	0.7”	4.4 ms	replaces previous NFM:good
30%	0.8”	4.1 ms	replaces previous NFM:good
50%	1.0”	3.2 ms	Replaces previous NFM:medium

If observing conditions satisfy the above constraints 90% of the time or more, observations will be classified as A (i.e., fully within constraints), for 50% of the time they will be classified as B (i.e., mostly within constraints). They will be classified as C otherwise. At Phase I the Turbulence Category must be specified for each run. Observations with different AO modes (WFM-NOAO, WFM-AO, NFM-AO) should be specified in different Runs.
Details: https://www.eso.org/sci/observing/phase2/ObsConditions.MUSE.html.

Phase 2 begins with the ESO web letter release, which defines the end of the telescope time allocation process. Service and Visitor mode observations with ESO instruments are performed by means of Observing Blocks (OBs), which contain all the information necessary to obtain a single observation. These include the target position, the instrument and exposure setup parameters, special scheduling requirements, the time constraints, the finding charts, and possibly also ephemerides lists.
As of P102, Service and Visitor Mode OBs are prepared by using p2, the web-based Phase 2 interface.
In particular, Service Mode users are expected to provide OBs (containing one acquisition and one or more observing templates) that include finding charts and a README file containing a general description of the observing run.
Generic guidelines for Phase 2 and p2 are available at:
http://www.eso.org/sci/observing/phase2/p2intro.MUSE.html
http://www.eso.org/sci/observing/phase2/SMGuidelines.html

As of Period 105, the preparation of MUSE OBs (all modes) can be done directly within the p2 environment with the help of the new ObsPrep tab. ObsPrep provides a new user friendly GUI that displays the target FoV and enables the selection of suitable VLT guide star, reference star for blind offset acquisition, NGS (for NFM) and TTS (WFM-AO). In

[4] **Important**: in the Phase 1 proposal preparation tool all turbulence categories from Table 10 and Table 11 appear as allowed even for NFM. For NFM please restrict them as per Table 10.

addition, it allows user to visualize and define the observing offsets pattern. All relevant parameters defined within ObsPrep tab are automatically propagated within the OB.
Finding Chart for MUSE observations (all modes) can be easily prepared by using the Finding Chart Generation (p2fc) service available within the p2 environment.
Alternatively, for WFM-NOAO observations we provide a ds9 template showing the trapezoidal FoV of MUSE in WFM mode, together with the SGS metrology field regions surrounding it. A similar ds9 template showing also the region where suitable TTS should be located for the case of WFM-AO observations is also available. One should simply load the file as a ds9 region template. As of period 118, TTS (WFM-AO) is not required to provide in phase 1.

Finally, MUSE all modes ESO-compliant finding charts can be created by using fcmaker (Python 3 module). You can easily and quickly install the code using pip: pip install fcmaker
Detailed instructions on how to create ESO compliant MUSE finding charts are available at:
http://www.eso.org/sci/observing/phase2/SMGuidelines/FindingCharts.MUSE.html

MUSE p2 tutorials have been prepared to guide the User through the preparation of successful OBs (see the p2 Tutorial). In addition, after logging into p2 demo, under the MUSE programme ID 60.A-9253(R) Users can find a folder named USD Tutorial containing example of OBs specifically designed for different observing strategy.
Example OBs are not editable but can be exported if needed.
https://www.eso.org/p2demo/home

Finally, questions on Phase 2 preparation for service mode observations should be addressed to our Operations Helpdesk at https://support.eso.org

5.2 MUSE Observing modes

MUSE has two basic modes: WFM for surveys and general use offered both with and without AO, and NFM with AO only for achieving unprecedented spatial resolution across a sizeable field. Note that in AO mode the maximum airmass of observations is 1.9 and the sky transparency cannot be THK. In addition, NFM observations can be performed only under good to excellent conditions (i.e., Turbulence category up to 50%) and at relatively low airmass (i.e., LOS seeing@500nm up to ~1").

In WFM only, there are two choices of wavelength range - the nominal (N) mode, which suppresses the 2nd-order overlap of blue light at red wavelengths (see Section 3.7), and the extended (E) mode, which does not use the blue cut-off filter and thus extends into the blue but suffers from the 2nd-order contamination redwards of 850 nm.
The available instrument modes are presented in Table 13.

Table 13: *Summary of instrument modes, filter names and spectral ranges (*). See Section 3.7 about 2nd order contamination in the red for WFM-NOAO-E and WFM-AO-E instrument modes.*

MUSE instrument mode	Spatial setting	Filter name	Spectral range (nm)
WFM-NOAO-N	WFM	Blue	480-930
WFM-NOAO-E	WFM	Clear	465-930(*) with 2nd order contamination at 850-930 nm
WFM-AO-N	WFM	Blue-Na	480-582, 597-930
WFM-AO-E	WFM	Na	465-576, 601-930(*)
NFM-AO-N	NFM	Blue-IR	480-578, 605-930 Note: the Na Notch filter is located in GALACSI

5.3 MUSE Target acquisition

The first template to be included in the OB is the acquisition template. For both seeing limited instrument modes (WFM-NOAO-N and WFM-NOAO-E), there are two templates that can be used for acquisition: wfm-noao_acq_preset if there is no need to do an interactive centering and the telescope pointing precision, 2"-3", is good enough. For precise centering wfm-noao_acq_movetopixel must be used and instructions for field centering must be given in the README file and on the finding chart. In addition, should the target FoV not contain a relatively bright source then we strongly suggest using a reference star for blind offset, which can be located few arcmin away from the target. For both WFM-AO instrument modes (WFM-AO-N and WFM-AO-E), the template to be used for acquisition is wfm-ao_acq_movetopixelLGS. For NFM-AO mode, the acquisition template is MUSE_nfm-ao_acq_LGS.
In addition, the template wfm-noao_acq_presetRRM must be used for an acquisition OB in Rapid Response Mode. This latter template is an exact copy of the normal preset template with the addition of two hidden (from the user) keywords for bookkeeping and logistics.

The main parameters of the acquisition templates are the following:

- Instrument Mode, as defined in Table 13, e.g., WFM-NOAO-N

- Position Angle on the sky (measured from North through East). The convention for position angles with respect to the FOV is detailed in Figure 45.
- (Optionally) Position of the VLT Guide Star. The VLT Guide Star must be between R band magnitudes 8 and 12 (in Vega), and located within the VLT guide star area (see Table 14)
  Providing the VLT guide star is not mandatory but is useful when combining observations taken at different days or when doing mosaic observations with MUSE. The quality of the astrometry in the headers of the raw data depends directly on the quality of the astrometry of the guide star.
- For WFM-AO acquisition only, position and magnitude of the AO tip-tilt star (TTS) with the possibility to provide an alternative TTS (optional but highly recommended) to mitigate potential difficulties during the acquisition sequence caused by inaccurate TTS parameters (e.g. high proper motion star, double star, wrong magnitude…). If accurate target centring is required then the use of a reference star is highly recommended. TTS star magnitude must be between R=6 and R=17.5. A TTS magnitude of 18.5 can be specified If the programme requests excellent seeing conditions that could translate to better than 0.6"@700 nm image quality at the airmass of observation. In addition, note that:
  - the TTS must be chosen such that it remains in the TTS patrol field defined in Table 14 for all on-target (i.e., OBJECT) positions in the subsequent observing template;
  - Differential tracking is not possible with WFM-AO observations, they are however allowed in TTS-free mode (i.e. WFM-AO with only the correction

provided by the lasers, but no TTS);

TTS free mode: for WFM-AO a mode without TT star, can be selected by setting the parameter "Perform acquisition with TTS" (SEQ.AO.TTS) in the acquisition template to "no". The HO laser corrections together with the telescope field-stabilization help improve image quality (see Fig. 12 of Hartke et al. (2020) SPIE).

- For NFM-AO acquisition only, position and J-band Vega magnitude of the NGS, the following constraints apply:
  - Unresolved objects (**sources with FWHM < 300 mas**) can be used as NGS providing its magnitude within an aperture of 1.5" diameter from its centroid is in the range 7 < J ≤18.0 (Vega). However, under excellent conditions (i.e., Turbulence category = 10%) the NGS faintest limit can be J<18.5 as long as the airmass of observation is not above 1.2.
  - Extended objects **(sources with FWHM > 300 mas)** can be used as NGS providing its magnitude within an aperture of 1.5" diameter from its centroid is in the range 7 < J ≤17 (Vega).
  - Very bright NGSs with J and V-band magnitudes between ~5.5-7.0 can be observed. Note that MUSE integrations time will be short, in some cases shorter than 1s, and overheads very large due to the approximately 1 minute readout time. If saturation of the main target in MUSE is an issue, then the first observing template should be a no-offset and NEXPO=1 observation that will be used to determine an optimal integration time by the night observer.
  - The NGS must always be within 3.35" of the field center if the NGS is an extended source (SEQ.NGS.EXTENDED=T), and **5.00"**[5] if the NGS is a point source (SEQ.NGS.EXTENDED=F).
    - Note that it is still possible to observe objects for which the distance between the science object and the NGS is larger than 3.35" or 5.00" (up to 2x3.35"=6.7" or 2x5.00"=10.0"). However, in this case, when designing the observations, the OB target coordinates should correspond to the instrument field center and not to the science object RA and DEC. In other words, the center of the MUSE FOV should correspond to the barycenter between the NGS and the science target. But note that AO performance has not been fully characterized for off-axis NGS.
  - If the NGS is the science object itself (i.e., NGS is on-axis) then the coordinates of the NGS can be left to 0 and the template will automatically take the coordinates of the target as the NGS;
  - If the NGS is the science target and has a high proper motions then its coordinates in the acquisition template must be left to 0, and the proper motion should be given in the target tab of the OB.
- Exposure time of acquisition exposure. Typical integration times vary between 10 seconds (if there is a V<17 point source in the FOV) and 2 minutes (when the

[5] After IRLOS upgrade there was a small decentering of the optics and the ranges in different directions are not the same. Therefore, until we correct this we have reduced the allowed range from 5.90" to 5.00".

brightest point source is V<20). If there is a need of precise (<1" error) pointing in fields where only faint extended sources are present, blind offsets through a reference source are recommended (only applicable to WFM)

- (Optionally) Blind offsets. The user has the possibility to apply some offsets with respect to a bright reference star centered in the FOV of MUSE, in case no bright source is visible in the FOV for direct acquisition and precise pointing is necessary. For the WFM case (i.e., AO and NOAO), the reference star can be either selected within or outside the MUSE FoV. Blind offset in NFM is not supported.
- The convention is to provide telescope offsets (arcsecs in RA and DEC) to move the telescope from the target to the reference star.

  RA_REFSTAR = RA_TARGET + ΔRA
  DEC_REFSTAR = DEC_TARGET + ΔDEC

  In that case, the sequence is the following:
  - The telescope points to the reference star by including offsets from the target
  - The reference star is centered in the MUSE FOV.
  - The offsets are cancelled, and the telescope moves to the target position.
  - For those familiar with the instruments, this definition of blind offsets is identical to the one used for HAWK-I and CRIRES.

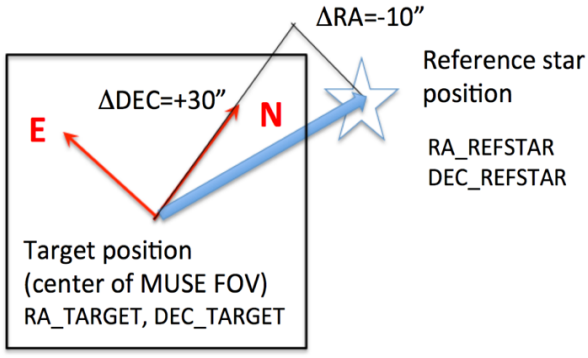
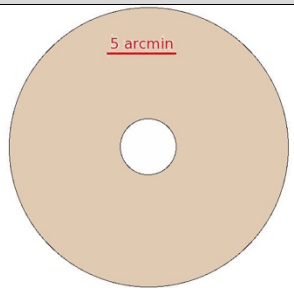
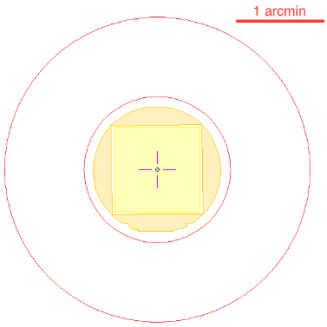
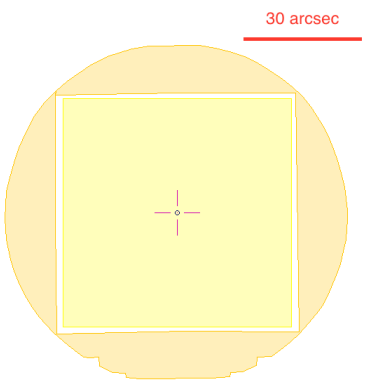
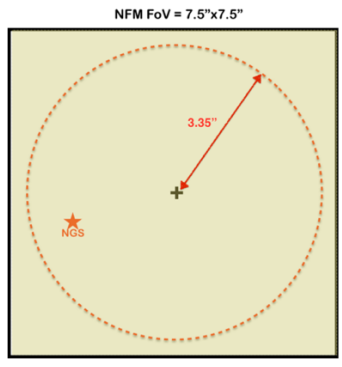


Figure 45 *Blind offset acquisition convention*.

- Slow Guiding (True/False, in WFM and WFM-AO only): The use of the SGS is strongly recommended whenever individual exposure times on the science targets are larger than 4 min. The SGS will acquire a reference image and detect guide stars after acquisition, then lock on these stars and correct for small motions such as derotator wobble, which is important for long exposures, in particular close to the zenith. The user does not need to provide secondary guiding stars in acquisition, these are automatically found by the system. If all individual exposure times are shorter than 4 min., the user has the option not to use SGS because no correction will be sent to the telescope (see Section 2.1.2.2). Do not activate the SGS if you do differential tracking.

Table 14: *Description of the different guide stars used for acquisition, and their corresponding region of sky with respect to the centre of the MUSE FOV.*

	Guide Star Area	Shape
VLT guide star	10 arcmin radius circle inside the unvignetted Nasmyth FOV 4 arcmin diameter circle excluded	
WFM-AO TTS	Between 1.725 and 3.59 arcmin diameter from the MUSE field center (covered area: 7.8 arcmin^2) The radius of the inner and outer circle is 52” and 107”	
SGS guide stars (WFM only)	SGS metrology fields, ~ 1.5arcmin square field, MUSE FOV excluded	
NFM NGS	Within 3.35” from the field center for extended NGS (SEQ.NGS.EXTENDED=T) and 5.00” for point sources (SEQ.NGS.EXTENDED=F).	

5.4 MUSE science observations

The science observation templates have to agree with the instrument mode defined in the acquisition template. The science template MUSE_wfm-noao_obs_genericoffset should be used for WFM-NOAO regardless the selected filter (i.e., Nominal or Extended). Similarly, for WFM-AO-N and WFM-AO-E observations the user should select the MUSE_wfm-ao_obs_genericoffsetLGS template. Finally, for observations in NFM the available template is MUSE_nfm-ao_obs_genericoffsetLGS.

These templates allow the user to perform observations including a sequence of telescope and position angle (PA) offsets, which is the recommended strategy for MUSE. It has been found that by rotating the instrument by +90, +180 or +270 degrees between exposures compared to the PA of the first exposure, the patterns of the slicers and channels (which appear as throughput variations in the flat-field image; see Figure 19) can be averaged out. The combination of a small dithering pattern (with offsets typically smaller than 1 arcsec, but larger than a spaxel) and 90 degrees rotations is currently the best strategy to reject cosmics and get a more uniform combined dataset in terms of noise properties.

The science template allows the user to perform a number of exposures and offset the telescope and/or the instrument derotator to adjust pointing and PA in between each offset position. In addition, the user should specify the type of exposures: “O(BJECT)” or “S(KY)” within the specified offsets list.

Important note for WFM-AO observations: users should verify that the TTS chosen in the acquisition remains within the allowed TTS area defined in Table 14 for all OBJECT positions. This constraint does not apply to SKY positions because during SKY observations, the tip-tilt loop is open and only the high-order correction with the LGS remains active. Note also that there is no particular additional constraint on PA offsets with AO.

Important note for NFM observations: The science template for NFM is very similar to that used for the WFM (AO and NOAO). As for the WFM case, we suggest breaking the total exposure time on source in sub-exposures and applying a small dithering pattern. To improve the quality of background it is recommended to combine observations taken with 90-degree rotation offsets but due to the larger overheads we recommend limiting the observations to a single PA per OB, if you have multiple OBs on one target.

All of these is better done using the ObsPrep tool in P2.

However, the following restrictions apply:

- For proper pipeline functioning an exposure of at least 150 s should be included in the OB, either OBJECT or SKY. The pipeline uses sky emission lines to correct the wavelength solution, and in NFM these are much fainter. For exposures with UIT

lower than 150 s there can be errors larger than 0.4 Å, while for UIT larger than 150 s the errors are mostly below this value.

- The maximum size of the dithering offset between two consecutive on-object exposures should not be larger than 1.0" in NFM (corresponding to ~40 NFM pixels);
- Rotations between exposures are allowed only if the NGS is on-axis (i.e., target is the NGS and placed at the FoV center). Combining rotations with small dithering (i.e., offsets) is possible as long as the defined offsets keep always the NGS within 0.2" from the initial position (i.e., the location of the NGS prior the start of any science template). In other words, each offset applied before any rotation should not place the NGS beyond 200 mas from its original position during the acquisition. But we note again that to rotate with the loop closed increases overheads as it is done in steps of 10 degrees.
- The offsets pattern for on-object exposures should always be designed such as to keep the NGS within 3.35" from the field center for extended objects (SEQ.NGS.EXTENDED=T), and 5.00" for point sources (SEQ.NGS.EXTENDED=F), otherwise the loop will open.

The total number of exposures performed is the combination of two parameters: NOFF (number of offsets specified in the list, see below) and NEXPO (number of exposures per offset). The instrument takes NEXPO exposures at a given offset position, then offsets the telescope to a new position. In total, NOFF x NEXPO exposures are taken by the template. It is normally recommended to use NEXPO=1 and always do a small offset between subsequent exposures. For very bright targets, needing short integration times not to saturate, it is usual to specify NEXPO>1 to increase SNR.

The use of the (S)KY exposure type allows the user to select less crowded regions on sky to take exposures which will be used for sky evaluation / sky subtraction. The typical exposure time of these SKY positions is shorter than the OBJECT ones but will depend on the actual conditions of the observations. Typically, in dark time one gets ~0.75e^-/min at 550nm from the sky while the RON is ~2.5e^- rms (i.e. variance 6.25) on average. The transition between read-out noise limited and sky-noise limited conditions occurs after about 10 min in dark time.

NFM very bright NGSs: If saturation of the main target in MUSE is an issue, then the first observing template should be a no-offset and NEXPO=1 observation that will be used to determine an optimal integration time by the night observer.

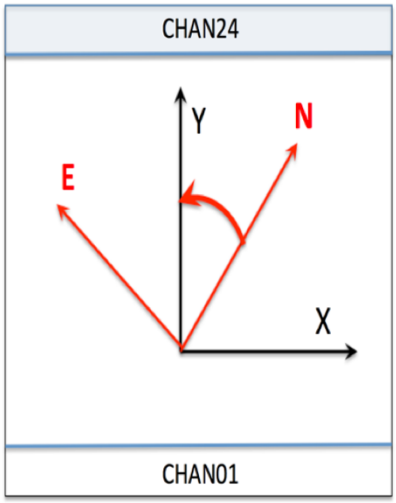
Similarly, to other VLT instruments, telescope offsets are defined relative to the previous telescope position, therefore the offsets are cumulative, e.g. a sequence of [0, -2, 4, -2] will finish at the original position. The offsets are defined in units of arcseconds in the reference frame selected (DETECTOR or SKY). The convention is detailed below in Figure 46 and Figure 47. If the first image is to be taken at the preset coordinates, the first set of offsets should be 0,0. If there are fewer offset values than the defined total number of exposures, the template will return at the beginning of the list of offsets and apply them again. However, the number of offsets provided should be identical in x and y directions. For example, if the number of exposures is 5 and the series of offsets (in "SKY" convention) is:

ΔRA	0	-10	5
ΔDEC	2	7	3

Then the offsets applied to the telescope will be:

ΔRA_{VLT}	0	-10	5	0	-10
ΔDEC_{VLT}	2	7	3	2	7

In addition, the user can provide a list of PA offsets to be sent to the instrument before starting the exposures at the new position. Like telescope offsets, PA offsets are cumulative. When in "DETECTOR" framework, if both telescope offsets and PA offset are provided, the telescope offsets are sent with respect to the current PA of the instrument, before applying the PA offset.



- If the user offsets are given in "**SKY**" convention, telescope offsets are sent in arcsecs, positive in the direction of East (RA) and North (DEC), respectively.
- If the user offsets are given in "**DETECTOR**" convention, telescope offsets are sent in arcsecs, positive in the X and Y directions, respectively, where the X and Y axes are defined relative to the 24 channels of MUSE.
- The **position angle** of a MUSE observation is measured positive East from North (red oriented angle). Positive position angle offsets are sent to the derotator in the same direction (see examples below).

Figure 46 *Offsets and position angle conventions.*

Example 1: Telescope offsets only, "SKY" convention

Total number of offsets:	5
Number of exposures per offset:	1
List of exposure types:	O,S,O,O,S
List of integration times:	1200,120,1200,1200,120
Offsets coordinate type:	SKY
List of ΔRA offsets:	0,-30,30,-1,-29
List of ΔDEC offsets:	0,-20,20,3,-23
List of PA offsets:	0

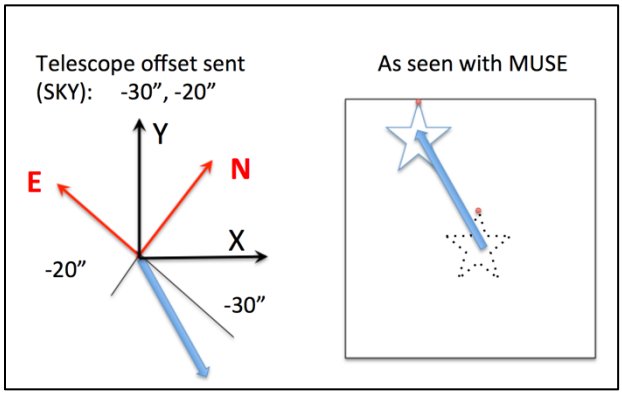


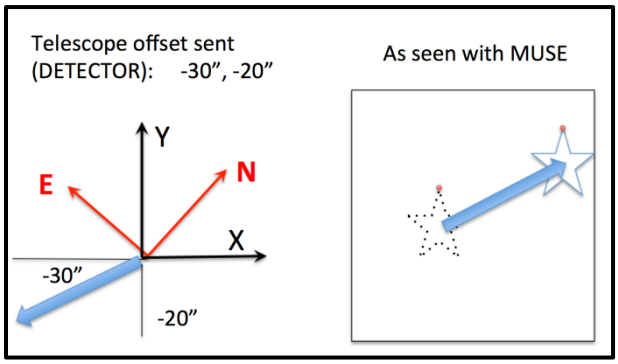
Figure 47 *Observation offsets convention.*

⇨ The telescope will (1) not move but make an 'object' exposure (1200s), (2) move and make a 'sky' exposure (120s), (3) move back to the origin and make an 'object' exposure (1200s), (4) move slightly and make an 'object' exposure (1200s), (5) move to the previous 'sky' position and make a 'sky' exposure (120s).

An illustration of the effect of the second offset is given in the figure.

Example 2: Telescope offsets only, "DETECTOR" convention

Total number of offsets:	7
Number of exposures per offset:	1
List of exposure types:	S,O
List of integration times:	120,1200
Offsets coordinate type:	DETECTOR
List of ΔX offsets:	-30,30
List of ΔY offsets:	-20,20
List of PA offsets:	0



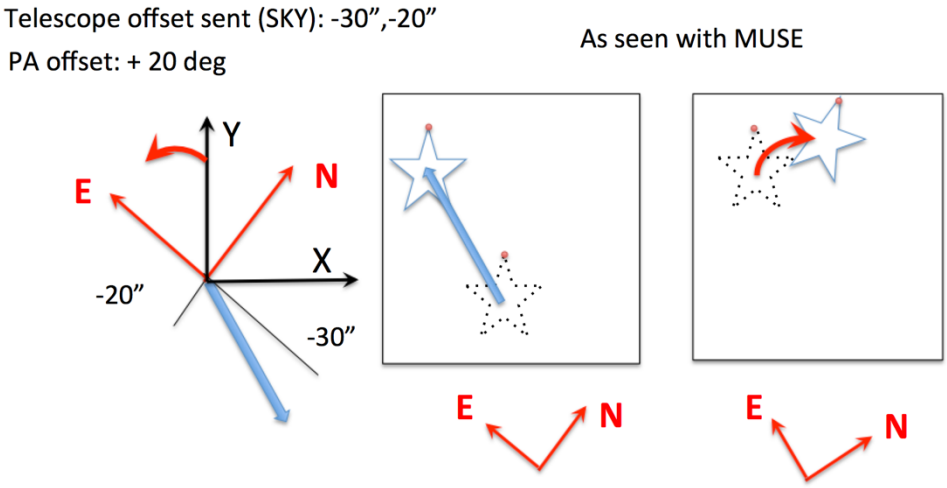
⇨ The telescope will (1) move and make a 'sky' exposure (120s), (2) move back to the origin and make an 'object' exposure (1200s), (3) to (7) repeat (1) and (2) until 7 exposures have been taken: therefore the last exposure will be of 'sky' type, and the telescope will finish the template at the 'sky' position, shifted from the preset coordinates.

⇨ Note that the list of integration times could be '120,1200,120,1200', the result would be the same, as well as if the ΔX list was '-30,30,-30,30,-30,30': each list is repeated as many times as required by the total number of exposures, and only the ΔX and ΔY offsets list lengths are linked.

An illustration of the effect of the first offset is given in the top-right figure.

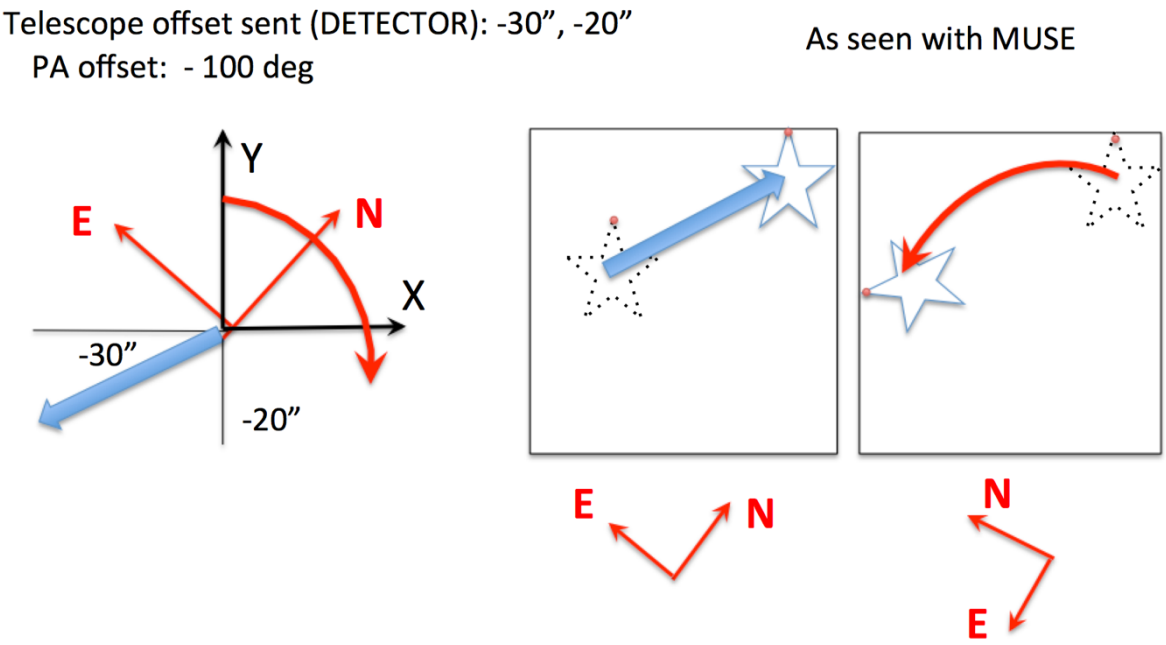
Example 3: Telescope offsets and PA offsets, "SKY" convention

An illustration of the effect of a (-30",-20") sky offset combined with a PA offset of 20 degrees is given in the figure:



Example 4: Telescope offsets and PA offsets, "DETECTOR" convention

An illustration of the effect of a (-30",-20") detector offset combined with a PA offset of -100 degrees is given in the figure:



5.5 Attached calibrations

Calibrations taken regularly during operations (see Section 7.1) provide daily flat-field and arc exposures, and illumination correction exposures are taken according to thermal variations during the night to account for repeatability (Section 7.1.3). If a MUSE observer believes more accuracy is needed it is possible to include arc and flat calibration in an observing OB as an attached calibration template, directly after the corresponding science template. Such attached calibrations are not recommended at this stage and are charged to the user.

Since P102 the templates for attached calibrations have been deprecated in favour of a single MUSE_cal_nightcalib template to be attached as the last template of the OB.

5.6 Instrument and Telescope Overheads

We provide here a summary of the telescope and instrument overheads (Table 15).

Table 15: *Summary of overheads.*

Acquisition and setup	
Telescope pointing, guide star acquisition (Preset) 2nd and following OBs in a concatenation	360 s 40s + 1 s/deg*(target separation)
Interactive acquisition loop	18 s
AO loops closure (in AO modes only)	180 s
SGS loop closure (in WFM and WFM-AO only)	20 s
Observations	
Detector setup	15 s
Detector readout + FITS file merging	60 s
Intra-exposure detector delay (for multiple exposures)	5 s
Small telescope offset (< 2 arcmin)	15 s
Large telescope offset (> 2 arcmin)	45 s
SGS loop closure after offsets	15 s
Derotator offset WFM	5 s + 0.11 s / degree
Derotator offset NFM (done in steps of 10 degrees if offset larger than 10 degrees)	5s + 1.1 s/degree
Attached calibration WFM	20s + 106s/flatfield + 112s/arc (1)
Attached calibration NFM	20s + 162s/flatfield + 148s/arc (1)
Return to origin	0 s if no offsets 15 s if there was no large offset 45 s if there was at least one large offset

[1]at least one arc per lamp is taken, making attached calibrations very “expensive.”

Execution time computations:

Example 1 : small telescope offsets, no PA offsets, no-AO mode

T_{total} = 360 s (preset) +
T_{acq} + 18 s (acquisition, 1 iteration) +
20 s (SGS loop closure) +
N x (15 s + UIT + 60 s) +
(N-1) x [5 s (intra-exposures delay) +
15 s (small telescope offset) +
10 s (SGS loop closure)]
+ 15 s (return to origin)

With T_{acq} the integration time of acquisition and UIT the integration time of each of the N exposures (assuming identical UITs).

Example 2: large telescope offsets and 90 degrees PA offsets between exposures in WFM-AO mode

T_{total} = 360 s (preset)+
T_{acq} + 18 s (acquisition, 1 iteration) +
180s (AO loops closure) +
20 sec (SGS loop closure) +
N x (15 s + UIT + 60 s) +
(N-1) x [5 s (intra-exposures delay) +
45 s (large telescope offset) +
5 s +
0.11 s x 90 (rotation) +
10 s (SGS loop closure)] +
45 s (return to origin)

With T_{acq} the integration time of acquisition and UIT the integration time of each of the N exposures (assuming identical UITs).

An alternative easy way to calculate the overhead is to create a MUSE mock OB by using the p2 demo in

https://www.eso.org/p2demo/home

Under the MUSE programme ID 60.A-9253(R) users can find a folder named USD Tutorials containing example OBs specifically designed for different observing strategies. By copying one of such OBs into a new one, the user is able to change the exposure times,

as well as the offsets and then to run the time calculator software in order to get the total integration and execution time. In Phase 1, users must provide the total execution time, which is given by the total exposures time plus overheads.

We request that during Phase 1 service mode users divide their total shutter open time for each target into one hour OBs using p2 and provide this info in the Time Justification section of the proposal.

At Phase 2, service mode users are strongly invited to check carefully the SM guidelines available at:

http://www.eso.org/sci/observing/phase2/SMGuidelines.MUSE.html

6 Templates

The table below show a summary of the available templates.

Table 16: Available templates summary.

Template name	Section	Comment
Acquisition templates		
MUSE_wfm-noao_acq_preset	6.1.1	Simple preset in WFM-NOAO
MUSE_wfm-noao_acq_movetopixel	6.1.2	To adjust pointing in WFM-NOAO
MUSE_wfm-noao_acq_presetRRM	6.1.3	For RRM use.
MUSE_wfm-ao_acq_movetopixelLGS	6.1.4	WFM-AO modes acquisition
MUSE_nfm-ao_acq_LGS	6.1.5	NFM-AO-N mode acquisition
Observation templates		
MUSE_wfm-noao_obs_genericoffset	6.2.1	Observation in WFM-NOAO modes
MUSE_wfm-ao_obs_genericoffsetLGS	6.2.2	Observation in WFM-AO modes
MUSE_nfm-ao_obs_genericoffsetLGS	6.2.3	Observations in NFM-AO-N mode
Night calibration templates (these templates are usually not needed by the users. The observatory provides)		
MUSE_wfm_cal_twilight	6.3.1.1	
MUSE_wfm_cal_specphot	6.3.1.2	
MUSE_wfm_cal_telluric	6.3.1.3	
MUSE_wfm_cal_astrom	6.3.1.4	
MUSE_nfm_cal_twilight	6.3.1.5	
MUSE_nfm_cal_specphot	6.3.1.6	
MUSE_nfm_cal_telluric	6.3.1.7	
MUSE_nfm_cal_astrom	6.3.1.8	
Attached night lamp calibrations template		
MUSE_cal_nightcalib	6.3.1.9	
Day calibration templates (also, not usually needed by users. Presented for completeness)		
MUSE_cal_bias	6.3.2.1	
MUSE_wfm_cal_specflat	6.3.2.2	
MUSE_wfm_cal_wave	6.3.2.3	
MUSE_nfm_cal_specflat	6.3.2.4	
MUSE_nfm_cal_wave	6.3.2.5	
Long term calibrations (output of these calibration observations is provided as part of static set of calibrations)		

MUSE_cal_dark	6.3.3.1	
MUSE_wfm_cal_geometry		Execute after astrometry.
MUSE_wfm_cal_wavelsf		To determine LSF
MUSE_nfm_cal_wavelsf		To determine LSF

6.1 MUSE acquisition templates

Full details on acquisition are provided in Section 0, including the parameters to define in p2. The main parameters of the acquisition are the instrument mode, position angle, exposure time for the acquisition, use of SGS (for WFM), and (optionally) definition of telescope guide star (WFM and NFM) and/or blind offsets (for WFM only).

6.1.1 MUSE_wfm-noao_acq_preset template signature file

MUSE_wfm-noao_acq_preset.tsf		
KEYWORD	**Range (Default)**	**Label in p2**
To be specified		
SEQ.SGS	T F (T)	Start slow-guiding?
TEL.TARG.OFFSETALPHA	-300..300 (0.0)	Alpha offset for the target (arcsec)
TEL.TARG.OFFSETDELTA	-300..300 (0.0)	Delta offset for the target (arcsec)
TEL.AG.GUIDESTAR	CATALOGUE/SETUPFILE/NONE (CATALOGUE)	Get Guide Star from
TEL.GS1.ALPHA	0....240000 (000000.000)	RA guide star (as HHMMSS.TTT)
TEL.GS1.DELTA	-900000..900000(000000.000)	DEC of guide star (as +-DDMMSS.TTT)
INS.DROT.POSANG	0....360 (0)	Position Angle on Sky (deg)
INS.MODE	WFM-NOAO-E, WFM-NOAO-N	Instrument Mode

6.1.2 MUSE_wfm-noao_acq_movetopixel template signature file

MUSE_wfm-noao_acq_movetopixel.tsf		
KEYWORD	**Range (Default)**	**Label in p2**
To be specified		
DET.UIT1	0.0..3600 (1)	Integration Time (seconds)
SEQ.SGS	T F (T)	Start slow-guiding?
TEL.TARG.OFFSETALPHA	-300..300 (0.0)	Alpha offset for the target (arcsec)
TEL.TARG.OFFSETDELTA	-300..300 (0.0)	Delta offset for the target (arcsec)
TEL.AG.GUIDESTAR	CATALOGUE/SETUPFILE/NONE (CATALOGUE)	Get Guide Star from
TEL.GS1.ALPHA	0....240000 (000000.000)	RA guide * (as HHMMSS.TTT)

TEL.GS1.DELTA	-900000.....900000 (000000.000)	DEC guide * (as +-DDMMSS.TTT)
INS.DROT.POSANG	0.0....360 (0)	Position Angle on Sky (deg)
INS.MODE	WFM-NOAO-E, WFM-NOAO-N	Instrument Mode

6.1.3 MUSE_wfm-noao_acq_presetRRM template signature file

This template should be used for rapid response mode, when observation of highly time critical targets is desired.

MUSE_wfm-noao_acq_presetRRM.tsf		
KEYWORD	**Range (Default)**	**Label in p2**
To be specified		
SEQ.SGS	T F (T)	Start slow-guiding?
TEL.TARG.OFFSETALPHA	-300..300 (0.0)	Alpha offset for the target (arcsec)
TEL.TARG.OFFSETDELTA	-300..300 (0.0)	Delta offset for the target (arcsec)
TEL.AG.GUIDESTAR	CATALOGUE/SETUPFILE/NONE (CATALOGUE)	Get Guide Star from
TEL.GS1.ALPHA	0....240000 (000000.000)	RA of guide star (as HHMMSS.TTT)
TEL.GS1.DELTA	-900000..900000 (000000.000)	DEC of guide star (as +-DDMMSS.TTT)
INS.DROT.POSANG	0....360 (0)	Position Angle on Sky (deg)
INS.MODE	WFM-NOAO-E, WFM-NOAO-N (WFM-NOAO-N)	Instrument Mode
Hidden		
SEQ.RRM.REGISTER	T, F (T)	(Register OB in RRM)
SEQ.RRM.VISITOR	T, F (T)	(Allow RRM activation in VM)

6.1.4 MUSE_wfm-ao_acq_movetopixelLGS template signature file

MUSE_wfm-ao_acq_movetopixelLGS.tsf		
KEYWORD	**Range (Default)**	**Label in p2**
To be specified		
DET.UIT1	0..3600 (1)	Integration Time (seconds)
SEQ.SGS	T F (T)	Start slow-guiding?
TEL.TARG.OFFSETALPHA	-300..300 (0.0)	Alpha offset for the target (arcsec)
TEL.TARG.OFFSETDELTA	-300..300 (0.0)	Delta offset for the target (arcsec)
TEL.AG.GUIDESTAR	CATALOGUE/SETUPFILE/NONE (CATALOGUE)	Get Guide Star from
TEL.GS1.ALPHA	0….240000 (000000.000)	RA of guide star (as HHMMSS.TTT)
TEL.GS1.DELTA	-900000…..900000 (000000.000)	DEC of guide star (as +-DDMMSS.TTT)
SEQ.AO.TTS	T F (T)	Perform acquisition with TTS
TEL.TTS1.ALPHA	0….240000 (000000.000)	RA of Tip-tilt star (as HHMMSS.TTT)
TEL.TTS1.DELTA	-900000…..900000 (000000.000)	DEC of Tip-tilt star (as +-DDMMSS.TTT)
TEL.TTS1.RMAG	6..18.5	Mag. of Tip-tilt star
TEL.TTS2.ALPHA	0….240000 (000000.000)	RA of alternative Tip-tilt star (as HHMMSS.TTT)
TEL.TTS2.DELTA	-900000…..900000 (000000.000)	DEC of alternative Tip-tilt star (as +-DDMMSS.TTT)
TEL.TTS2.RMAG	6..18.5	Mag. of alternative Tip-tilt star
INS.DROT.POSANG	0….360 (0)	Position Angle on Sky (deg)
INS.MODE	WFM-AO-E, WFM-AO-N (WFM-AO-N)	Instrument Mode

6.1.5 MUSE_nfm-ao_acq_LGS template signature file

MUSE_nfm-ao_acq_LGS.tsf		
KEYWORD	**Range (Default)**	**Label in p2**
To be specified		
DET.UIT1	0..3600 (1)	Integration Time (seconds)
TEL.AG.GUIDESTAR	CATALOGUE/SETUPFILE/NONE (CATALOGUE)	Get Guide Star from
TEL.GS1.ALPHA	0....240000 (000000.000)	RA of guide star (as HHMMSS.TTT)
TEL.GS1.DELTA	-900000.....900000 (000000.000)	DEC of guide star (as +-DDMMSS.TTT)
SEQ.NGS.ALPHA	0....240000 (000000.000)	RA of Natural Guide object (as HHMMSS.TTT)
SEQ.NGS.DELTA	-900000.....900000 (000000.000)	DEC of Natural Guide object (as +-DDMMSS.TTT)
SEQ.NGS.MAG	4..19.5	J Mag. of the Natural Guide object
SEQ.NGS.COLOR	0.	Color of on-axis guide object
SEQ.NGS.EXTENDED	T F (NODEFAULT)	Specify if the guide object is extended or not
INS.DROT.POSANG	0....360 (0)	Position Angle on Sky (deg)

6.2 Observation Templates Tables

Full details on observing templates are provided in Section 5.4, including the main parameters to define in p2, in particular the definitions and conventions for offsets.

6.2.1 MUSE_wfm-noao_obs_genericoffset template signature file

MUSE_wfm-noao_obs_genericoffset.tsf		
KEYWORD	**Range (Default)**	**Label in p2**
To be specified		
SEQ.NEXPO	1..1000 (1)	Number of exposures per offset
SEQ.NOFF	1..100 (NODEFAULT)	Total number of offsets
SEQ.OBSTYPE.LIST	O S (O)	Observation type list, O/S
SEQ.OFFSET.COORDS	SKY DETECTOR (SKY)	Offset coordinate type selection
SEQ.OFFSET.POSANG.LIST	-360..+360 (0)	List of relative offsets in position angle (deg)
SEQ.OFFSET1.LIST	-600..600 (NODEFAULT)	List of relative offsets in RA or X (arcsec)
SEQ.OFFSET2.LIST	-600..600 (NODEFAULT)	List of relative offsets in DEC or Y (arcsec)
SEQ.UIT.LIST	0..3600 (NODEFAULT)	List of UITs
SEQ.RETURN	T F (T)	Return to origin?

6.2.2 MUSE_wfm-ao_obs_genericoffsetLGS template signature file

MUSE_wfm-ao_obs_genericoffsetLGS.tsf		
KEYWORD	**Range (Default)**	**Label in p2**
To be specified		
SEQ.NEXPO	1..1000 (1)	Number of exposures per offset
SEQ.NOFF	1..100 (NODEFAULT)	Total number of offsets
SEQ.OBSTYPE.LIST	O S (O)	Observation type list, O/S
SEQ.OFFSET.COORDS	SKY DETECTOR (SKY)	Offset coordinate type selection
SEQ.OFFSET.POSANG.LIST	-360..+360 (0)	List of relative offsets in position angle (deg)
SEQ.OFFSET1.LIST	-600..600 (NODEFAULT)	List of relative offsets in RA or X (arcsec)
SEQ.OFFSET2.LIST	-600..600 (NODEFAULT)	List of relative offsets in DEC or Y (arcsec)
SEQ.UIT.LIST	0..3600 (NODEFAULT)	List of UITs
SEQ.RETURN	T F (T)	Return to origin?

6.2.3 MUSE_nfm-ao_obs_genericoffsetLGS template signature file

MUSE_nfm-ao_obs_genericoffsetLGS.tsf		
KEYWORD	**Range (Default)**	**Label in p2**
To be specified		
SEQ.NEXPO	1..1000 (1)	Number of exposures per offset
SEQ.NOFF	1..100 (NODEFAULT)	Total number of offsets
SEQ.OBSTYPE.LIST	O S (O)	Observation type list, O/S
SEQ.OFFSET.COORDS	SKY DETECTOR (SKY)	Offset coordinate type selection
SEQ.OFFSET.POSANG.LIST	-360..+360 (0)	List of relative offsets in position angle (deg)
SEQ.OFFSET1.LIST	-600..600 (NODEFAULT)	List of relative offsets in RA or X (arcsec)
SEQ.OFFSET2.LIST	-600..600 (NODEFAULT)	List of relative offsets in DEC or Y (arcsec)
SEQ.UIT.LIST	0..3600 (NODEFAULT)	List of UITs
SEQ.RETURN	T F (T)	Return to origin?

6.3 Calibration Templates Tables

6.3.1 Night calibration templates

6.3.1.1 MUSE_wfm_cal_twilight template signature file

This template is used to perform the twilight flat calibration.

MUSE_wfm_cal_twilight.tsf		
KEYWORD	**Range (Default)**	**Label in p2**
To be specified		
SEQ.ADU.TARGET	1..60000 (21000)	Target number of counts
SEQ.DROT.POSANG	0..360 (0)	Position angle on sky (deg)
SEQ.UIT.START.DUSK	0.1..600 (1.0)	Start integration times at twilight time (s)
SEQ.NEXPO	1..1000 (10)	Maximum number of exposures
INS.MODE	WFM-NOAO-E WFM-NOAO-N WFM-AO-E WFM-AO-N (NODEFAULT)	Instrument Mode

6.3.1.2 MUSE_wfm_cal_specphot template signature file

This template is used to perform all WFM spectrophotometric standard star calibration.

MUSE_wfm_cal_specphot.tsf		
KEYWORD	**Range (Default)**	**Label in p2**
To be specified		
DET.UIT1	0.1..3600 (NODEFAULT)	Integration Time (seconds)
SEQ.NEXPO	1..1000 (1)	Number of exposures per offset
SEQ.NOFF	1..100 (1)	Total number of offsets
SEQ.OBSTYPE.LIST	O S (O)	Observation type list, O/S
SEQ.OFFSET.COORDS	SKY DETECTOR (DETECTOR)	Offset coordinate type selection
SEQ.OFFSET.POSANG.LIST	-360..360 (0)	List of relative offsets in Position Angle (deg)
SEQ.OFFSET1.LIST	-600..600 (0)	List of relative offsets in RA or X
SEQ.OFFSET2.LIST	-600..600 (0)	List of relative offsets in DEC or Y
SEQ.RETURN	T F (T)	Return to origin?
INS.MODE	WFM-NOAO-E WFM-NOAO-N WFM-AO-E WFM-AO-N (SAMEAS)	Instrument mode to calibrate

6.3.1.3 MUSE_wfm_cal_telluric template signature file

This template is used to perform a telluric standard star calibration.

MUSE_wfm_cal_telluric.tsf		
KEYWORD	**Range (Default)**	**Label in p2**
To be specified		
DET.UIT1	0.1..3600 (NODEFAULT)	Integration Time (seconds)
SEQ.NEXPO	1..1000 (1)	Number of exposures per offset
SEQ.NOFF	1..100 (1) (NODEFAULT)	Total number of offsets
SEQ.OBSTYPE.LIST	O S (O)	Observation type list, O/S
SEQ.OFFSET.COORDS	SKY DETECTOR (DETECTOR)	Offset coordinate type selection
SEQ.OFFSET.POSANG.LIST	-360..360 (0)	List of relative offsets in Position Angle (deg)
SEQ.OFFSET1.LIST	-600..600 (0)	List of relative offsets in RA or X (arcsec)
SEQ.OFFSET2.LIST	-600..600 (0)	List of relative offsets in DEC or Y (arcsec)
SEQ.RETURN	T F (T)	Return to origin?
INS.MODE	WFM-NOAO-E WFM-NOAO-N WFM-AO-E WFM-AO-N (SAMEAS)	Instrument mode to calibrate

6.3.1.4 MUSE_wfm_cal_astrom template signature file

This template is used to perform the astrometric calibration, on a regular basis.

MUSE_wfm_cal_astrom.tsf		
KEYWORD	**Range (Default)**	**Label in p2**
To be specified		
SEQ.UIT.LIST	0..3600 (NODEFAULT)	List of UITs
SEQ.NEXPO	1..1000 (1)	Number of exposures per offset
SEQ.NOFF	1..100 (NODEFAULT)	Total number of offsets
SEQ.OBSTYPE.LIST	O S (O)	Observation type list, O/S
SEQ.OFFSET.COORDS	SKY DETECTOR (SKY)	Offset coordinate type selection
SEQ.OFFSET.POSANG.LIST	-360..360 (0)	List of relative offsets in Position Angle (deg)
SEQ.OFFSET1.LIST	-600..600 (0)	List of relative offsets in RA or X (arcsec)
SEQ.OFFSET2.LIST	-600..600 (0)	List of relative offsets in DEC or Y (arcsec)
SEQ.RETURN	T F (T)	Return to origin?

6.3.1.5 MUSE_nfm_cal_twilight template signature file

This template is used to perform the twilight flat calibration. Note that the target number of counts refers to the average over the frame. Typically, we can have peak counts near 50,000 ADUs and at the wavelength extremes near 5,000 ADUs. These values are obtained with a target number of counts of 30,000 ADUs, approx..

MUSE_nfm_cal_twilight.tsf		
KEYWORD	**Range (Default)**	**Label in p2**
To be specified		
SEQ.ADU.TARGET	1..60000 (21000)	Target number of counts
SEQ.DROT.POSANG	0..360 (0)	Position angle on sky (deg)
SEQ.UIT.START.DUSK	0.1..600 (1.0)	Start integration times at twilight time (s)
SEQ.NEXPO	1..1000 (10)	Maximum number of exposures

6.3.1.6 MUSE_nfm_cal_specphot template signature file

This template is used to perform a NFM spectrophotometric standard star calibration.

MUSE_nfm_cal_specphot.tsf		
KEYWORD	**Range (Default)**	**Label in p2**
To be specified		
DET.UIT1	0.1..3600 (NODEFAULT)	Integration Time (seconds)
SEQ.NEXPO	1..1000 (1)	Number of exposures per offset
SEQ.NOFF	1..100 (1)	Total number of offsets
SEQ.OBSTYPE.LIST	O S (O)	Observation type list, O/S
SEQ.OFFSET.COORDS	SKY DETECTOR (DETECTOR)	Offset coordinate type selection
SEQ.OFFSET.POSANG.LIST	-360..360 (0)	List of relative offsets in Position Angle (deg)
SEQ.OFFSET1.LIST	-600..600 (0)	List of relative offsets in RA or X
SEQ.OFFSET2.LIST	-600..600 (0)	List of relative offsets in DEC or Y
SEQ.RETURN	T F (T)	Return to origin?

6.3.1.7 MUSE_nfm_cal_telluric template signature file

This template is used to perform a telluric standard star calibration in NFM. Note that the mode is not selectable as there is a single NFM: NFM-AO-N.

MUSE_nfm_cal_telluric.tsf		
KEYWORD	**Range (Default)**	**Label in p2**
To be specified		
DET.UIT1	0.1..3600 (NODEFAULT)	Integration Time (seconds)
SEQ.NEXPO	1..1000 (1)	Number of exposures per offset
SEQ.NOFF	1..100 (1) (NODEFAULT)	Total number of offsets
SEQ.OBSTYPE.LIST	O S (O)	Observation type list, O/S
SEQ.OFFSET.COORDS	SKY DETECTOR (SKY)	Offset coordinate type selection
SEQ.OFFSET.POSANG.LIST	-360..360 (0)	List of relative offsets in Position Angle (deg)
SEQ.OFFSET1.LIST	-600..600 (0)	List of relative offsets in RA or X (arcsec)
SEQ.OFFSET2.LIST	-600..600 (0)	List of relative offsets in DEC or Y (arcsec)
SEQ.RETURN	T F (T)	Return to origin?

6.3.1.8 MUSE_nfm_cal_astrom template signature file

This template is used to perform the NFM astrometric calibration.

MUSE_nfm_cal_astrom.tsf		
KEYWORD	**Range (Default)**	**Label in p2**
To be specified		
SEQ.UIT.LIST	0..3600 (NODEFAULT)	List of UITs
SEQ.NEXPO	1..1000 (1)	Number of exposures per offset
SEQ.NOFF	1..100 (NODEFAULT)	Total number of offsets
SEQ.OBSTYPE.LIST	O S (O)	Observation type list, O/S
SEQ.OFFSET.COORDS	SKY DETECTOR (SKY)	Offset coordinate type selection
SEQ.OFFSET.POSANG.LIST	-360..360 (0)	List of relative offsets in Position Angle (deg)
SEQ.OFFSET1.LIST	-600..600 (0)	List of relative offsets in RA or X (arcsec)
SEQ.OFFSET2.LIST	-600..600 (0)	List of relative offsets in DEC or Y (arcsec)

SEQ.RETURN	T F (T)	Return to origin?

6.3.1.9 MUSE_cal_nightcalib.tsf

This template replaces the two deprecated templates below starting in P102.
These templates perform wavelength and internal flat calibration directly following science exposures, at the same telescope and derotator position. These calibrations are useful when a very accurate wavelength or flat-field correction is necessary for the science observations, and they are charged to the user's programme.

MUSE_cal_nightcalib.tsf		
KEYWORD	**Range (Default)**	**Label in p2**
To be specified		
SEQ.ARC	T F (T)	Attached night arcs?
SEQ.FLATFIELD	T F (T)	Attached night flat fields
SEQ.NARCS	1…5 (1)	Number of arcs per arc lamp
SEQ.NFLATS	1…10 (1)	Number of flats

6.3.1.10 MUSE_wfm_cal_waveatt DEPRECATED in P102

This template is the equivalent of MUSE_wfm_cal_wave in case of attached calibration.
The default values are those used during the daily calibrations.

MUSE_wfm_cal_waveatt.tsf		
KEYWORD	**Range (Default)**	**Label in p2**
To be specified		
SEQ.LAMP3.UIT	0..3600 (0.7)	Integration time on Neon penray lamp (s)
SEQ.LAMP4.UIT	0..3600 (19)	Integration time on Xenon penray lamp (s)
SEQ.LAMP5.UIT	0..3600 (1)	Integration time on HgCd High Power lamp (s)
SEQ.LAMP6.UIT	0..3600 (0)	Integration time on Neon High Power lamp (s)
SEQ.NEXPO	1..1000 (3)	Total number of exposures

6.3.1.11 MUSE_wfm_cal_specflatatt DEPRECATED in P102

This template is the equivalent of MUSE_wfm_cal_specflat in case of attached calibration. The default values are those used during the daily calibrations.

MUSE_wfm_cal_specflatatt.tsf		
KEYWORD	**Range (Default)**	**Label in p2**
To be specified		
DET.UIT1	0..3600 (0.35)	Integration Time (seconds)
SEQ.NEXPO	1..1000 (4)	Total number of exposures
SEQ.DROT	0.0..360.0 (0.0)	Derotator pos. angle (+- DDD.TTT)

6.3.2 Daily daytime calibration templates

6.3.2.1 MUSE_cal_bias template signature file

Parameters for bias exposures include number of biases to be taken and the binning factor (always 1 for science exposure).

MUSE_cal_bias.tsf		
KEYWORD	**Range (Default)**	**Label in p2**
To be specified		
SEQ.NEXPO	1..1000 (11)	Total number of exposures

6.3.2.2 MUSE_wfm_cal_specflat template signature file

This template is used to perform the daily flat-field calibration, as described in Section 7.1

MUSE_wfm_cal_specflat.tsf		
KEYWORD	**Range (Default)**	**Label in p2**
To be specified		
DET.UIT1	0..3600 (0.35)	Integration time in seconds
SEQ.NEXPO	1..1000 (4)	Total number of exposures
INS.MODE	WFM-NOAO-E WFM-NOAO-N WFM-AO-E WFM-AO-N (NODEFAULT)	Instrument Mode
SEQ.LAMP.SWITCHOFF	T F (T)	Switch off the calibration lamps?

6.3.2.3 MUSE_wfm_cal_wave template signature file

This template is used to perform the daily wavelength calibration, as described in Section 7.1

MUSE_wfm_cal_wave.tsf		
KEYWORD	**Range (Default)**	**Label in p2**
To be specified		
SEQ.LAMP3.UIT	0..3600 (0.88)	Integration time on Neon penray lamp (s)
SEQ.LAMP4.UIT	0..3600 (12)	Integration time on Xenon penray lamp (s)
SEQ.LAMP5.UIT	0..3600 (0.65)	Integration time on HgCd High Power lamp (s)
SEQ.LAMP6.UIT	0..3600 (0)	Integration time on Neon High Power lamp (s)
SEQ.NEXPO	1..1000 (5)	Total number of exposures
INS.MODE	WFM-NOAO-N WFM-NOAO-E WFM-AO-E WFM-AO-N (NODEFAULT)	Instrument Mode
SEQ.LAMP.SWITCHOFF	T F (T)	Switch off the calibration lamps?

6.3.2.4 MUSE_nfm_cal_specflat template signature file

This template is used to perform the daily flat-field calibration, as described in Section 7.1

MUSE_nfm_cal_specflat.tsf		
KEYWORD	**Range (Default)**	**Label in p2**
To be specified		
DET.UIT1	0..3600 (30)	Integration time in seconds
SEQ.NEXPO	1..1000 (4)	Total number of exposures

6.3.2.5 MUSE_nfm_cal_wave template signature file

This template is used to perform the daily wavelength calibration, as described in Section 7.1. Note that LAMP3 corresponds to Ne, LAMP4 to Xe, and LAMP5 to HgCd.

MUSE_nfm_cal_wave.tsf		
KEYWORD	**Range (Default)**	**Label in p2**
To be specified		
SEQ.LAMP3.UIT	0..3600 (7)	Integration time on Neon penray lamp (s)
SEQ.LAMP4.UIT	0..3600 (190)	Integration time on Xenon penray lamp (s)
SEQ.LAMP5.UIT	0..3600 (8)	Integration time on HgCd High Power lamp (s)
SEQ.LAMP6.UIT	0..3600 (0)	Integration time on Neon High Power lamp (s)
SEQ.NEXPO	1..1000 (5)	Total number of exposures

6.3.3 Long-term daytime calibration templates

6.3.3.1 MUSE_cal_dark template signature file

This template is used to perform dark calibrations.

MUSE_cal_dark.tsf		
KEYWORD	**Range (Default)**	**Label in p2**
To be specified		
DET.UIT1	0..3600 (3600)	Integration time (seconds)
SEQ.NEXPO	1..1000 (3)	Total number of exposures

6.3.3.2 MUSE_wfm_cal_geometry template signature file

This template is used to perform the geometrical calibration, as described in Section 7.1. It should be noted that the geometrical calibration goes in pair with the astrometrical calibration. The RMS of the WCS solution gives an indication of the overall quality of the field reconstruction.

MUSE_wfm_cal_geometry		
KEYWORD	**Range (Default)**	**Label in p2**
To be specified		
SEQ.NEXPO	1..1000 (80)	Total number of exposures
SEQ.ONTIME.LIST	"(40 0 40 0)"	List of lamp on time (s) (Neon Penray, Xenon Penray, HgCd, Neon High Power)
SEQ.YSHIFT	0..40.767 (0.069)	Y offset applied on the mask (arcsecs)
INS.MODE	WFM-NOAO-E WFM-NOAO-N (NODEFAULT)	Instrument Mode

Page left intentionally almost blank

7 Calibrating and Reducing MUSE data

7.1 MUSE calibration plan

Calibration	Number of exposures	Frequency	Phase	Purpose
Bias	11	Daily	Day	Master bias, bias characteristics
Dark	5x20 min	Monthly	Day	Master dark, dark current
Flat-field with continuum lamp	11	Daily (a)	Day	Illumination correction, Tracing solution, Background light, Instrument throughput
Wavelength	5 per lamp: Ne, Xe, HgCd	Daily (a)	Day	Wavelength solution Dispersion characteristics
Line Spread Function	15 per lamp: Ne, Xe, HgCd	90 days	Day	For monitoring. It is recommended to use the daily arcs for LSF computation
Geometrical calibration: multi-Pinhole mask with arc lamps (HgCd and Neon Penray together)	70	90 days	Day	Relative location of the slices. WFM and NFM use same calibrations.
Flat-field with sky	>3	Weekly	Twilight	Illumination correction
Flat field illumination correction	1 (b)	Every 1-2h	Night	To account for temperature variations of Illumination correction.
Attached Flat-field with continuum lamp	N (c)I	On request	Night	High-precision flat-fielding
Attached Wavelength	N (cb)	On request	Night	High-precision wavelength solution
SPECTROPHOTOMETRIC CALIBRATION	1	(d)	Night	Absolute flux calibration Telluric correctionI(e)
ASTROMETRY	1	90 days	Night	Astrometric model

Table 17: *MUSE Calibration plan*

(a) WFM-NOAO-E done every day starting P101. All other modes are done if observed the previous night.
(b) During WFM-NOAO Science Verification, normal flat-field calibrations were also done between 1 to 3 times per night depending on temperature variations. Now we are obtaining approximately every 1-2 hours a very short flat in nominal mode for illumination correction in both modes.
(c) The number of exposures is defined by the user in template MUSE_cal_nightcalib.
(d) During clear or photometric nights in which MUSE science OBs are executed
(e) Note that we do not observe a telluric star right after or before each exposure. If a telluric star is desired, then the user must provide it and the time will be charged to the program. OBX files of our standard stars can be found in the Tools section of the MUSE web pages (http://www.eso.org/sci/facilities/paranal/instruments/muse/tools.html).

We summarize in Table 11 the main calibrations performed as part of the standard calibration plan for MUSE. These calibrations are performed on a regular basis. Note that WFM and NFM modes do not share same calibrations except for bias, darks, and the geometry calibration.

7.1.1 Wavelength calibration

Wavelength calibration is performed on a daily basis. For each MUSE instrument mode used in science observations, 5 exposures are taken with each of the 3 available arc lamps (HgCd, Xe, Ne) illuminating the entire FOV. The location of these reference emission lines on the detector is used by the pipeline to derive an overall wavelength solution. Details on the emission line wavelengths are provided for each lamp as a reference in Table 20 to Table 22.

Using the new MUSE_cal_nightcalib template MUSE observers can submit an “attached” wavelength calibration to be performed directly following their science observation (not recommended).

7.1.2 Flat-field calibration

Every day and for each MUSE instrument mode used in science observation, 11 exposures are taken with the continuum lamp illuminating the entire FOV. The data reduction software uses these exposures to estimate the tracing solution, as well as the illumination and throughput as a function of position and wavelength.

During Science Verification, in addition to the daily calibrations, flat-field calibration observations were performed on a nightly basis, at a frequency of 1 to 3 times per night depending on temperature variations. After analysing the 2nd Commissioning observations of MUSE we have determined that a full set of flats is not necessary for the appropriate correction of the science data, and that instead we can use illumination correction observations taken during the night. These observations account for any temperature dependence of the flat field. See below.

Using the new MUSE_cal_nightcalib template MUSE observers can submit an “attached” flat-field calibration to be performed with the continuum lamp directly following their science observation (not recommended).

7.1.3 Nightly illumination correction

Every hour the system asks the observer to obtain an illumination correction observation. This is a single flat field in Nominal mode which is used by the pipeline to correct for any temperature variation in the illumination pattern of the slices of the individual channels. The service mode or visitor mode users do not need to provide an OB for this calibration.

7.1.4 Twilight sky flat calibration

This calibration takes evening twilight exposures to correct for overall illumination on sky.

Exposures are taken according to the sky brightness:

- a reference exposure is taken, and the average ADU level is estimated.
- Depending on this level, we estimate the integration time for the next exposure required in order to maintain a constant (and high) ADU level.
- This sequence is continued until the conditions are no longer appropriate for twilight exposures or the maximum number of exposures to be taken is reached (whichever comes first)

7.1.5 Geometrical (spatial) calibration

Geometrical calibration is performed monthly. Both WFM and NFM share the same geometrical calibration which is taken in WFM. The instrument is set up in WFM with a multi-pinhole mask (WFM_SMP) covering the entire FOV (more details on this mask are given for reference in Section 8.3). The mask is translated vertically by 0.034" between each exposure, and a total of 70-80 exposures are taken to fully cover all slices by the pinholes.

These exposures are analysed by the DRS to derive the relative location and orientation of each slice in each channel. Already processed geometry tables will be provided in the instrument package.

7.1.6 Spectro-photometric calibration

The spectro-photometric calibration is performed daily, whenever possible (i.e. under photometric conditions), using observations of a field containing a spectrophotometric standard star. Several high SNR exposures (~ 10 000 ADU at peak) of the star are used to derive the flux calibration curve. The stars used for this calibration are taken from the reference list of standard stars:

https://www.eso.org/sci/observing/tools/standards/spectra.html

Note that the peak flux level can vary depending on the seeing at the time of the exposure. The level mentioned above is for approximately 1" seeing. The user can expect variations by a factor of two above or below this level depending on conditions at the time of the observations.
If the science has been observed under no photometric conditions, and as such no spectro-photometric calibration has been obtained, user should use the standard star frame part of the pipeline static calibrations.

7.1.7 Telluric correction and PWV constraint

Bands of O_2 at ~580 nm, δ, 629 nm, γ, 688 nm, B, and 759 – 771 nm, the strong A-band, are present in the spectrum of MUSE, and nothing can be done to avoid them and should be corrected by the observation of a telluric star. Telluric absorption features of H_2O are also present and are stronger at wavelengths longer than 700 nm, albeit not nearly as problematic as in the JHK NIR bands. Although for O_2 not much can be done, the user can exercise some level of control over the amount of H_2O absorption by using the constraint on precipitable water vapour, PWV, when creating OBs at Phase 2. The median value at Paranal is 2.5 mm of H_2O, and any user intending to request a value below the median will need to request a waiver with a proper scientific justification.[6] The effect in the transmission in the most affected wavelength windows can be seen in Figure 48.

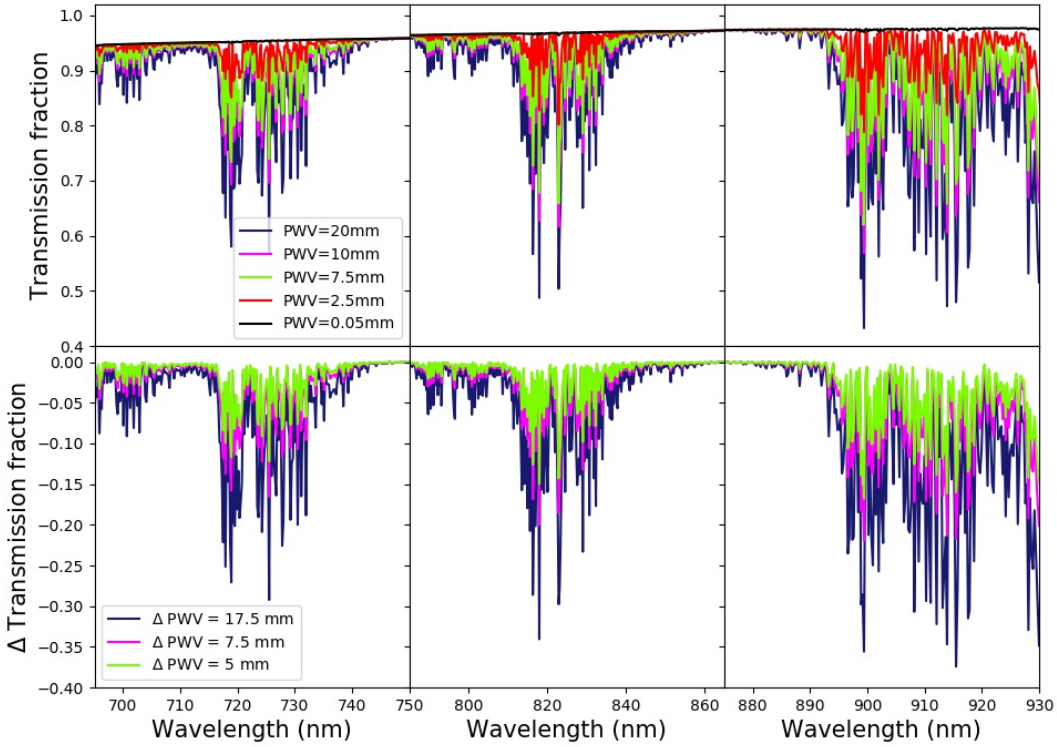


Figure 48 *Water vapour telluric absorption. The top panels show the fractional atmospheric transmission as a function of wavelength for several values of PWV, while the bottom panels show for each PWV the absorption difference from the meadian Paranal value absorption at 2.5 mm of H_2O.*

[6] The ETC has been modified so that the user can experiment with different values of the PWV. Before P104 the ETC used by defect 10 mm of H_2O.

To correct the spectrum from telluric absorptions there are two options. The first one is the use of the observations of one of the specphot stars as discussed in the previous section. This option is fully backed by the pipeline as long as the star used is in the list of MUSE specphot standards, and the template used to observe it is MUSE_wfm__cal__telluric.

The second option is the use of the program Molecfit (Smette et al., 2015, A&A 576, A77) , Kausch et al., (2015, A&A 576, A78) to fit the telluric absorptions directly in the target spectrum.
Note that data from template MUSE_wfm_cal_telluric can be processed by the MUSE pipeline as long as the star observed with this template is one of those supported. The External Verification Module (EVM) within p2 automatically checks that the target used with this template is a supported star. Additionally, from P98 onwards, esorex triggers a warning if it finds that the specro-photometric or telluric standard templates were carried out with non-supported stars. A list of supported stars can be found in Table 18 and in the MUSE pipeline manual (http://www.eso.org/sci/facilities/paranal/instruments/muse/doc.html).

Table 18: *List of spectrophotometric standard stars that are supported by the MUSE pipeline for telluric corrections.*

Star name	Ra (2000)	Dec (2000)	Comment
WD0308-565	03 09 48.241	-56:23:48.20	
EG21	03:10:31.153	-68:36:05.29	
GD71	05:52:27.614	15:53:13.750	
HD49798	06:48:04.690	-44:18:58.400	
LTT3218	08:41:32.500	-32:56:34.000	
GD108	10:00:47.254	-07:33:31.010	
GD153	12:57:02.337	22:01:52.680	
EG274	16:23:33.750	-39:13:47.500	
GJ754.1A	19:20:34.920	-07:40:00.070	EG131, very good telluric
LTT7987	20:10:56.846	-30:13:06.640	
LDS749B	21:32:16.239	00:15:14.400	
Feige110	23:19:58.398	-05:09:56.160	

7.2 MUSE data reduction

The output of an exposure with the instrument is a raw frame, which has the following multi-extension FITS format:

- **Primary extension (Extension 0, header only):** contains the keywords specific to the exposure and common to all channels, such as information about the observing program, telescope, overall instrument and weather conditions, etc. Note that some of the parameters monitored by the SGS system make it into keywords in the primary headers of the science images, the most important ones been OCS.SGS.FWHM.* and OCS.SGS.FLUX.*, that can be used to monitor the image quality and transparency during the exposure. But please note that the image quality monitoring keywords should be taken with caution because the SGS filter is very wide, and it is thus affected by atmospheric dispersion.
- **Extensions 1 to 24:** contains for each channel a short header (with information specific to the detector) and the image frame corresponding to this particular channel. The order of the extensions in the FITS file does not follow the order of the channel numbers so they should be addressed with their extension name CHAN01, CHAN02, CHAN03 …. CHAN22, CHAN23, CHAN24 corresponding to the channel number. The size of the image frame, in the absence of binning, is 4224 x 4240 (including the overscan regions, see Section 2.1.2.4.3).
- **Extensions beyond 24** (for science exposures) contain information from the SGS, Auto Guider (for WFM), and SPARTA subsystems (AO only), taken in parallel to the science exposures, when SGS is activated. The SGS will record images with the TCCD and produce stack median images every ~ 2 min. These median images can be averaged over the entire science exposure to give a deeper image of the region surrounding the MUSE FOV. The addition of these extensions have been an ongoing development, therefore they might not be present on older data. As of November 2019 the implemented extensions are:

    - **SGS_IMG (WFM mode):** an image of size 1024x1024 contains the average of all the stacked median images taken during the science exposure.
    - **SGS_CUBE (WFM mode):** a cube of 1024x1024xN pixels, containing all N stacked median images taken during the science exposures.
    - **SGS_DATA (WFM mode):** a FITS table containing information from the SGS system in the form of (4+NSTARSx10)xN entries, for the N measurements done using NSTARS (NSTARS<10) stars detected in the SGS. For each measurement, the 4 first columns give general information about the time and the offsets sent to the telescope, while the last 10 x NSTARS entries give information on each star.
    - **AG_DATA (WFM mode):** a FITS table containing information about the guide star (GS) from the telescope Auto Guider (AG). It contains three columns giving the time of the measurement, and the FWHM in x and y, with a typical periodicity of 11 to 45 seconds. If there is no SGS star these data can be used to check the image quality during the exposure.

- **ASM_DATA:** a FITS table containing the Atmospheric Site Monitoring (ASM) data
- **SPARTA_TT_ACQ_IMG (AO modes):** a FITS image of size 280x280 used to acquire the IRLOS NGS star.
- **SPARTA_ATM_DATA (AO modes):** a FITS table containing atmospheric turbulence information as determined by the SPARTA Real Time Computer.
- **SPARTA_CN2_DATA (AO modes):** a FITS table containing the atmospheric turbulence profile estimated by the SPARTA Real Time Computer.
- **SPARTA_TT_CUBE (AO modes):** a FITS cube showing a subsample of the TTS images obtained during the observations.

The MUSE Data Reduction Software (DRS) has been developed to fully reduce MUSE raw science observations using the associated calibrations. Data reduction is performed following a number of calibration recipes. The final output of the DRS is a FITS datacube (with RA, DEC and wavelength as the three axes), as well as a number of quality control (QC) parameters for each recipe. Full details on installing and using the MUSE DRS are provided in the MUSE Pipeline Manual, which can be found at the webpage below: https://www.eso.org/sci/facilities/paranal/instruments/muse/doc.html

Note that given the data volume and complexity of MUSE exposures, data reduction can be extremely resource intensive on computer architecture, especially on memory. It is not recommended that data be reduced on personal computer, rather a multi-core workstation with at the very least 32 GB RAM is recommended. However, for the end-cube production and combination of multiple datacubes a machine with at least 150 GB RAM is needed.

The MUSE pipeline is extensively described in the paper “The Data Processing Pipeline for the MUSE Instrument” by Weilbacher et al. 2020 (https://ui.adsabs.harvard.edu/abs/2020arXiv200608638W/abstract).

MUSE data are now processed by Quality Control Garching using the ESO calibration pipelines with the best available calibration data. The reduced datacubes (one per OB), as well as the combined multi-cubes (i.e. stack datacubes from multiple OBs) can be downloaded directly from the Phase 3 query form in the ESO Archive. However, it should be noted that for the AO cases (WFM-AO-N, WFM-AO-E and NFM) the reduced datacubes provided by the ESO Science Archive have being obtained without the use of the pipeline recipe specifically dedicated to the correction of the Raman lines. Users interested in the spectral regions affected by the Raman lines might have to process the raw data independently, including the Raman lines correction in the pipeline workflow.

Page left intentionally almost blank

8 Reference material

8.1 Detector cosmetics

We provide in Table 19 for reference the detectors showing 1 or several bad columns, with the corresponding region affected on the detector.

Table 19: List of defects identified for each detector (arranged by channel) by the MUSE pipeline as a DQ issue. Each detector is identified by its name (DET_ID) and associated IFU number. The last columns give (when relevant) the number of bad columns (bc), bad pixels (bp), and the rectangular region showing defects marked as [x1:x2,y1:y2] in pixel positions on the raw data frames.

CHANNEL	IFU	DET_ID	DET_INDEX	DQ Cosmetics
1	24	egeria	6	None
2	1	victoria	6	None
3	10	flora	6	2055bp(1bc) [1828,2058:4112]
4	4	juno	6	None
5	15	vesta	5	None
6	2	hebe	5	None
7	12	circe	5	6025bp(3bcs) [2800:2802,2057:4068]
8	3	massalia	5	None
9	18	thalia	4	None
10	20	lutetia	4	4111bp(2bcs) [2156,2057:4112]
11	21	parthenope	4	None
12	11	hygiea	4	2034bp(1bc) [1567,23:2056]
13	17	harmonia	3	2056bp(1bc) [1101,1:2056]
14	19	irene	3	None
15	15	astraea	3	None
16	8	pallas	3	None
17	7	thetis	2	None
18	16	iris	2	None
19	9	kalliope	2	None
20	6	fortuna	2	None
21	13	proserpina	1	2054bp(1bc) [1411,1:2054]
22	5	eunomia	1	2051bp(1bc) [2673,6:2056]
23	23	metis	1	None
24	22	melpomene	1	None

8.2 Arc lamps list

We provide in Table 20, Table 21 and Table 22 the list of lines identified in the arc lamps used for wavelength calibration.

8.2.1 HgCd arc lamp

Table 20: list of wavelengths and relative fluxes for the HgCd arc lamp.

Wavelength (Angstroms)	Relative Flux
4339.2232	30
4347.4945	80
4358.335	5500
4412.9894	2
4662.352	25
4678.1493	1200
4799.9123	3800
4916.068	85
4960.1	3
4980.64	0.5
5025.6	3
5045.8	0.5
5085.8217	7150
5120.637	0.5
5154.6605	32
5290.74	0.5
5316.776	1
5354.034	10
5365.5	0.5
5460.75	35000
5549.634	1
5675.81	8
5769.61	7000
5790.67	6600
5803.782	8
5859.254	4
5871.975	0.5
5890.2	1
6072.64	6
6099.1421	4
6111.495	2
6123.27	5
6234.36	18
6325.1661	11
6330.0133	2
6438.4695	2800
6716.34	15
6778.1157	1
6888.564	0.5
6907.46	160
6965	6
7067	8
7081.901	40
7091.86	13
7177.8	0.5
7269.9	2
7345.6704	25
7367.3	0.5
7372.5	1
7383.2	18
7397	4
7504.1	6
7514.8	8
7552.1	0.5
7603	2
7635.2	30
7675.2	2
7724.2	12
7728.825	22
7821.2	1
7948.2	10
8005	30
8006.1	2
8014.8	8
8067	3
8070.7	2
8013.8	10
8115.4	42
8163.4	1
8195.6	2
8200.3089	4
8264.2	8
8408.3	14
8424.5	13
8521.4	3
8625	140
8652.7	1
8758.1	6
8763	1
8773.1	0.5
8783.7	0.5
8887.5	0.5
8988.9	1
9039.2	1
9067.2	0.5
9123.1	10
9138	2
9243.1	5
9253.9	1
9255	15
9499	35

8.2.2 Xe arc lamp

Table 21: list of wavelengths and relative fluxes for the Xe arc lamp

Wavelength (Angstroms)	Relative Flux
4500.978	9
4524.6805	7
4582.7472	3
4603.03	1
4624.2756	33
4671.2258	70
4690.97	2
4697.0208	11
4734.1518	20
4792.619	4
4807.019	24
4829.708	15
4843.2934	13
4916.507	16
4923.152	21
4972.71	1
5028.2794	4
5044.92	0.5
5261.95	1
5292.22	2
5337.89	2
5392.795	1
5394.738	1
5418.02	2
5439.923	1
5440.39	1
5532.78	6
5552.385	1
5566.615	2
5567.77	2
5570.91	3
5697	3
5716	2
5824	7
5875.018	6
5889.12	1
5894.988	6
5934	7
5974.152	0.5
5978.29	0.5
5998.115	0.5
6030	4
6111.8	5
6163.8	6
6178.303	3
6179.665	10
6182.42	14
6198.26	5
6200.892	3
6201.49	2
6224.168	0.5
6261.212	1
6265.302	1
6273.23	0.5
6286.011	2
6293	3
6318.062	19
6333.97	0.5
6344.98	0.5
6355.77	0.5
6419	1
6469.705	12
6472.841	6
6487.765	7
6498.717	5
6504.2	7
6521.508	1
6533.159	3
6543.36	1
6554.196	4
6595.561	11
6608.87	0.5
6632.464	6
6668.4	20
6679.8	2
6728.008	30
6767.12	1
6778	6
6827.315	25
6846.8	8
6860.19	1
6866.838	6
6872.107	18
6882.155	50
6910.82	1
6925.53	7
6935.8	4
6976.182	12
6982.05	2
6991.65	0.5
7019.02	4
7035.53	1
7048	5
7078.46	0.5
7119.598	110
7136.57	0.5
7200.79	1
7244.94	4
7257.94	10
7262.54	3
7266.49	7
7284.7	38
7316.272	27
7321.452	22
7336.48	15
7355.58	8
7386.003	29
7393.793	36
7400.41	8
7424.05	3
7441.94	4
7451	5
7473	15
7492.23	3
7501.13	3
7514.7	1
7559.79	9
7584.68	80
7600.77	2

7642.024	290
7664.3	12
7740.31	6
7783.66	5
7790	1
7802.651	30
7881.32	8
7887.393	96
7937.41	6
7967.342	125
8003.26	1
8029.67	13
8057.258	48
8061.339	45
8101.98	8
8109.46	1
8118.29	0.5
8171.02	6
8206.336	215
8231.6336	20000
8266.52	120
8280.1162	8500
8297.71	2
8324.58	3
8346.8217	795

8372	2
8392.37	2
8409.1894	1370
8437.55	1
8522.55	7
8530.1	9
8576.01	30
8624.24	17
8648.54	56
8692.2	24
8696.86	23
8709.7	11
8739.37	180
8758.2	34
8819.4106	37800
8851.44	3
8862.32	240
8885.71	3
8908.73	125
8930.83	170
8952.3	6800
8981.05	45
8987.57	90
9025.98	17
9032.18	23

9045.4466	8888
9096.13	25
9112.24	5
9131.59	4
9152.12	10
9162.652	10800
9167.52	70
9203.2	45
9211.38	27
9222.39	6
9245.18	2
9301.95	33
9306.64	36
9334.08	1
9374.76	250
9412.01	65
9441.46	5
9442.68	30
9445.34	100
9488	4
9497.07	27
9505.78	3
9513.377	450
9585.14	6

8.2.3 Ne arc lamp

Table 22: list of wavelengths and relative fluxes for the Ne arc lamps

Wavelength (Angstroms)	Relative Flux
4704.3949	0.5
4708.8594	0.5
5031.3484	0.5
5037.7512	5
5080.383	3
5154.4271	0.5
5188.6122	0.5
5193.1251	0.5
5193.224	0.5
5203.8962	0.5
5210.5672	0.5
5222.3517	0.5
5234.0271	0.5
5298.1891	0.5
5330.7775	18
5341.0938	15
5400.5616	38
5433.6513	0.5
5562.691	7
5656.6588	8
5662.5489	0.5
5689.8163	5
5719.185	4
5748.2985	16
5760.5885	0.5
5764.4188	90
5804.4496	20
5811.4066	0.5
5820.1558	50
5852.4878	3250
5872.8275	40
5881.895	2700
5901.409	40
5906.4294	18
5913.633	6
5918.9068	2
5919.029	2
5934.4522	3
5944.834	4400
5961.6228	3
5965.471	25
5975.122	1250
5987.9074	16
5991.6477	3
6000.9275	4
6029.9968	1500
6064.5359	5
6074.3376	3800
6096.163	4800
6118.0187	1
6128.4498	270
6143.0627	10000
6163.5937	3700
6174.802	12
6182.146	20
6189.0649	2
6205.7775	6
6217.2812	3500
6246.7294	5
6266.4952	7000
6293.7447	4
6304.7893	2600
6313.6855	6
6332.766	9600
6382.9914	11500
6402.248	21000
6421.7044	2
6444.7118	7
6506.5277	12000
6532.8824	5500
6598.9528	7100
6652.0925	48
6678.2766	12000
6717.043	9200
6738.032	1
6929.4672	12450
7024.05	1300
7032.4128	34000
7051.2922	47
7059.1079	205
7112.3075	1
7173.938	2650
7245.1665	17000
7304.8422	1
7438.8981	5200
7472.4383	80
7488.8712	1000
7535.7739	920
7544.0439	370
7833.0281	0.5
7839.052	5
7927.1172	7
7936.9957	20
7943.1805	120
8082.4576	210
8118.5495	50
8128.911	20
8136.4061	250
8248.6826	5
8259.3795	45
8266.0769	97
8300.3248	620
8365.7464	85
8377.507	2900
8418.4265	470
8463.3569	52
8484.4424	22
8495.3591	1650
8544.6952	30
8571.3535	35
8582.9031	19
8591.2583	550
8634.6472	630
8647.0412	64
8654.3828	1050
8680.794	215
8681.9216	215
8704.1122	45
8771.6575	100

8781.969	1000
8792.5056	5
8830.9067	6
8853.8669	450
8865.701	240
8919.5007	102
8988.5564	25
9148.672	130
9201.7588	95
9220.468	72
9226.691	17
9275.5191	8
9300.8532	70
9310.5833	8
9313.9731	25
9326.5072	55
9373.3079	15
9425.3797	40
9459.211	18
9486.6825	18
9534.164	45
9547.4052	20
9665.42	45

8.3 Description of the WFM_SMP mask

The geometrical calibration is performed by translating a multipinhole mask covering most of the WFM FOV of the instrument (Figure 49). It is composed of 12 vertical lines of 57 pinholes covering a rectangular region of 55.6 x 58.5 arcsecs on each side with a regular grid. By translating the mask vertically, we are able to have pinholes entering and exiting each slice of the instrument during the geometrical calibration.

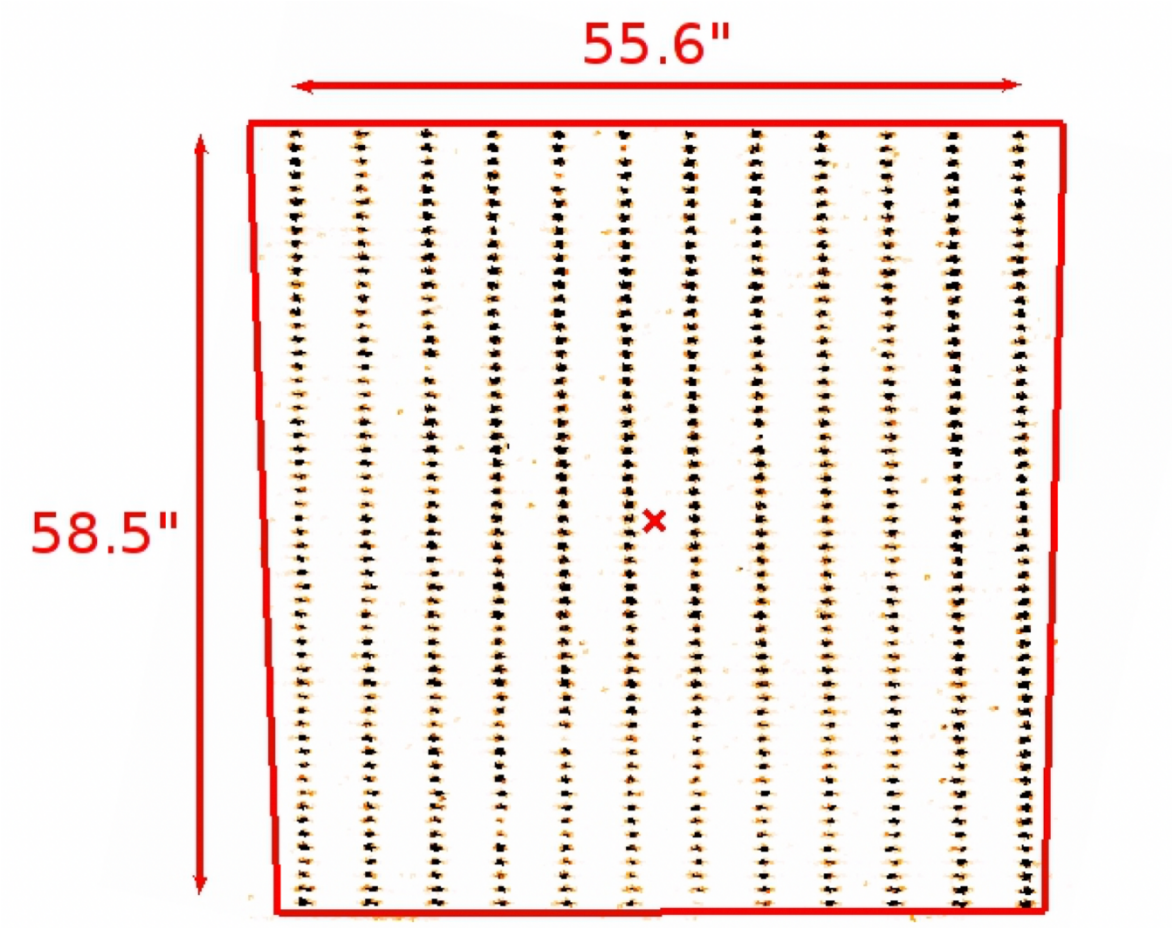


Figure 49: *Arrangement of the WFM_SMP mask used for geometrical calibration, as viewed on a reconstructed image when illuminated with internal lamps. We overlay the trapezoidal shape of the FOV in red.*

8.4 Log of instrument changes

Changes in software or hardware can have implications on the necessary calibration data set to reduce science data. For example, a change of detector invalidates all the previous bias, darks, flat fields, and geometry calibration files. For that reason, we keep a table with all the changes in reverse chronological order. This table is kept in the MUSE News URL:

https://www.eso.org/sci/facilities/paranal/instruments/muse/news.html

8.5 ds9 template

We provide a ds9 template showing the trapezoidal FOV of MUSE for the different WFM modes, together with the SGS metrology field regions surrounding it.

One can simply download the .tpl files from the ESO webpages at

https://www.eso.org/sci/facilities/paranal/instruments/muse/tools.html

8.6 Version history

- Version for P106 Phase 1 and 2
  - Added performance data for WFM-AO and NFM-AO modes. See Figure 27 and Figure 38.
  - Added warning about large overheads for NFM rotations
  - Added recent important references for MUSE data analysis.

- Version 11 for P105 Phase 2:
  - Modified maximum distance of reference NGS in NFM to 5.90” when using the small-scale field selector for point sources, identified in the NFM acquisition OB with the selectable keyword SEQ.EXTENDED=F. Several places 2.2.3, 0, 5.4, and Table 14.
  - Added info on the effect of airmass on AO performance for NFM observations. Section 4.5.1.
  - Added ADC problem frame. Section 3.9.7.
  - Added information of the NFM ADC section. Section 3.6.
  - Description of some new extensions that have been added to the raw frames. Section 7.2.

- Version 10 For P105 Phase 1:
  - Added information about new Turbulence Categories replacing Seeing in Phase 1. See Table 10 and Table 12.
  - Relaxed offset size in NFM from 0.2” to 1.0” if no rotations. See Section 5.4.
  - Remove restriction of only SKY offsets in AO modes. See Section 5.4.
  - Added recommendations of having one exposure with an UIT of at least 150s in NFM OBs. See Section 5.4.

- Version 9.7 – 9.10

  For P104 Phase II. Added PWV constraint in the discussion of Telluric correction, and the plot of transmission versus PWV. Added info for new Phase 1 tool to be used for DDT. Added section discussing the NFM ADC performance. Reformatted TOC to not use hyperlinks. Added to overhead table preset time for OBs in concatenation. Added throughput in bluest part of spectrum for -E modes.

- Version 9.1

  For P104 Phase I. Revised classification criteria for NFM-AO observations. Added new overheads for the attached calibrations.

- Version 8.24

  Added section on performance of 3 laser degraded mode operations in WFM-AO.

- Version 8.15

  This version is released for P103 Phase II. It contains changes for NFM-AO-N observations. A new section on performance taken from the literature has been added.

- Version 8.12

  This version contains preliminary performance information for the NFM-AO-N mode. It is released in support of the P103 Phase I stage.

- Version 8.5

  Document has been cleaned of bad links. Modified range of notch filter and made it homogenous in the different tables. Added new version of some figures to fix broken document. Homogenized the notch filter wavelength ranges.

- Version 8.3

  Document updated for Instrument Package for P102. Template description, Sec. 7, aligned to IP P102. Added resolution vs wavelength table in Sec. 3.2.

- Version 8

  Document upgraded to include information on GALACSI and WFM AO observations, to be used for Science Verification and P101.

- Version 7

  Uncorrupted version. All table and Figure numbers now correct.

- Version 6

  Several links have been updated. This version should be used for P97 Phase II onwards.

- Version 5.10

  In this version we changed the versioning number to the PDM scheme.
  Released for P96 Phase II. Note that this version documents the recent changes to the detector system including the change of detector in channel 01 to eliminate the problem of the glowing pre-amplifier. To reduce bias and dark structure we are now continuously wiping the CCDs between exposures.

- Version 1.3.1

  Released for P96 Phase I on 4 March 2015. Minor change added RRM acq_Preset template info.

- Version 1.3.0

  Released for P95 Phase I on 8 Sep 2014. Note that there was no version 1.2

--- End of document ---